Faculdade de Engenharia da Universidade do Porto

Dental Pressure Detection and Nerve Stimulation Demonstration Prototype

Beatriz Alves Pereira

Mestrado em Engenharia Biomédica

Supervisor: Professor José Machado da Silva

Second Supervisor: Doctor Jorge Marinho

September 1, 2018

O presente trabalho foi desenvolvido no âmbito do projeto "NIMAS - Novos Implantes Médicos AtivoS-032348-02/SAICT/2017" financiado por fundos europeus estruturais e de investimento (FEEI-FEDER) da competência da Comissão Diretiva do Programa Operacional Competitividade e Internacionalização, e pelo Orçamento de Estado da competência da Fundação para a Ciência e a Tecnologia (FCT).

U.PORTO
FEUP FACULDADE DE ENGENHARIA
UNIVERSIDADE DO PORTO

MEB - MESTRADO EM ENGENHARIA BIOMÉDICA **2017/2018**

A Dissertação intitulada

"Dental Pressure Detection and Nerve Stimulation Demonstration Prototype"

foi aprovada em provas realizadas em 21-09-2018

o júri

Presidente Prof. Doutor Joaquim Gabriel Magalhães Mendes
Professor Auxiliar do Departamento de Engenharia Mecânica da FEUP - U.Porto

Prof. Doutor José Alberto Peixoto Machado da Silva
Professor Associado do Departamento de Engenharia Eletrotécnica e de Computadores - FEUP - U. Porto

Dr. João Carlos Azevedo Gaspar
Diretor de Grupo de Investigação do INL - International Iberian Nanotechnology Laboratory

O autor declara que a presente dissertação (ou relatório de projeto) é da sua exclusiva autoria e foi escrita sem qualquer apoio externo não explicitamente autorizado. Os resultados, ideias, parágrafos, ou outros extratos tomados de ou inspirados em trabalhos de outros autores, e demais referências bibliográficas usadas, são corretamente citados.

Beatriz Alves Pereira
Autor - Beatriz Alves Pereira

Faculdade de Engenharia da Universidade do Porto

Abstract

Advances in bioelectronics and microtechnologies have offered a series of new techniques, allowing us to witness the birth of a new generation of medical implants, namely the bionic devices, which are able to restore functions in the body. These include neurostimulation and neural recording devices, which provide great benefits in the treatment of neurological diseases or restoration of sensitivity and movement, such as, e.g., by means of a cochlear implant. In the domains of dental medicine, neurostimulation has been explored in the treatment of dry mouth and of some facial pain conditions, being these the two only applications known so far.

The purpose of this work is to respond to the need for evolution of this field of medicine in areas such as neuro-stimulation and intelligent implants, through the development of a bionic device capable of capturing different levels of force applied during mastication and mandibular occlusion and translate them into proportional electrical stimuli.

The developed prototype integrates two modules, one meant to be installed in a dental prothesis and the other placed at the ends of the trigeminal nerve. The first module integrates a piezoelectric sensor that captures the force applied during the bite, amplifies this signal and converts it into a four-level digital code. This information is then transmitted to the second module, responsible for handling the reception of this information, converting these four levels into a proportional nerve stimulation current value with a digital-to-analogue converter (DAC). The DAC circuit is designed so that for each level of applied force a 1 mA current step occurs, leading to a maximum stimulation intensity of 3 mA. In order to perform the wireless communication between modules in the future, a conversion of the data to serial before the transmission, and its conversion, again, to parallel, is the receiver, is required. The electrical stimulation is monophasic, with small current peaks applied to the trigeminal nerve.

Resumo

Avanços no campo da bioeletrónica e da microtecnologia têm oferecido uma panóplia de novas técnicas, permitindo a disponibilização de uma nova geração de implantes médicos, nomeadamente os dispositivos biónicos, capazes de restaurar funções no organismo. Aliado a estes desenvolvimentos, a neuro-estimulação permite grandes benefícios no tratamento de doenças neurológicas e na restauração dos sentidos e movimentos, tomando-se como exemplo a doença de Parkinson e o implante coclear, respetivamente. No domínio da medicina dentária, a neuro-estimulação ainda tem escassos exemplos de atuação, destacando-se como exemplos únicos conhecidos o tratamento de sensação de dor facial ou de boca seca.

O propósito deste trabalho vem no sentido de dar resposta à necessidade de evolução deste campo da medicina em áreas como a neuro-estimulação e os implantes inteligentes, através do desenvolvimento de um dispositivo biónico capaz de captar diferentes níveis de força aplicados durante a mastigação e oclusão mandibular e traduzi-los em estímulos elétricos proporcionais.

O protótipo desenvolvido integra dois módulos, idealizados para que um seja instalado numa prótese dentária e outro nas extremidades do nervo trigeminal. O primeiro módulo integra um sensor piezoelétrico que regista a força aplicada aquando da mordida, trata do condicionamento deste sinal e converte-o num formato digital. Esta informação é transmitida, de seguida, para o segundo módulo, responsável por tratar da receção desta informação, convertendo os quatro níveis de força detetados em valores proporcionais da corrente de estimulação, através de um conversor digital/analógico (DAC). O circuito DAC é dimensionado de maneira a que, por cada nível de força aplicada, ocorra o somatório de 1 mA de corrente, levando a uma intensidade máxima de estimulação de 3 mA. Para que no futuro a comunicação entre módulos seja feita por wireless, a conversão dos dados para série antes da transmissão é requerida, assim como uma conversão, novamente, para paralelo, após a transmissão dos dados entre módulos. A estimulação elétrica é monofásica, com pequenos picos de corrente aplicados ao nervo trigeminal.

Acknowledgements

After a long walk of 5 years, here comes the culmination of such a difficult journey. As such, these thanks go not only to the people who accompanied me during this year of work, but also those who were present throughout my academic journey.

First, I would like to thank Prof. José Machado da Silva, my supervisor, for all the patience, dedication and availability. Also to Dr. Jorge Marinho, my co-supervisor, for all the availability, even at a distance, always shown me.

Then, I would like to thank the whole team of the 18th floor of Electrical Engineering, Mathematics and Computer Science building of the Delft University of Technology, who welcomed me during 5 months in an internship. I would like to thank to Prof. Ir. Peddy French for the knowledge that he gave me about biosensors. I also want to give special thanks to Prof. Ir. Wouter Serijn, leader of the Bioelectronics group and my co-supervisor in TU Delft, for the constant availability, teaching, help and advices he always showed.

Two other very important people during 6 months of work in the Department of Electrical and Computer Engineering of FEUP, Vasco Correia and Pedro Alves. Vasco for being the biggest help when the solutions failed and when I did not see the light at the end of the tunnel; Mr. Pedro Alves for all knowledge and concern.

I can not fail to thank a very special friend who accompanied me in the most enriching experience I had and that contributed a lot to that, Inês Gonçalves, my “tuga de laranja” partner. Thank you for all the friendship moments as we wrote the document, for all the hours spent in lab I-03 and for all the support when I thought the thesis was endless.

The reason that made me integrate so well in FEUP, BEST Porto, to all the moments that gave me, to the memories I take from all these people and all the skills that made me discover that I did not even know I had. But most of all, a big thank you to a small mafia of neighbors who meets randomly and who heard me complain about this dissertation - "BEST AREAL". Especially to Miguel Carvalho for forcing me to relativize things and for all the patience until the last minute of delivery of the thesis, to João Camacho for being the greatest counselor, to João Guedes and Simão Lúcio for 8.4 always open and ready to receive me at any time, to Luis Monteiro for believing in me more than myself and a biggest thank you to the best of all, Márcia Saraiva, for all the minutes of support during this semester that was an authentic roller coaster and for having suffered with me until the delivery of this great work.

For the 50 reasons that show me every day how they are with me and never abandon me, the best friends in the world, Ines, Bruna, Sofia, Andreia and Carolina.

Lastly, most importantly, those who make me wake up every day, knowing that I am not alone, before the thanks, an apology for all the unanswered calls, for the bad mood, for all the times I cried for six months, my parents and my sister. Today I can say that I am the image of their education.

A thank you, too, to the rest of my family, who have always been at the distance of a phone call.

Beatriz Alves Pereira

“the sea's only gifts are harsh blows and, occasionally, the chance to feel strong”

Primo Levi

Contents

List of Figures

List of Tables

Nomenclature

ADC	Analogue-to-Digital Converter
ASIC	Application-Specific Integrated Circuit
CMOS	Complementary Metal Oxide Semiconductor
CMRR	Common-Mode Rejection Ratio
DAC	Digital-to-Analogue Converter
ECT	Electroconvulse Therapy
EMS	Electrical Muscle Stimulation
FES	Functional Electrical Stimulation
FPAA	Field Programmable Analog Array
IA	Instrumentation Amplifier
IC	Integrated Circuit
IMD	Implantable Medical Devices
IPFM	Integral Pulse Frequency Modulation
MEMS	Micro Electro-Mechanical Systems
MNT	Mechano-Neuro-Transduction
MOSFET	Metal-Oxide-Semiconductor Field Effect Transistor
NMES	Neuromuscular Electrical Stimulation
OTA	Operational Transconductance Amplifier
PCB	Printed Circuit Board
PISO	Parallel-In Serial-Out
POSFET	Piezoelectric Oxide Semiconductor Field Effect Transistor
PVDF	Polyvinylidene Fluoride
PZT	Poly-Zirconate-Titanate
RF	Radio-Frequency
SIPO	Serial-In Parallel-Out
SNR	Signal-to-Noise Ratio
SoC	System-on-Chip
TENS	Transcutaneous Electrical Stimulation
TNP	Trigeminal Neuropathic Pain
TDP	Trigeminal Deafferentation Pain
PHN	Postherpic Neuralgia

ε	Dielectric constant of the medium
ρ	Piezoresistivity coefficient
q	Charge source produced by the piezoelectric element

Chapter 1

Introduction

1.1 Motivation

The mouth and oral functions are of high importance for humans in several physiologic and social aspects, such as eating and communication. The different structures in the oral cavity are not individually specialized in a particular function, acting together for a specific purpose. The normal regulation of oral functions depends on information received from several sensory organs, including the periodontal mechanoreceptors.

Over the years, with the advances of technology and the discover of new materials, allied to the increase of the human average life expectancy, oral health care needs have increased and the treatment with dental implants has become more recurrent in society, with a larger and more effective set of solutions for different dental problems, with a success rate of 85% for 10 years [21]. Lighter implants with better biomechanical and biocompatible materials or with a natural tooth-like aesthetics are examples of these advances [3].

Biomechanical factors, like excessive loads on the implant during a bite, are the cause of most complications in the implanted prostheses, such as, porcelain fracture, unrestrained cement or screw, abutment screw loosening, problems in the attachment of the implant due to the irreversible loss of dental hard tissue, and early implant failure after loading [3, 22, 23]. Consequently, these circumstances require repairs or changes in the implant, causing extra costs for the patient [2, 20]. Often, the origin of failures in the implants, along with the emergence of headaches, neck pain, dorsal and lombar disorders resides in the lack of sensitivity to the forces exerted by the patient in the implants. This occurs due to the fact that people lose the somatosensory feedback otherwise provided by the teeth nerves. Furthermore, the periodontal mechanoreceptors work as a gyroscope for the brain and their absence results in postural instability [24]. There are also some studies that show a relationship between trigeminal nerve stimulation and the activation of some cortical areas and, in the absence of such stimulation, lead to dementia and stress diseases [25]. Lastly, excessive loads result in an increase of strain on the bone and may lead to unexpected and unwanted tooth movements. The microstrains on the bone may cause a deficit in the bone remodelling and pathologic overload ultimately resulting in bone loss.

1.2 Objectives

The central aim of the present work addresses the reestablishment of this somatosensory feedback in people with teeth loss. In other words, it is intended to develop a bionic device able to capture different applied force levels during chewing and mandibular occlusion, detecting and translating this mechanical information into different electrical stimuli. These stimuli will be then sent to the brain allowing restoring neuronal activity during mastication in order to recover the dental sensitivity in the area, triggering in the organism an appropriate motor response of defence or decrease in muscle contraction.

The very final purpose of this project is to develop two electronic modules interconnected through a wireless link. One of the modules will be placed inside the dental implant, using a piezoelectric sensor capable of producing a charge signal proportional to the force applied on the implant. Thus, there is an analogue-to-digital conversion of this signal translated into a series of electrical pulses that are sent to the second module. The second module is placed near to the endings of inferior/superior alveolar branches of a trigeminal nerve. It is responsible for a digital-to-analogue conversion of the received pressure information, leading to a certain amount of current to be discharged through electrodes, and finally applied in the form of electrical pulses to the nerve. Nociceptive stimuli run then through the sensory pathway to the thalamus and from here directly to the sensorial cortex, causing the brain to generate an adequate motor response of the masticatory muscles, stopping in a more adequate way the parafunctional mastication movements. In this dissertation, and in order to simplify and prove the functional operation of the demonstration prototype, the goal is to implement all this process by directly connecting the two modules, i.e., without wireless communication.

The work to be developed in this dissertation focus on the development of the circuits for the transmitter and receiver modules, i.e., pressure sensing, conditioning and an analogue–to–digital converter (ADC) in the first one and a digital-to-analogue converter (DAC) and current stimuli generator in the second one. Furthermore, the work is also focused on the development of data conversion technique for its transmission between modules.

1.3 Structure of the Dissertation

The present dissertation is composed of six chapters: Introduction, Stomatognathic System, Developments in Medical Devices and Nerve Stimulation, Design and Implementation of Prototype Device, Results and Discussion, Conclusion and Future Work.

This first chapter highlights the problem in question, describing its scientific background, and the motivation for the development of a prototype in order to solve this problem. The chapter ends with the description of the overall structure of the dissertation along with the contents of the different chapters.

Chapter 2 describes in more detail the scientific background about Stomatognathic System, namely the fundamental functional and structural complexities to provide biting, chewing, among other important human activities. Moreover, the functions of periodontal mechanoreceptors essential to promote tooth sensitivity, as well as the process of creation and transmission of these nerve stimuli, are underlined. Finally, a broad approach is taken to the current oral implantology in the market and most frequent problems in its biomechanics, related disorders and costs for the patient.

In Chapter 3 a state of the art around the most current medical devices on the market is presented, insisting on the greatest advances in bioelectronics and micro/nanotechnology, focused on low power consumption. A second part of the chapter deals with the medical applications of electrical stimulation in the most varied fields of medicine, as well as the stimulation technologies associated with microelectronics - biopotential amplifiers and stimulation circuits, and the most relevant requirements in nerve electrical stimulation. Finally, a summary of the technological developments in facial and oral field is made.

Chapter 4 describes the general block diagram of the prototype device to be developed and the details followed to design the corresponding circuits. The design of the circuit sensing and conditioning, ADC, DAC, current stimuli generator and the conversion technique for data transmission between two modules are fully detailed.

Chapter 5 demonstrates all the results obtained in each of the prototype blocks and a discussion based on the perspectives of these results.

Lastly, in Chapter 6, the conclusions of this dissertation are highlighted with a summary and critical discussion on the most important obtained results. A vision for future work to be carried out in order to create a full-custom system, is also presented.

Chapter 2

Stomatognathic System

The stomatognathic system comprises bones, muscles, joints, teeth, lips, tongue, cheeks, glands, arteries, veins and nerves. This system shows functional and structural complexities that are fundamental to provide humans with the capabilities to perform speech, biting, chewing and swallowing, among other activities. These structures correspond to the temporomandibular joint, teeth and mastication muscles, which are influenced and controlled by neuromuscular pathways [1].

The biting and chewing are crucial for the correct working of the entire digestive system, along with teeth that assume an important role in the oral health. The normal regulation of these oral functions depends on sensorial organs activity, namely of the periodontal mechanoreceptores [26].

2.1 Teeth

The teeth originate in the dental arcade and present some anatomical differences depending on their function for an oral activity, namely biting and chewing. Over time these structures suffered several evolutions associated to the evolution of the human behavior, namely to the type of feeding and the reduction of cranial structure.

The teeth are divided in four groups: incisors – associated to cutting; canines – to tearing; premolars – to tearing and chewing; molars – to chewing. The first two groups correspond to the anterior teeth and the last two groups to the posterior teeth. There are two dental arcades, one in maxilla (superior) and another in mandible (inferior)[1], Figure 2.1. The internal structure of the teeth is presented in Figure 2.2 and corresponds to the internal organization of each tooth, providing motor and sensory characteristics. The major division of the internal structure is the crown (segment that contacts the outside) and the root (inside of the mandible or maxilla). The crown consists of enamel, corresponding to the most robust and most mineralized substance in the body. This structure is firstly created by hydroxyapatite and after by a crystalline calcium phosphate.

[1]In common language it is also called superior maxilla and inferior maxilla.

The enamel is supported by underlying dentin. Then, in the innermost part of the crown is the pulp. The pulp is the central part of the tooth created by soft connective tissue with blood vessels and nerves which come into the tooth through a hole on root apex. The root is covered by a bone substance denominated cementum. Between cementum and alveolar bone there are fibers, the periodontal ligaments, whose aim is to create a surrounding for the tooth stability. The gum in healthy mouths has a triangular form allowing the division between dental crowns. The tooth apex is an opening at the root end, through which blood vessels and nerves pass from the alveolar region to the pulp cavity, offering thermal and mechanical sensitivity to the teeth [2].

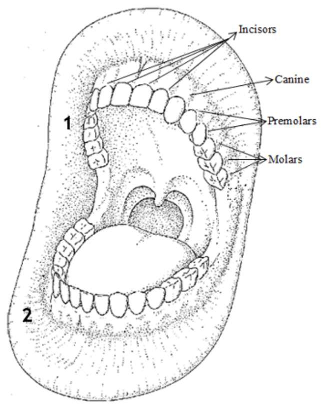

Figure 2.1: Representation of oral cavity and external structure of teeth. This structure classifies the teeth in: incisors, canines, premolars and molars. (1) Superior dental arcade; (2) Inferior dental arcade (adapted from [1])

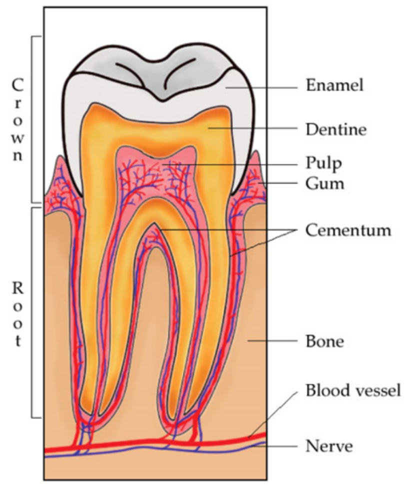

Figure 2.2: Representation of the teeth internal structure. It is mainly divided in crown and root. The crown presents an external zone, the enamel, and more internally is the pulp. Belonging to the root is the cementum (adapted from [2]).

2.2 Periodontal Mechanoreceptors

The teeth are being constantly subjected to mechanical stress in result of activities such as speech or chewing that require tongue movement, contact with other teeth and food intake.

The periodontal mechanoreceptors allow the brain to receive information about forces applied on teeth and their directions and the damping of excessive forces exerted on them, limiting and preventing the repetition of these forces. These mechanoreceptors are located among the collagen fibers of the periodontal ligament. When a tooth is mechanically stimulated the collagen fibers, and consequently the periodontal mechanoreceptors, encode the magnitude and the rate of the applied forces and send this information to the central nervous system from endings of the inferior/superior alveolar nerve converging in the trigeminal nerve and then to the brain. The trigeminal nerve is the fifth cranial nerve and is divided into three branches: ophthalmic, maxillary and mandibular (Figure 2.3). This nerve has mainly a sensory function, although there is a small region which has a motor function. For this reason it is called a mixed nerve. These sensorial functions, besides allowing teeth sensitivity, contribute also to the sensitivity of the facial skin and the oral cavity. As for the motor functions, the trigeminal nerve is responsible for the innervation of muscles that participate in chewing, swallowing and speech functions. Thus, the masticatory forces are regulated in proportion to the hardness of the substances to be chewed [26].

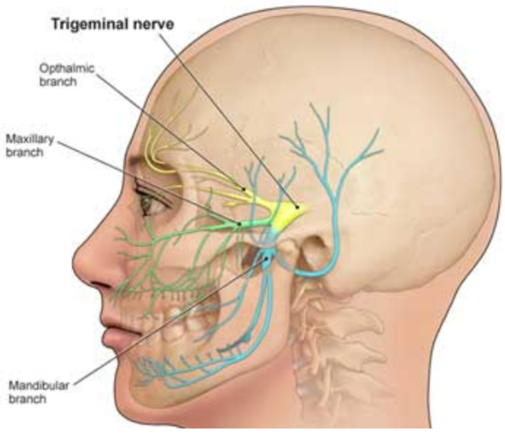

Figure 2.3: Representation of trigeminal nerve and its three branches: ophthalmic (yellow), maxillary (green) and mandibular (blue) [3].

All 32 teeth in a full dentition have periodontal mechanoreceptors, but studies reveal that the posterior teeth (premolars and molars) have reduced incidence of receptors and a decreased number of labelled neurons in the trigeminal ganglion, comparing with the anterior teeth (incisors and canines). The periodontal afferents exhibit a high sensitivity to the changes in static force below 1 N and with conduction velocities of information reaching an average of 54 m/s [26].

2.2.1 Nerve Stimuli Creation Process

The neural cell or neuron is the basic unit of the nervous system. Since it is electrically excitable, it receives and transmits information through chemical and electrical signals. Depending of its structure and function, the neuron is divided into three principal parts: the soma or cell body; the dendrites, numerous extremities; and the axon, a single long nerve fiber. All these cells share reception, triggering, signalling and secretion functions (Figure 2.4). When an electric impulse occurs, which acts as an input to the target neuron, this signal is received by its dendrites and sent to the soma where a trigger can be generated if a certain threshold is reached. The trigger is called an action potential with the property of all-or-none spike that is the principle that the force by which a nerve responds to a stimulus is independent of the stimulus amplitude. If this stimulus exceeds a certain threshold, the nerve will give a complete response; otherwise, there is no response. The soma includes also the cell nucleus which synthetizes several essential proteins for cell functioning. The action potential generated on trigger point is propagated through the axon, without loss of amplitude (in a regenerative manner) that allows to cover long distances. The nerve impulse is unidirectional and the input signals are always sorted as analogue signals. The junction between the axon and the next neural cell allows their intercommunication, resulting in the release of neurotransmitters from the axon endings to the dendrites of the receptor cell, leading to the synapse process to occur. After this action, a new electric impulse follows. This process promotes the communication of a stimulus across several neurons that, due to the shape and amplitude of the action potential, remains constant; the information is contained in the number of spikes and the time elapsed between them. The neurotransmitter signal can be considered the output of the neuron and its amplitude depends on the number and frequency of the action potentials that are generated. The synapse can have excitatory or inhibitory roles, corresponding to increasing or decreasing the chance of an action potential, respectively [4, 27].

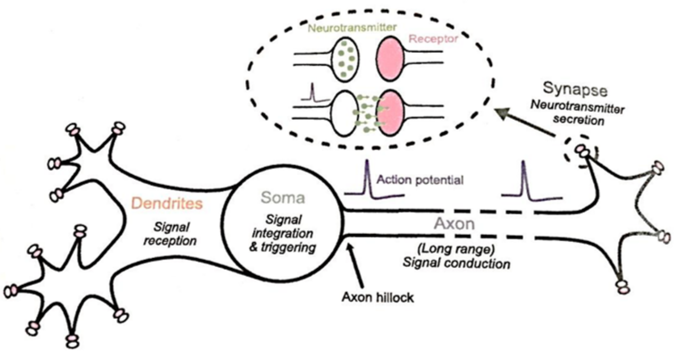

Figure 2.4: Scheme of the general organization of all nerve cells. The signal is created in the form of action potentials. Reception occurs in the dendrites, signal integration and triggering in the soma and conduction in the axon. The neurotransmitter secretion for the receptor cell is named synapse [4].

The axon can be myelinated, existing then a discontinuous insolation layer. The spaces where myelin is inexistent are called *Nodes of Ranvier*. This feature improves the velocity of the action potential [4].

The action potential manifests changes in the voltage over the cell membrane of the neuron. The cell membrane has two layers of phospholipids forming a seal between the inside and the outside of the cell (cytoplasm and extracellular fluid, respectively). The voltage in the membrane, given by $V_m = V_{in} - V_{out}$ is defined as the difference between the potentials of the cytoplasm – characterised by a high concentration of potassium (K^+) and anions (A^-) - and the extracellular fluid – characterised by a surplus of sodium (Na^+) and chloride (Cl^-). Although the membrane is a very good isolator, the diffusion of ions through the membrane is possible through proteins in the membrane, ion channels, and the concentration gradients are maintained by these proteins. The charge movement forms an electric field across the membrane, leading to a conduction current that opposes the diffusion current. The voltage at which the conduction and diffusion current is in equilibrium for an ion type is called the Nernst voltage and is given by [4]:

$$V_x = \frac{RT}{z_x F} ln \frac{c_{i,x}}{c_{o,x}}, \tag{2.1}$$

where V_x is the Nernst potential for one specific ion type x, R is the gas constant [8.314 J/mol K], T is the temperature [K], F is the Faraday's constant [9.6×10^4 C/mol], z_x is the valence of the ion and $c_{i,x}$ and $c_{o,x}$ are the intracellular and extracellular ionic concentrations [mol/cm^3], respectively. The different ion channels can be modelled with a voltage source that is equal to the Nernst potential in series with a conductance $g_{m,x}$ that represents the conductivity of each ion channel, as it is presented in Figure 2.5. As the Nernst potentials of the individual ions are unequal, the total membrane is in a dynamic equilibrium, i.e., there is a constant flux of ions through the membrane. The V_m potential is more negative because $3Na^+$ ions are pumped for every $2K^+$ ions and can be modelled by two current sources. The membrane is characterized by a membrane capacitance C_m. The cellular membrane is characterized by a resting potential $V_m = -70$ mV determined by the values of V_x and $g_{m,x}$. When V_m becomes more negative (hyperpolarizing) or a little more positive (depolarizing), the values of $g_{m,x}$ are maintained approximately constant and the membrane responds in a passive (electronic) way [27, 4].

The neural stimulation can be considered at three different levels [4]:

1. The electrode level – the electrodes and the tissue to be stimulated are modelled using an equivalent electrical circuit, forming the load of a stimulator;
2. The tissue level – the tissue is modelled as a volume conductor and the electrical stimulation promotes an electric field within that volume conductor;
3. The neuronal level – as can be observed in Figure 2.5 by the electrical model of a cell membrane, the electric field influences the local extracellular membrane potential of

a neuron, triggering or supressing an action potential.

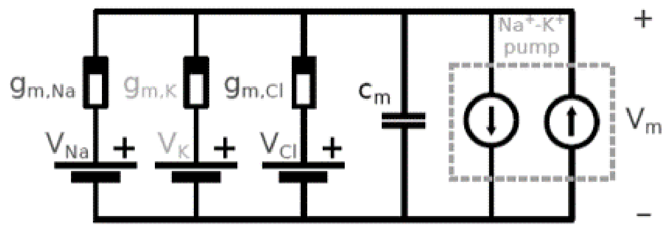

Figure 2.5: Representation of the electrical model of a cell membrane. The voltage sources (V_x) of the specific ion species represent the Nernst potentials; g_m of respective ion channels is the conductance; the current sources represent the pump of each ion; C_m is the capacitance of the membrane; V_m is the voltage in the membrane that changes when an action potential occurs due to the nerve stimulation [4].

2.2.2 Transmission of Nerve Information

The transmission of information throughout the organism is processed on afferent and efferent channels. The afferent channels send stimulus through sensitive nerves to the brain. Here, the information is processed and returns on efferent channels by motor nerves to target structures where they are translated into a mechanical response [28].

When some kind of stimulus is provoked in the superior/inferior dental arch, the periodontal arch suffers this impact, stimulating the afferent nerve fibers to send the nerve impulse up to the trigeminal spinal tract nucleus. The information process occurs in the interneurons to the trigeminal motor nucleus. Once they are reached, the efferent nerve fibers drive the proper mechanical response to facial muscles, depending on the stimulus (Figure 2.6) [5]. Take the example of a sudden increase in the consistency of food during chewing, such as in the case of a bone that is cracked inadvertently; the excess tension exerted at the level of the periodontal ligament will lead to the conduction of a stimulus that will be processed in the brain as a stop response of the chewing activity to prevent further dental contact, which could otherwise seriously damage the tooth.

2.3 Biting Forces

The physiology of the stomatognathic system involves a range of force magnitudes applied to the teeth. The force magnitudes vary with the anatomic function and so with the tooth region in the dental arch, as well as the state of dentition. In the 70s, *Helkimo* became the first scientist to record force values in the human bite through a specially designed apparatus provided with a strain gauge attached to metal beams united into forks. He concluded that the average bite force values are higher in men than women, and that higher values of force are reached in the molar region, decreasing until the incisive region.

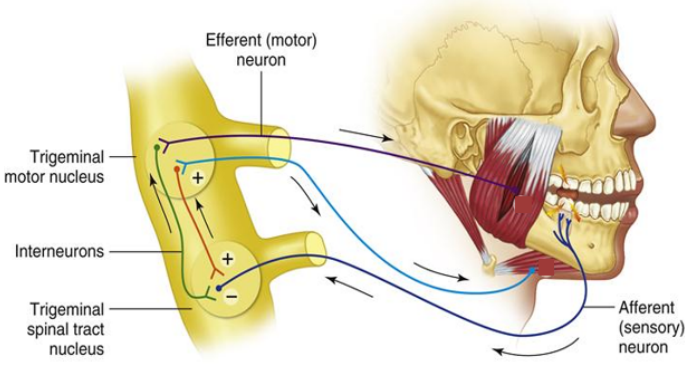

Figure 2.6: Schematic representation of the transmission of nervous information process. When the afferent sensory neurons are stimulated information is sent to the trigeminal spinal tract nucleus where processing occurs. The trigeminal motor nucleus send the stimulus response by efferent motor neurons to target structures [5].

Furthermore, these values tend to decrease with increasing age, especially in women, due to teething deterioration [23].

With the technology evolution, the studies related to the recording of forces applied in the bite also evolved. Above all, the record of these values is important in the construction of dental implants and to the choice of materials with which they are produced, since they have to be prepared to suffer high mechanical stress. More recent data report an average magnitude value for the maximum bite force of 570 ± 165 N for full natural dentition, decreased to 170 ± 20 N in patients with complete dentures, and in a group of patients with maxillary dentures and implant-supported mandibular overdentures the maximum bite force recorded was 325 ± 30 N [29].

2.4 Oral Implantology

Due to oral problems there is often the need for extraction of one or more teeth. Implantology is seen as the standard procedure for the replacement of anatomy and function of teeth. Studies show that 6-10% of the world population is completely edentulous and that only in the developed world, about 130 million teeth are lost annually. In 2012, more than 30 million implants were manufactured, a market that has been growing at around 6% per year. Solutions to replace teeth loss are expected to hit a market representing 46 million units, exceeding 9 billion euros, in 2020 [20].

When placing a dental implant some planning is needed allowing to gather considerations of aesthetics and biomechanics. Factors related to the force applied when chewing have also to be considered to evaluate the resistance of the implant.

When a dental extraction occurs, the alveolar bone is reabsorbed and the periodontal ligament ceases to exist and, consequently, leads to loss of periodontal receptors and of dental sensitivity in the region.

2.4.1 Prostheses and components

A large set of solutions for the lack of dentition exists in the market, with more than 2000 types of implants. It is possible to identify in the dental prostheses three functional factors: support, retention and number of artificial teeth. Regarding the prosthesis support, one can have support on other teeth, on the gum, or on other implants. The retention corresponds to the permanence of the prosthesis in the dental arch and may be removable or permanent. The number of teeth in the prosthesis can be partial or total [2].

The removable prostheses supported on natural teeth and/or on gum are fabricated in acrylic or in metal (skeletal), Figure 2.7. These have the great advantage of allowing for the recovery of the ability to chew, solving aesthetic defects, helping to recover from phonetic problems and allowing an easy hygiene. These prostheses have a lower cost comparing to the permanent prostheses. However, the existence of excessive forces on the teeth which serve as pillars of the structure along with the slack that the prosthesis gains over time become a disadvantage.

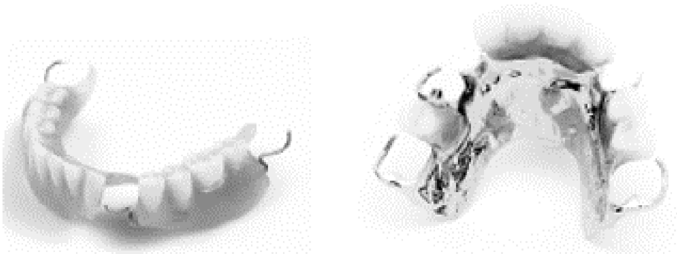

Figure 2.7: Dental removable prosthesis in acrylic (left) and in metal (right) [2].

The permanent prostheses are more complex than the removable ones. In this case it is possible to divide the prosthesis in three main elements: implant, abutment and crown (Figure 2.8) [6]. The implant is placed in the bone structure and the crown is the part placed on the top, near the gum. The abutment allows the connection between the implant and the crown. The material used in the construction of the implant and the abutment is usually titanium due to its biocompatibility and the great mechanical properties, offering a good resistance in the activities which these prostheses are subject to, such as chewing. The crown is made of a ceramic material – alumina, which is also biocompatible - covered with a pigmentation colour that resembles that of natural teeth. In order to promote the implant stability and the bone growth, titanium oxide coatings are used. This solution reduces the movements on the gum associated to the removable prostheses, offering greater resistance and structure. There is a principal disadvantage allied to the cost comparing to the removable prostheses [2].

2.4.2 Biomechanics of dental implants

The maintenance of the biomechanical loads depends on the characteristics of the applied forces and the functional surface area over which the load is dissipated. The size of

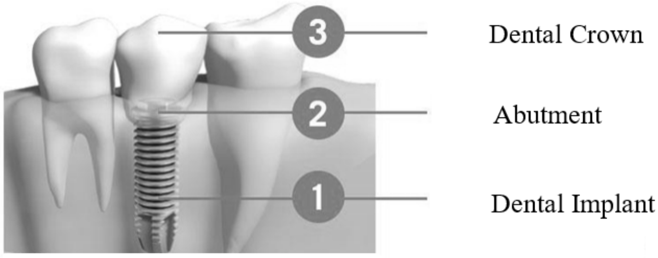

Figure 2.8: A permanent prosthesis and its constituents. (1) Dental Implant; (2) Abutment; (3) Dental Crown (adapted from [6]).

the implant body has many associated biomechanical factors, including abutment screw loosening, crestal bone maintenance, implant survival and implant component or body fracture. According to *Goodacre et al.* [20] there are numerous mechanical complications in the implants that can be caused by overloads and that carry costs for patients. Table 2.1 presents the problems with greater incidence in the loss of implants and the associated costs, in a period of 5 years.

The forces applied to dental implants can be characterized according to their magnitude, duration, type, direction and magnification. In particular, the type of forces that can be imposed on dental implants may be of compression, tension or shear. Dental implants have the greater resistance to compression forces [23].

As previously mentioned, the periodontal ligaments along with the biomechanical design of the natural tooth, the nerve and blood vessel complex, surrounding type of bone, among other characteristics, avoid the risk of occlusal overload to the tooth environment. Consequently, the support system of an implant in the absence of the periodontal ligament and the nerve/vessel complex finds a stress environment really higher, presenting a biomechanical risk for the implant failure [22].

Table 2.1: Most frequent problems in dental implants and cost per person in a period of 5 years [20].

Most frequent problems	**Cost per person**
5% loss of dental implants	15000 € in total dentures per jaw
14% fractures	9000 € in total dentures per jaw
30% screw and abutment loosening	100 € per implant

2.4.3 Disorders related to dental implants

As has been mentioned above, in cases of dentition absence, the patient loses dental sensitivity due to the loss of periodontal mechanoreceptors, which cannot be restored with the conventional mechanical dental implants currently on the market.

Besides the loss of sensitivity, teeth loss affects also other biomechanical behaviors. The jaw is a strategic point of the human body in posture, vision and balance control. It works as a gyroscope for the brain; the posture complex contracting/relaxing of postural gravity and anti-gravity muscular groups depend on how accurate is data information processed on the complex brain situs of oculo-chephalo-gyrus [20]. For this reason, changes that occur in trigeminal nerve stimulation can influence and lead to imbalances both in the vestibular system[2] and oculomotor system [24].

Chewing movements activate many cortical areas of the somatosensory supplementary motor and insular cortices, along with the striatum, thalamus and cerebellum through the stimulation and the increase of oxygen levels in the brain. The mastication may provide a "drug-free" release for stress and dementia related diseases, often accompanied by cognitive dysfunctions such as impaired spatial memory and amnesia. One of the problems in patients with dental implants is the impairment of mastication function and, consequently, low stimulation values in the brain which, in more serious cases, can lead to developing dementia [25].

2.5 Conclusion

In conclusion, the stomatognathic system assumes an enormous complexity, which is fundamental for the welfare of the human. Dental implants are a solution for tooth loss, however, they currently do not allow the restoration of dental sensitivity, which leads to problems of impairment of mastication function, unbalanced diet, dental overload, decline in body posture and balance and cognitive disfunctions. These problems lead to high costs and diminished quality of life for the patient.

[2] Vestibular system is the sensory system that provides the leading contribution to the sense of balance and spatial orientation for the purpose of coordinanting movement with balance.

Chapter 3

Developments in Medical Devices and Nerve Stimulation

Medical devices have been developed and improved over the years, with the purpose of promoting access to areas of the body so far not possible, as well as facilitating the understanding of physiological functions, prevention, early diagnosis and also their minimally invasive treatment. Advances in bioelectronics and micro/nanotechnology fields allied to the discovery of new biomaterials and new techniques, such as the coating with thin biocompatible materials, have allowed improvements in the biocompatibility, sensitivity, longevity and reliability of these devices [7].

The major current challenges for medical devices are low power consumption and miniaturization, so that more efficient operation is ensured over longer periods of time, the increase of data processing power and faster wireless communications [30]. One can find in the literature mainly three types of in-body medical devices (Figure 3.1): devices implanted inside the body (implantable); devices to be swallowed like pills (ingestible); and devices injected underneath the skin through needles (injectable) [7].

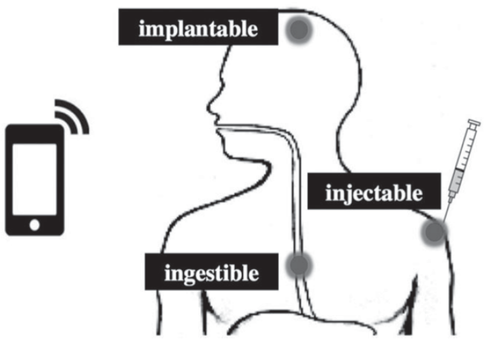

Figure 3.1: The three types of in-body medical devices: implantable, ingestible and injectable [7].

These in-body medical electronic implants can be used as sensors to detect physiological parameters or as stimulators to stimulate the nervous system. They can be presented as devices that communicate wirelessly with an external monitoring/control equipment (e.g., a smartphone); or as devices connected to the exterior of the body through a cable penetrating through the tissues for power and/or data transmission [31]. The first wireless implants combined inductive coupling at a frequency of 20 MHz or lower. Since this technology has been associated to the several limitations, such as slow data rates and high sensitivity to misalignments among inductors, the wireless antenna communication recently emerged. The literature reports antenna designs as: (1) Planar Inverted-F Antennas, typically working with implantable devices; (2) Helical antennas, typically working with ingestible devices; and (3) Loop or dipole antennas employed for injectable devices [7]. The application-specific integrated circuit (ASIC) technology has paved the way for wireless sensing platform development, with minimal power consumption. A typical system-on-chip (SoC) ASIC comprises a sensor, a signal conditioning circuit, a microcontroller and radio communication circuitry, allowing the exchange of information after processing the captured signals and presenting them as the output variables.

With the introduction of these microsystems new challenges appeared concerning power consumption and autonomy, and consequently the development of energy transferring and harvesting technologies using different power sources, such as the increase of energy density in batteries, use of acoustic waves, radio-frequency (RF) or inductive power transfer [31, 14].

The in-body devices require a power source for operation, ideally with dimensions similar or smaller to those of the device. Miniaturized implantable batteries or "microbatteries" (in the order of 10 mm diameter or less), specifically in Li and Li-ion on two-dimensional and three-dimensional thin-film, non-rechargeable or rechargeable have been developed [32]. With the purpose of solving problems regarding batteries' lifetime fully-passive operation devices have also been developed [31].

Power harvesting technologies rely on harvesting radiated energy (electromagnetic or ultrasounds), tissue motion and heartbeat, thermal gradients in the body, human movement, and glucose oxidization. Fully-passive operation is intended to completely eliminate the power storage requirements (for example, external interrogators as part of a hat in the case of brain implants or part of a T-shirt in the case of pacemakers) [7]. Supercapacitors are other approaches used to store energy to improve the autonomy of the device.

The implantable medical devices (IMD) are placed inside the human body through a surgical operation serving all kinds of sensing and stimulating functionalities. Some of the most representative implantable technologies are summarized in Table 3.1, highlighting:

1. Pacemakers: one of the most popular implantable medical devices placed inside the chest or abdomen to help control cardiac arrhythmias. The most modern pacemakers don't exceed 30 mm in length and allow additionally to communicate critical diagnostic information about the patient to external devices [7, 33].

2. Intra-cranial pressure monitors: they allow monitoring the intra-cranial pressure which, in extreme cases, results in cerebral edema, cerebrospinal fluid disorder, head injury and localized intracranial mass lesion [7].

3. 3. Neurosensors: they have recently gained interest in many applications, including Epilepsy, Parkinson's and Alzheimer's. These devices operate without internal power supplies or wires/cables, exhibiting a highly simplified implant circuit topology (Figure 3.2) [7].

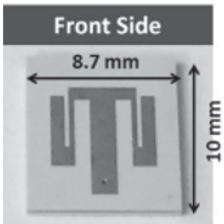

Figure 3.2: Example of a Neurosensor [7].

Examples like cardiac stents capable of wirelessly transmitting artery status, insulin pumps that monitor and correct blood sugar levels (Figure 3.3) and implants capable of detecting the presence of oral cancers aspire to the future in the field of implantable devices [7, 34, 35].

(a) Representation of a cardiac stent capable of wirelessly transmitting artery status [34].

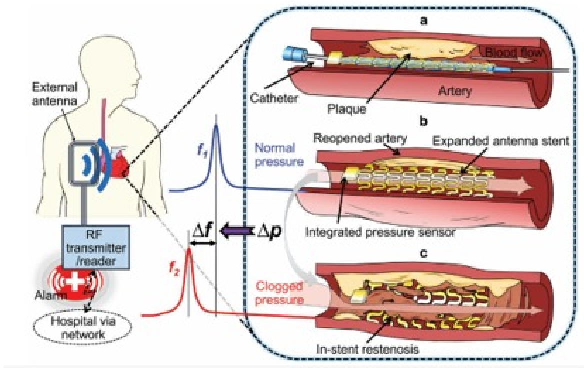

(b) Example of an insulin pump with monitorization of blood sugar levels [35].

Figure 3.3: Future of the implantable devices field.

The ingestible medical devices are miniature capsules ingested through the mouth like a pill. These devices can collect images, transmit videos in real time, detect several physiological parameters, etc, while they travel through the gastrointestinal tract. For these reasons, ingestible devices typically use high-frequency telemetry links to achieve high data rates, better image resolution and device miniaturization. The collected data are transmitted to a monitoring or control device for display and post-processing. Some examples of these devices are summarized in Table 3.1, notably:

1. Imaging capsules: correspond to small endoscopy capsules capable of capturing images of the gastrointestinal tract and digestive system. These devices include a module to obtain the images, another module to control and acquire the images and a last module to process and transmit the information (Figure 3.4) [7].

Figure 3.4: Example of an imaging capsule to the gastrointestinal tract [7].

2. Ingestible sensors: ingestible capsules with dimensions similar to the intestinal lumen providing information to reveal the state of gut health and disorders, and another physiological parameters in the body [36]. More recently, these capsules are able to measure the concentration of different gases during digestion in the gut, which in abnormal cases may be indicative of painful constipation, irritable bowel syndrome and colon cancer [7].

3. Drug delivery capsules: Electronic pills used to deliver a certain drug in the gastrointestinal tract [7].

In the future, developments in this area are expected to include personalized drug delivery capsules to treat digestive disorders and diseases (Figure 3.5), ingestible sensors to confirm the correct pills dosage for a patient, etc.

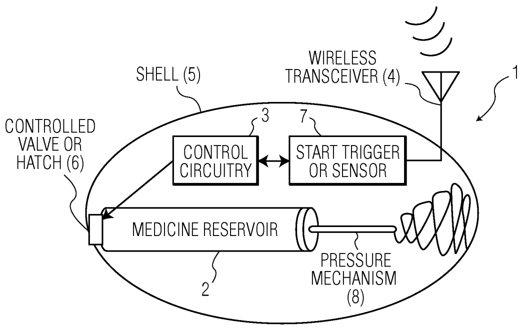

Figure 3.5: Functional representation of a drug delivery capsule [8].

The injectable medical devices are characterized by minimally invasive nature, smart capabilities and low-frequencies. For these reasons they are seen as the next generation of medical devices. Table 3.1 reports the main examples of these medical devices. It is possible to divide the term “injectable” in different classes, distinguished below:

1. Micro-sensors: Sensors injected into the human body by a needle. The length of the sensor has the thickness of a human hair and is made of hydrogel sensitive to oxygen. The reading of the device is made with an optical reader and the light is shined on the skin. One of the examples is the monitoring of peripheral artery disease (Figure 3.6 (a)) [7].

2. Micro-stimulators: These sensors are also injected into the human body by a needle but contrary to previous examples a micro-stimulator includes stimulating electrodes, an antenna for biotelemetry and power harvesting, and electronics used to control the stimulation (Figure 3.6 (b)) [7].

3. Three-dimensional medical electronics which are directly built into the human body through sequential injections (Figure 3.6 (c)) [7].

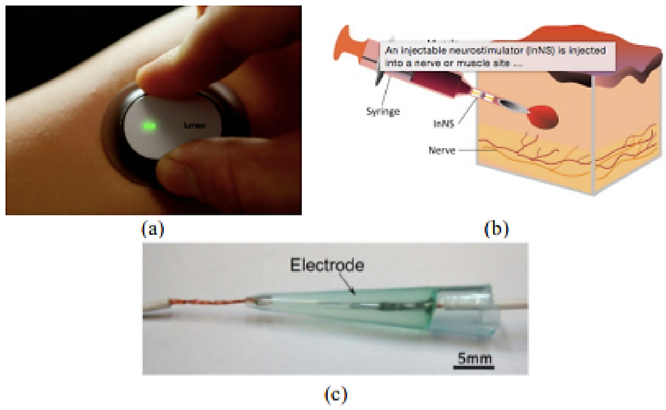

Figure 3.6: (a) Example of a micro-sensor injected by a needle; (b) Representation of the micro-stimulator injection process; (c) Electrode formed via sequential material injections [7].

The reunion of all these characteristics defines a new approach of implants denominated Smart Implants, able to collecting and sending information between the implant and different structures in the body.

Neural stimulation is another approach which has gained more importance in recent years in the medical devices domain. There are three main components which characterize a system responsible to stimulate a nerve: the pulse generator which, as the name implies, generates a set of pulses; the lead wires that carry the pulses to the stimulation spot; the electrodes capable of delivering the same pulse to the tissue [37]. Neuro-stimulators have been applied using electrical, magnetic and more recently optical and acoustic stimuli to stimulate the nervous system.

The neuro-bionic devices like the cochlear implant, retinal neuro-stimulator, stimulators in the subthalamic nucleus, etc., provide great benefits in the treatment of neurological diseases such as Epilepsy, Parkinson, Tinnitus, Tourette syndrome, spinal cord injuries, chronic pain or restoration of sensitivity and movement in different structures

[7, 14, 32]. Still in the field of neural stimulation many studies have been conducted in the mechano-neuro-transduction (MNT) area which integrates micro electro-mechanical systems (MEMS) [14, 38, 39].

Subsequently, the electrical stimulation technique will be addressed in particular, once the work is focused on this stimulating field. Electrical stimulation uses an electric current to artificially recruit neurons in order to exploit the nervous system, forcing the generation of action potentials (activation) or preventing their generation (inhibition). The electrical stimulation field has different types of stimulation, with specific characteristics such as electrical muscle stimulation (EMS), Russian electrical stimulation, neuromuscular electrical stimulation (NMES), functional electrical stimulation (FES) and transcutaneous electrical stimulation (TENS). In the EMS, the generator and electrodes are attached to the skin, sending electrical impulses to the patient's muscles for rehabilitation medicine [40]. The Russian electrical stimulation is identical to EMS but uses medium frequency (in the kHz range) alternating stimulating currents delivered in a pulsed (burst or interrupted) mode. NMES uses electrodes in contact with muscle, allowing a more rapid propagation of the stimulus comparing with EMS. FES is a technique that uses low energy electrical pulses to artificially generate body movements in individuals who have been paralyzed due to injury to the central nervous system. TENS focuses on reducing the level of pain and inflammation through the application of low amplitude electric currents over painful areas [41]. The electrical stimulation may have different designations, depending on the stimulation's local in the body. In the surface and transcutaneous stimulation, the electrodes are positioned outside the body. The percutaneous stimulation is characterized by the electrodes being located inside the body, however, the lead wires come from outside the body, to connect to the pulse generator (for the example, percutaneous tibial nerve stimulation to treat the overactive bladder syndrome). Lastly, the implantable stimulation where electrodes, lead wires and the pulse generator are inside the body (like in the cochlear implants and cardiac pacemakers cases). An implantable stimulation, where the electrodes, the lead wires and the pulse generator are inside the body, promotes more independent stimulation without the need of external wires which are uncomfortable and impractical for the patient [37].

The electric stimulating signal characteristics, such as amplitude, pulse width, and stimulation rate are determined by the stimulation field. Interleaving stimulation is an additional concept, which permits improved treatment results. The electrical energy to recruit neurons is applied by electrodes which can be configured as monopolar, bipolar or tripolar. The monopolar configuration recurs to two electrodes, an active electrode and another operating as ground allowing a more spread stimulation field. In the bipolar configuration one electrode is the cathode and the other is the anode producing a focused stimulus. The tripolar configuration uses three electrodes, one as the cathode while the other two electrodes both act as the anode. Electrode polarity controls the shape and density of the electrical field, as determined by the distance between the electrodes and the number of positive versus negative electrodes used [4]. A more detailed explanation of these concepts will be presented later in this chapter.

The main concern for any implantable stimulator is safety. In order to create a suitable charge balance in the body during the stimulation, stimulating circuits with monophasic and biphasic waveforms have been proposed [38, 42, 43]. Furthermore, current nerve stimulator designs have also automatic calibration techniques to maintain charge balance [4, 38].

Table 3.1: Most representative implantable, ingestible and injectable wireless medical devices (adapted from [7]).

Implantable Devices	**Ingestible Devices**	**Injectable Devices**
Pacemakers	Imaging of the digestive system	Neuro-stimulators
Defibrillators	Medication adherence	Glucose sensors
Intra-cranial pressure monitors	Heart failure detection	Oxygen sensing sensors
Cardiovascular pressure monitors	Gastrointestinal disorder detection	Peripheral artery disease monitors
Deep brain neurosensors	Drug delivery capsule	Athletes' muscle performance trackers
Retinal stimulators	pH sensing of the esophagus	Shoulder subluxation rehabilitation
Cochlear implants	Pressure/temperature sensing of the gastrointestinal tract	Knee osteoarthritis rehabilitation
Parkinson's stimulators	Gastric stimulators	Hand contraction treatment
Brain computer interfaces for prosthetic limbs		Ulcers treatment
Chronic pain stimulators		Hemicranias treatment
Glucose monitors		Urinary incontinence treatment
Drug infusion systems		
Identity verification chips		

Then a state of art presentation of the electrical stimulation devices will be made, as suggested in the Table 3.2. Furthermore, the typical stimulation parameters used in each clinical application are described. The primary factors that determine whether current flows are enough to produce a desired clinical effect are the impedance of the body tissues in the path of the current, electrode size and position, stimulation parameters, and electrical characteristics of the tissue to be excited. These parameters are generally interrelated for the various clinical areas in which electrical stimulation is used.

By observing the table, it is possible conclude that, in the cardiac field, the cardiac pacing recurs to a typical values of current in order of mA while cardiac defibrillators use higher current values, in order of A, once cardiac defibrillator needs a high-energy stimulation of the heart in the form of an electrical shock.

Although it is rarer, it is possible to find some applications of monophasic stimulation, namely electroventilation, since its stimulation frequency is really small (in the order of Hz) and also its pulse duration (in order of μs), not allowing effects of load accumulation.

In general, it is observed that when the electrodes are applied to skin, the stimulation force is more than when the electrodes are implanted in contact with the target tissue. This is because when the stimulation is applied on the skin, the losses are greater until reaching the target tissue, and therefore the applied current also must be higher, so that it is effective. See the example of diagnostic stimulation of brain and spinal cord with maximum stimulation current of 1,5 A and vagus nerve stimulation with a current stimulation between 0,25 to 35 mA.

It should also be noted that the gastric pacing and restoration of lost sight are the clinical applications with the lowest stimulation current.

Table 3.2: Clinical applications and typical parameters used in the stimulation of tissues with electrical currents [9].

Clinical Application	**Typical Method of Current Delivery**	**Typical Waveform**	**Typical Current or Voltage**
Cardiac pacing	Implanted electrodes in contact with heart (electrode impedance 250 Ω to 1 kΩ)	Biphasic current pulse 20 to 40 ms in duration with charge-balancing phase	0,1 to 8 V peak delivered from 5 to 10 μF capacitor and 50 to 200 mA
Cardiac defibrillation	Implanted electrodes in contact with heart (electrode impedance 30 to 60 Ω)	Biphasic capacitor discharge 5 to 10 ms Monophasic or biphasic capacitor-discharge pulse 5 to 10 ms	2 to 10 A or 30 to 40 A (depends of the capacitor)
Cardiomyoplasty	Electrodes across skeletal muscle, looped under the nerve branches	1 to 16 pulses per burst, at a pulse repetition rate of 10 to 60 Hz; burst delivered in synchrony with cardiac activity	0,1 to 8 V peak delivered from 5 to 10 μF capacitor

Table 3.2 – *Continued on next page*

Table 3.2 – *Continued from previous page*

Clinical Application	**Typical Method of Current Delivery**	**Typical Waveform**	**Typical Current or Voltage**
Electroventilation	Implanted electrodes in contact with phrenic nerve or innervation point of diaphragmatic muscles	0,8 s bursts of balanced monophasic pulses 10 μs in duration at 35 Hz 0,8 s bursts of balanced biphasic current pulses 1 to 10 ms in duration (phrenic nerve) or 25 to 100 ms in duration (muscles) at 30 Hz	200 mA to 1,5 A or 1 to 10 mA (depends of the compliance voltage)
Diagnostic stimulation of peripheral nerves	Bipolar pair electrodes applied to skin over target nerve	Monophasic current pulses 50 μs to 2 ms in duration	0 to 100 mA
Diagnostic stimulation of brain (cortex) and spinal cord	Bipolar pair electrodes applied to skin	50 μs wide transformer isolated square wave	100 to 1000 V with a maximum current of 1,5 A (at a rate of current rise of 0,1 A/μs)
Pain relief	Implanted electrodes in contact with spinal cord or targeted peripheral nerve; transcutaneous electrical nerve stimulation (TENS)	Monophasic or biphasic pulses 210 μs/50 to 150 μs in duration delivered at 30 to 80 Hz/10 to 150 Hz	0,1 to 12 V peak and 10 to 150 mA
Vagus nerve stimulation (VNS)	Implanted electrodes in contact with vagus nerve; electrode impedance 1 to 7 kΩ	Monophasic current pulses 130 to 1000 μs in duration delivered at 30 Hz for 30 s every 5 min	0,25 to 35 mA
Deep brain stimulation (DBS)	Thin electrode implanted deep into parts of the brain that are involved in control of movement; electrode impedance 600 Ω to 2 kΩ	60 to 450 μs charge-balanced capacitor-discharge pulses delivered at 2 to 185 Hz	0,1 to 10,5 V peak

Table 3.2 – *Continued on next page*

Table 3.2 – *Continued from previous page*

Clinical Application	**Typical Method of Current Delivery**	**Typical Waveform**	**Typical Current or Voltage**
Gastric pacing	Implanted electrodes stitched to the stomach muscle wall of the antrum; electrode impedance 200 Ω to 1 kΩ	Monophasic or biphasic pulses 210 μs in duration delivered at 30 to 80 Hz Hemicranias treatment	10 to 600 μA
Restoration of lost sight	Implanted electrode array in contact with retina; typical electrode impedance 1 to 10 kΩ Implanted electrode array in contact with brain's visual cortex; typical electrode impedance 10 to 100 kΩ	Balanced biphasic current pulse 100 μs to 5 ms in duration; repetition rate 60 to 500 Hz	10 to 600 μA or 1 to 60 μA (depends of the compliance voltage)
Cochlear stimulation	Implanted electrode array in contact with cochlea; typical electrode impedance 1 to 10 kΩ	Balanced biphasic current pulse 20 μs to 1,2 ms in duration at 2 kHz	30 μA to 2 mA
Functional neuromuscular stimulation (FNS)	Implanted electrodes in contact with muscle; electrode impedance 200 Ω to 2 kΩ	Balanced biphasic current pulse 25 to 500 ms in duration at 100 Hz	1 to 10 mA or 10 to 150 mA (depends of the compliance voltage)
Electrical muscle stimulation (EMS)	Electrodes placed over target muscles Interferential mode: at least two pairs of skin surface electrodes delivering high-frequency signals; electrode impedance 100 Ω to 1,5 kΩ at 4 Hz	Biphasic 10 to 15 ms waveforms at 10 Hz for denervated muscle Sinusoidal current: one channel at a frequency of 4 kHz, second channel at 4 kHz	0 to 100 mA RMS
Electroconvulsive therapy (ECT)	Electrodes applied to the forehead with impedance 250 Ω to 1,5 kΩ	10 s burst of 0,25 ms pulses delivered at 10 to 100 Hz	Up to 1 A with 2.5 kV

3.1 Electrical Stimulation Clinical Applications

The progress in neurostimulation technologies are providing relief to a large number of patients affected by debilitating disorders. These therapies include invasive and non-invasive approaches that involve the application of electrical stimulation to drive neural function. The next subchapters portray different medical devices with electrical stimulation at different parts of the body.

3.1.1 Cardiac field

The Pacemaker, one of the most well-known and used medical device in the world, relieves or eliminates the symptoms of bradycardia[3]. This device is composed by a power supply that is a battery and a power management electronic circuit, a pulse generator that generates the electric impulses, lead wires to carry the electric impulse to the electrodes and the electrodes which transmit the stimulus to cardiac tissue (Figure 3.7).

Figure 3.7: Components of a Pacemaker.

In a simple pacemaker the pacing pulses are generated at a constant interval, amplitude and waveform, being only a function of their circuit (Figure 3.8). This device generates a pacing pulse at a constant interval with a transistorized 1 kHz marker oscillator circuit to help record fast heart sounds. Early pacemakers did not consider that the patient's heart could have spontaneous electrical activity. An important development in the field of cardiac pacing was the inclusion of circuitry that could detect the patient's intrinsic heart activity and pace only when the heart's rate fell below a predefined rate (synchronous pacemakers) (Figure 3.9 (a)). It consists of a timing circuit, an output circuit and electrodes, as well as those of the asynchronous pacemaker, but it also has a feedback circuit. The timing circuit is configured to operate at a fixed rate and to promote an electrical response in the electrodes. The electrodes serve as a means of applying pulse and detecting the electrical signal of spontaneously occurring ventricular contractions that are used to inhibit the pacing timing circuit. The atrial-synchronous pacemaker is a more complicated circuit, as shown in Figure 3.9 (b). In this case, the pacemaker is designed to replace the locked heart conduction system. Here, it detects electrical signals corresponding to the contraction of the atria and uses appropriate delays to activate a stimulus pulse for the

[3]Bradycardia – A disease characterized by a very slow heart rate.

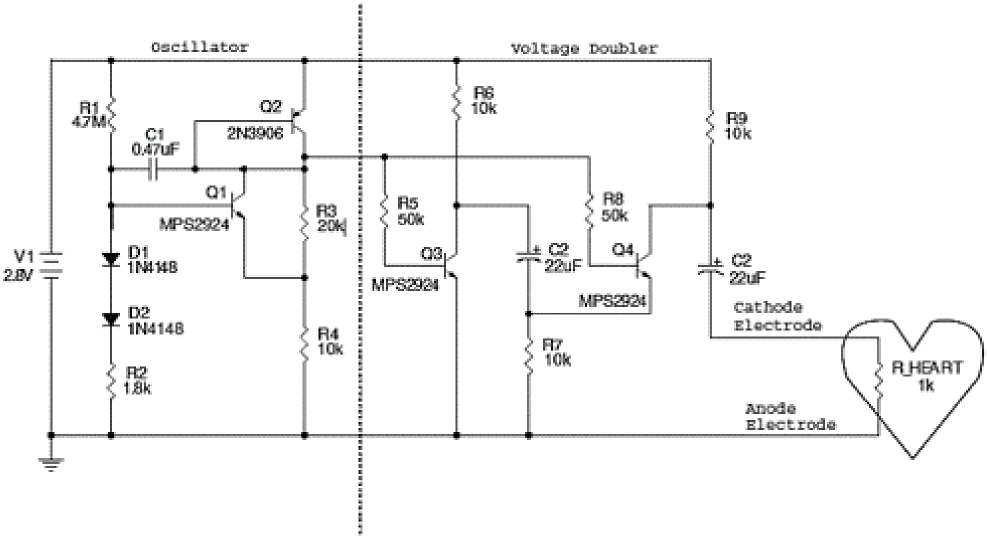

Figure 3.8: Early pacemakers had period and pacing pulse characteristics (amplitude, waveform and duration) that were only a function of the electric circuit [9].

ventricles. Since pacemaker sensing circuits usually limit their complexity to a low-power biopotential amplifier followed by a threshold detector, they detect intrinsic cardiac events based on the presence of a signal that surpasses the threshold voltage. Modern pacemakers make it possible to program the various timeouts and pacing pulse parameters in a non-invasive manner using a bidirectional RF link that communicates with the implanted device's microprocessor. This allows therapy to be tuned to the specific requirements of the patient. The latest batteries also have a longer lifetime which allows them to be replaced over longer periods of time.

Cardiac defibrillators allow high-energy stimulation of the heart in the form of an electrical shock, interrupting an accelerated heart rate and restoring a more normal rhythm. All recent defibrillators store energy in capacitors, which are charged to a certain voltage, depending on the energy needed. The defibrillation waveform is based on the discharge of this capacitor, either with an inductor (damped sine waveform) or with a switching circuit that truncates the exponential decay of the capacitor (truncated exponential waveform). Defibrillation waveforms are described by the number of phases in the defibrillation waveform, the defibrillation current tilt, and the duration of the defibrillation waveform (Figure 3.10). The implantable defibrillators are connected to leads located inside the heart or on its surface. These types of defibrillators typically use flyback converters to charge the energy-storage capacitor bank. Crude feedback loops are used in these devices to control the charge level. Photoflash electrolytic capacitors are commonly used to store the energy in implantable defibrillators.

The cardiomyoplasty allows the muscle stimulation in synchronism with the heart activity. Training is done with a low stimulation rate with only one pulse in a burst and over a period of six weeks increasing the repetition rate and the number of pulses in the

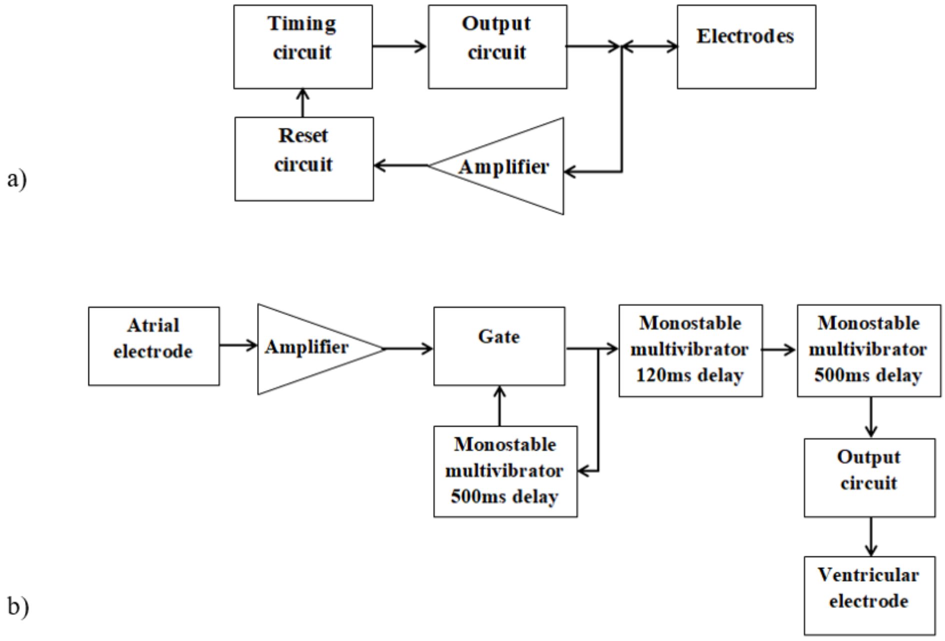

Figure 3.9: (a) Block diagram of a synchronous pacemaker. (b) Block diagram of an atrial-synchronous pacemaker (adapted from [10]).

burst.

3.1.2 Neurologic field

Electroventilation is the electrical stimulation of the phrenic nerve or the diaphragmatic muscles which can support ventilation. Patients with spinal cord injury, sleep apnoea, spasm of the diaphragm and damaged phrenic nerves resort to ventilatory support.

The electroanalgesia is a technique consisting in the application of electric currents to the spinal cord or a peripheral nerve to allay the pain with neuropathic characteristics (7-8% of adults in the general population suffer from neuropathic pain [44]). Neuropathic

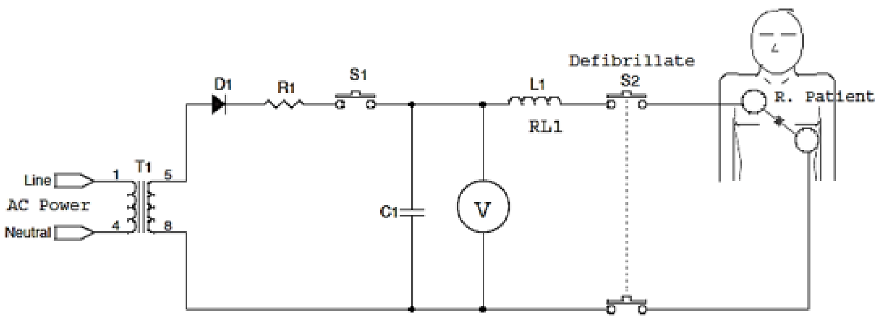

Figure 3.10: Simplified block diagram of a damped sine waveform defibrillator [9].

pain can result from traumatic or surgical injuries to peripheral nerves, infectious diseases, metabolic disorders, cancer and its treatment, and injuries or diseases that affect the central nervous system. This treatment suggests that the management of patients with chronic neuropathic pain is challenging, with more than 50% of patients experiencing only partial or no relief of their pain. The strategies used clinically can be both permanently implanted and nonsurgical applied devices. Figure 3.11 summarizes common neuromodulation devices and stimulation targets in the central and peripheral nervous systems. All

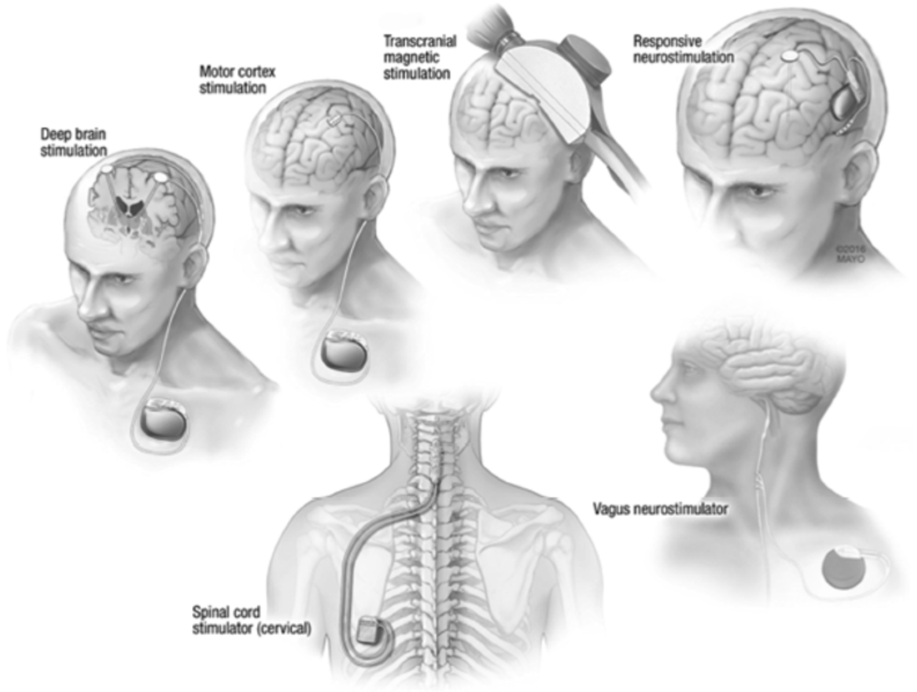

Figure 3.11: Illustration of common neuromodulation devices for the treatment of neurologic disorders [11].

these implantable neurostimulation systems include three main components: stimulating electrodes, a pulse generator which works like a battery pack, and electrode extenders to subcutaneously connect the electrodes to the pulse generator. Deep brain stimulation systems are designed as either rechargeable or non-rechargeable. Non-rechargeable systems store energy in a battery and the longevity of these systems depends on parameters used for the electrical signal, such as stimulation amplitude, stimulation rate, pulse width, number of active contacts, and battery capacity. Rechargeable systems must be recharged regularly [45].

Neurostimulators for the restoration of lost sight use electrical stimulation of the retina, the optical nerve, and the visual cortex for functionally restoring sights to blind people. Functional sight may be given to patients blinded by retinitis pigmentosa by means of using integrated circuits embedded in contact with the retina. The integrated circuits (ICs) contain an array of photovoltaic cells that directly power an array of microstimulators and electrodes to convert the image into a directly mapped electrical image, bypassing degenerated photoreceptors and directly stimulating the remaining nerve cells in the retina. For patients with blindness caused farther down in the optical nerve, the possibility exists of stimulating the visual cortex directly using microelectrode arrays to generate coherent images from phosphenes (sensation of a spot of light) elicited by the electrical stimulation (Figure 3.12) [7, 46]. Functional electrical stimulation (FES) is a rehabilitation strategy

Figure 3.12: Example of a retinal neuro-stimulator [7].

that applies electrical currents to the nerves that control paralyzed muscles in order to stimulate functional movements such as standing or stepping. This system includes either skin-surface or implanted electrodes, a control unit which often also receives motion information back from sensors, and a stimulus generator. The typical applications of this technique include controlling foot drop, enabling lower-limb paraplegics to stand or sit, and restoring hand function to the paralyzed upper limb. A general block diagram of this type of stimulator hardware is given in Figure 3.13, including the microcontroller, high-voltage, power supply, stimulation current control, and the stimulation pulse width and frequency generator.

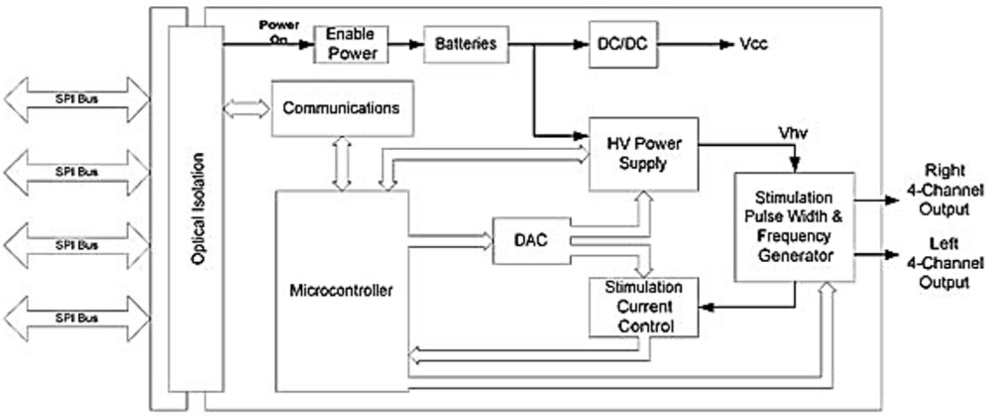

Figure 3.13: Block diagram of stimulator components [12].

Electroconvulsive therapy (ECT) is a relatively painless, effective procedure in the treatment of depression. A short, controlled set of electrical pulses is given for about one minute through electrodes on the scalp to produce generalized seizures. It is believed that the biological changes that result from seizure lead to a change in brain chemistry, which may be the key to restoring normal function.

Electrical stimulation for the treatment of bladder dysfunction and the lower urinary tract actives the motor fibers which innerves the detrusor muscle that produces bladder contraction, increases intravesical pressure, and can be used for bladder emptying. Also, it can be used to prevent urine leakage (incontinence). Some patients require continuous stimulation to prevent incontinence, and the high rate of stimulation requires a greater supply of energy over a longer period of time than is necessary for the cardiac pacemaker. For this reason, transcutaneous stimulation techniques are frequently used. Electrodes are typically placed on the second, third, and fourth sacral roots or nerves bilaterally. Leads from the electrodes are tunnelled subcutaneously between the costal margin and the iliac crest to a convenient site, where they are connected to a stimulator implanted in a subcutaneous pocket (Figure 3.14) [47]. One kind of transcutaneous stimulator is the

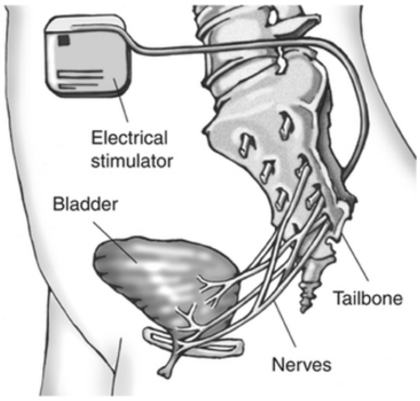

Figure 3.14: Sacral neuromodulation for lower urinary tract dysfunction [13].

RF unit shown in Figure 3.15. The implanted circuit is totally passive, with the internal secondary coil located bellow the skin and coupled to an external primary coil placed on it. The primary coil is driven by a 1 MHz RF oscillator that is switched on by the timing circuit to produce the desired pulses. The power supply for this external circuit is composed of replaceable or rechargeable batteries. The internal circuit consists of a capacitor C_1 to resonate the secondary coil to the oscillator frequency, a diode detector, and a filter capacitor C_2 to remove the RF component from the detected pulse waveform. The stimulus is then applied directly to the electrodes [10]. Intraspinal microstimulation is accomplished primarily with metal microelectrodes with diameters of 100 μm and small exposed surface areas. Stimulus amplitudes of μA, pulse durations last 100-400 μsec, and stimulus frequencies are in the range 10-60 Hz and are determined largely by the magnitude of the desired response.

The cochlear implants restore the lost hearing stimulating the spinal ganglion cells of the auditory nerves, bypassing non-functional hair cells to restore limited hearing in some types of deafness. The cochlear implant system really consists of two sections: an implanted stimulator connected to an electrode array inserted in the cochlea and an external speech processor (microphone) that codes the speech into stimulation patterns

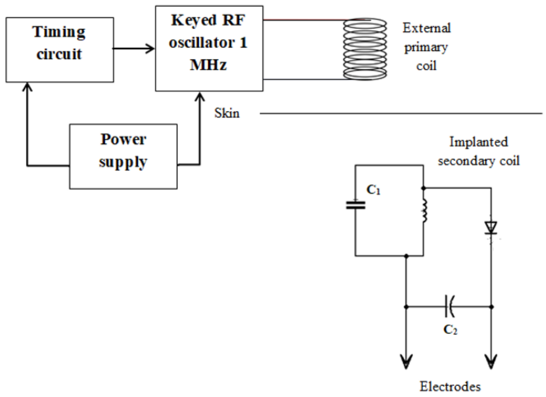

Figure 3.15: Transcutaneous RF-powered for the bladder electric stimulator (adapted from [10]).

that can be translated back into sounds by the brain. The external speech processor also powers the implant via an inductive energy transfer link (Figure 3.16). The block diagram

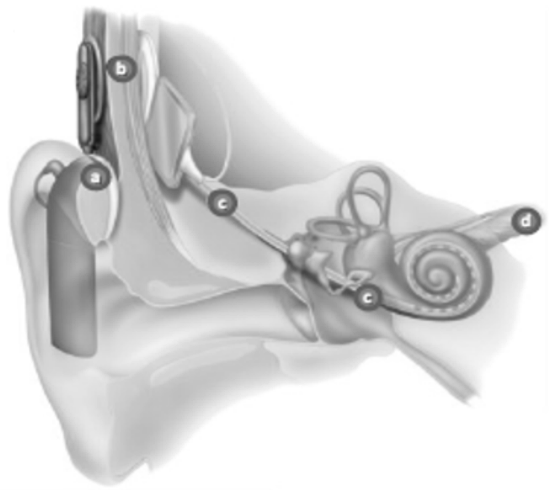

Figure 3.16: Representation of a cochlear implant and its components: a – microphone, b – external transmitter, c – receiver/stimulator, d – electrodes (adapted from [14]).

for a simplified version of a multichannel cochlear device is presented in Figure 3.17. The external unit has a microphone to pick up the sound and a speech processor circuit and this block is responsible to determine the specific features of the sound which will be used to control the stimulating electrodes. The processor is no more than a set of band-pass filters disposed such that the output signal of these filters represents the sound intensity in a specific band as a function of time. The signal from each band-pass filter controls a particular set of electrodes in the cochlea. The signal and power sufficient to drive the stimulator are thus transmitted by electrical induction by a technique similar to that shown in Figure 3.15 [10, 48].

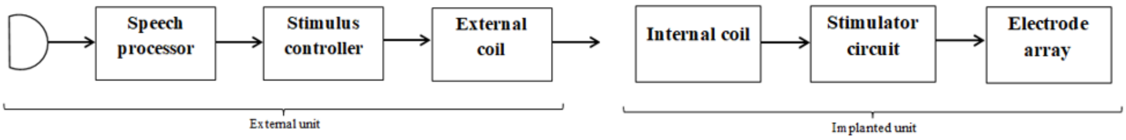

Figure 3.17: Block diagram of a cochlear prosthesis (adapted from [10]).

3.1.3 Gastric field

Gastric pacing is the electrical stimulation of the stomach, currently being used to reduce symptoms of nausea and vomiting for patients suffering from gastroparesis[3].

3.1.4 Muscle field

Electrical muscle stimulation (EMS) is used to strengthen muscles and facilitate voluntary motor function. These devices are used to maintain or increase range of motion, relaxation of muscle spasm, prevention or delay of disuse atrophy, muscle re-education, increased local blood circulation, and post-surgical stimulation of calf muscles to prevent blood clots [10].

The neurostimulation is a current therapy for the treatment or prevention of previously reported diseases. However, most neurostimulation systems available today provide a therapy delivered according to pre-programmed settings and don't automatically respond to changes in the patient's clinical symptoms or in the underlying disease (open-loop stimulation). For this reason, in recent years clinical experiences with closed-loop neurostimulation systems have emerged that modulate or adapt therapy in response to physiological changes, providing a more effective and efficient therapy. For example, open-loop spinal cord stimulation systems are generally effective in treating pain, however, they may provide therapy in excess or insufficient because the stimulation settings are not automatically adjusted based on the position of the patient's body. With a closed-loop system, it is possible to provide improved and more consistent pain relief by automatically adjusting the stimulation settings according to the patient's body position [49]. For instance, in a closed-loop stimulation the neural interface detects specific neurochemical changes in the brain to drive stimulation parameter tuning and deliver stimulation to the brain.

The most convenient way to apply electrical stimulation is through small portable units. These units have modifiable capabilities so therapists can set parameters and design personalized electrical stimulation programs that patients can use in the clinic or at home. Many come with pre-programmed schemes, from which the therapist can choose to have fixed parameters, depending on the purpose of the treatment (strengthening, muscle re-education, pain relief...). Most of these units can be locked so that patients can take them home without fear of changing program or parameter settings, and the patient only needs to turn the unit on to activate the set program [50].

[3]Gastroparesis – A stomach disorder in which food moves through the stomach more slowly than normal.

3.2 Overview in Microelectronics and Stimulation Technology

3.2.1 Biopotential Amplifiers

Over the years, the development of these medical devices has seen remarkable progress thanks to enormous advances in microelectronics technologies, electrodes technology, packaging and signal processing techniques. Issues such as reliable and fast bidirectional data communication, efficient power delivery to the implantable circuits, low noise and low power to the system recording part, and safe stimulation delivery to avoid tissue and electrode damage are some of the challenges faced by the microelectronics circuit designer.

Typically, signals from the physiological activity have very small amplitudes and must be amplified before processing. For most medical applications and to be biologically useful, all biopotential amplifiers must have a high input impedance, to provide minimal signal load to be measured. This is because the characteristics of biopotential electrodes can be affected by the electrical load they see, which, combined with excessive loading, can result in signal distortion. Typical biopotential amplifiers have input impedances of at least 10 MΩ [9].

On the other hand, the biopotential amplifier also allows protecting the organism. To that end, the biopotential amplifier must be insulated so that the current through the electrode circuit can be kept at safe levels and any artefact generated by that current can be minimized [9].

Each electrode-tissue interface has finite impedance which can result in offsets in the output signal. Probably, the most common problem in the detection and processing of the biopotential signals is the power line interference. The mains 50 Hz frequency and its harmonics can affect low-level signals, despite the use of differential amplification methods and the activation of the active potential of the body, which try to eliminate common-mode signals. Unfortunately, 50 Hz falls within the band where biopotentials and other physiological signals have most of their energy. The usual solution to reject unwanted in-band frequencies is a notch filter. As shown in Figure 3.18, simple implementation of a notch filter known as a twin-T filter requires only three resistors and three capacitors. If $C1 = C3$, $C2 = 2C1$, $R1 = R3$, and $R2 = R1/2$, the notch frequency occurs where the capacitive reactance equals the resistance ($XC = R$) and is given by:

$$f_{notch} = \frac{1}{2\pi(R1)(C1)}. \tag{3.1}$$

As the human body is a good conductor and for this reason acts like an antenna to capture an electromagnetic radiation in the environment, the biopotential amplifier has to be capable to reject common-mode signals (e.g. power line interference) through the CMRR (common-mode rejection ratio) characteristic of the biopotential amplifier. CMRR

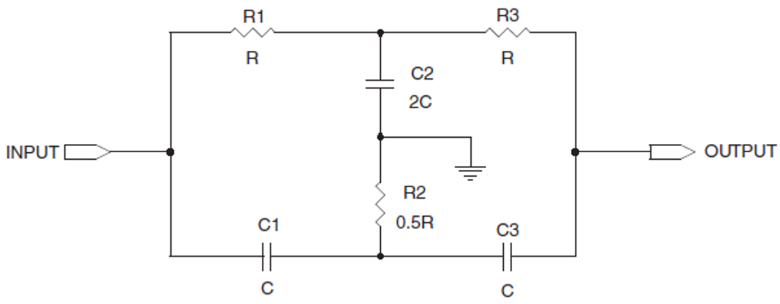

Figure 3.18: The notch frequency of the simple twin-T filter [9].

is defined as the ratio between the amplitude of the common-mode signal to the amplitude of an equivalent differential signal (the biopotential signal under investigation) that would produce the same output from the amplifier [9].

Noise and drift are additional unwanted signals that contaminate a biopotential signal under measurement. Both noise and drift are generated within the amplifier circuit. The former generally refers to undesirable signals with spectral components above 0,1 Hz, while the latter generally refers to slow changes at the baseline at frequencies below 0,1 Hz [9].

The output circuit of a biopotential amplifier does not present as many problems as the input circuit, only that the output impedance of the amplifier must be low in comparison to the load impedance, and the amplifier must be able to supply the power required by the amplifier to charge.

Another issue for biopotential amplifiers is that they enable rapid calibration. Biopotential amplifiers that need to have adjustable gains usually have an option by which different carefully calibrated fixed gains can be selected instead of having continuous control to adjust the gain [10].

The frequency bandwidth of a biopotential amplifier must be such that it amplifies, without attenuation, all the frequencies present in the electrophysiological signal of interest [9].

Some of current amplifier designs with increased functionality and performance and without penalties in chip size and power are featured in Figure 3.19 [15, 51]. The design in [15] employs an ac-coupled chopping technique[4] to reject electrode offsets and achieve low noise performance. The concept of this technique is shown in Figure 3.19 (a). The operational transconductance amplifier (OTA) is an active amplifying element that has not a power output driver circuit, as it does not need to bias any resistive elements other than the high-resistance pseudo-resistor in the feedback network [51]. Figure 3.19 (b), shows the simplified circuit schematic of a current feedback instrumentation amplifier (IA). For biomedical applications requiring high CMRR performance and accurate gain setting the use of an IA is desirable. A popular IA topology for integrated circuits is the current

[4] Chopping technique enables the design of amplifiers with high CMRR performance.

feedback technique. In a current feedback IA, the gain is adjusted precisely by the ratio of two resistors and the CMRR does not depend on the combination of resistors [15].

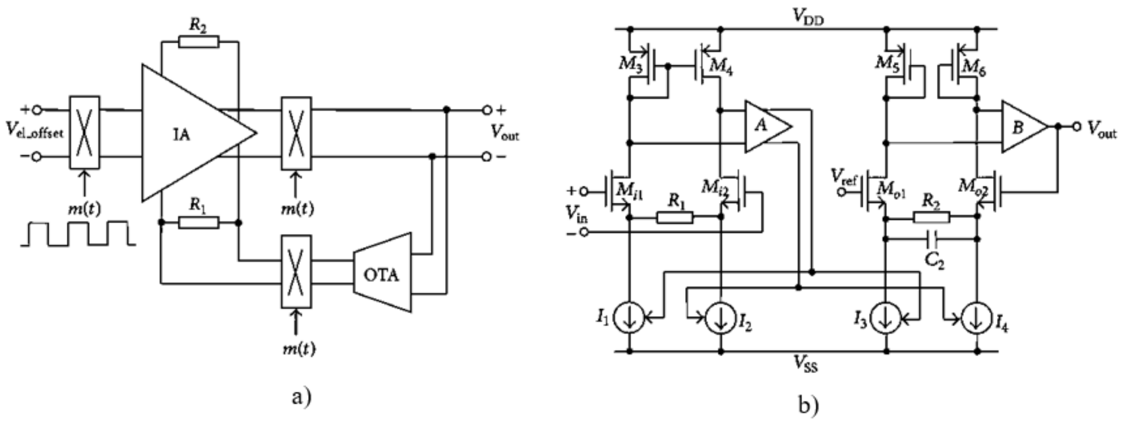

Figure 3.19: (a) Representation of an amplifier with noise reduction and electrode offset elimination; (b) Example of a current feedback instrumentation amplifier (adapted from [15]).

3.2.2 Stimulation Circuits

Once the stimulators are implanted within the body, the device must be as small as possible. This means avoiding the use of external components, while keeping energy consumption as low as possible to avoid the need for large batteries. Therefore, the voltage compliance of the circuit should be as high as possible to allow the lowest voltage supply possible [52].

The most commonly used forms of stimulation signal waves are those of Figure 3.20. The charge-balanced pulses of Figure 3.20 (a) ensure that no net charge is introduced into the body and that the current is driven to the tissue in one direction and after a brief interval in the other direction. This method is known as a balanced bidirectional pulse pair. Figure 3.20 (b) shows a circuit in which the monophasic pulses are produced only when the power source is switched along the path to the tissue and there is no way for the capacitance of the electrode-tissue interface to discharge. Not all stimulators provide a constant current stimulus. Some generate the stimulus current by discharging a capacitor into the tissue (Figure 3.20 (c)) or by using an impulse transformer to increase the voltage (Figure 3.20 (d)) [9]. The microfabrication of multi-electrode matrices has an increasing number of solutions to various challenges in all fields of biomedical. Microelectrode represent a new tool for the evaluation of electrical activity of excitable cells due to non-invasive contact, allowing long-term investigations. However, the microelectrodes still suffer from several drawbacks. The most important disadvantage is the rather poor electrical coupling of the planar electrode to the cell surface. This leads to a significant loss in the recorded

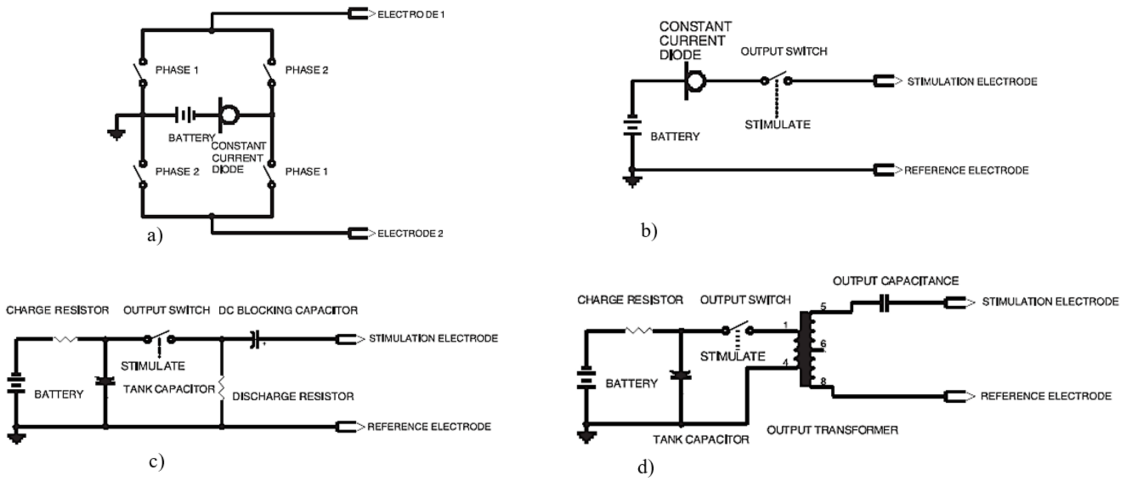

Figure 3.20: Representation of the most common stimulation signal waveshapes and the generic circuits used to produce them. (a) Charge-balanced circuit; (b) Circuit for monophasic pulses stimulation; (c) Stimulator with a capacitor discharging; (d) Stimulator by using an impulse transformer to step-up the voltage (adapted from [9]).

signal-to-noise ratio and a reduction in the efficiency of electrical stimulation. In addition, the large electrode dimensions and even greater inter-electrode distances in most of the available microelectrodes are not suitable for single-cell experiments. The electrode-membrane coupling can be improved by using three-dimensional electrodes with smaller sizes than the cell itself. Electrical stimulation of single cells using biphasic voltage pulses through three-dimensional electrodes creates a local electrical field which can be upscaling to very large sensing/recording arrays, that can result in high-throughput systems [53].

A general block diagram applied to most neural stimulators prostheses devices for treatment of neuronal diseases and for basic scientific experiments (e.g., cortical studies using animal models) is highlighted in Figure 3.21. First of all, for the reasons explained above, when the biological signal is recorded it needs to be amplified and then filtered. Thereafter, the analogue information is converted into a digital signal and sent to a digital controller like a microcontroller. Depending on the purpose of the system, the digital signal is processed and, according to the signal information, the pulse generator creates an electrical current that is drawn to the electrodes and allows neural stimulation of the tissue. These systems are commonly fed by a power supply as a rechargeable battery. The prototype depicted in the next chapter follows, therefore, an identical block diagram system.

3.3 Electrical Nerve Stimulation Requirements

The equivalent electrical model of the electrode system is typically divided into two parts: the electrode-tissue interface, with a capacitive branch (C_{dl}) and a faradaic branch (R_{CT}

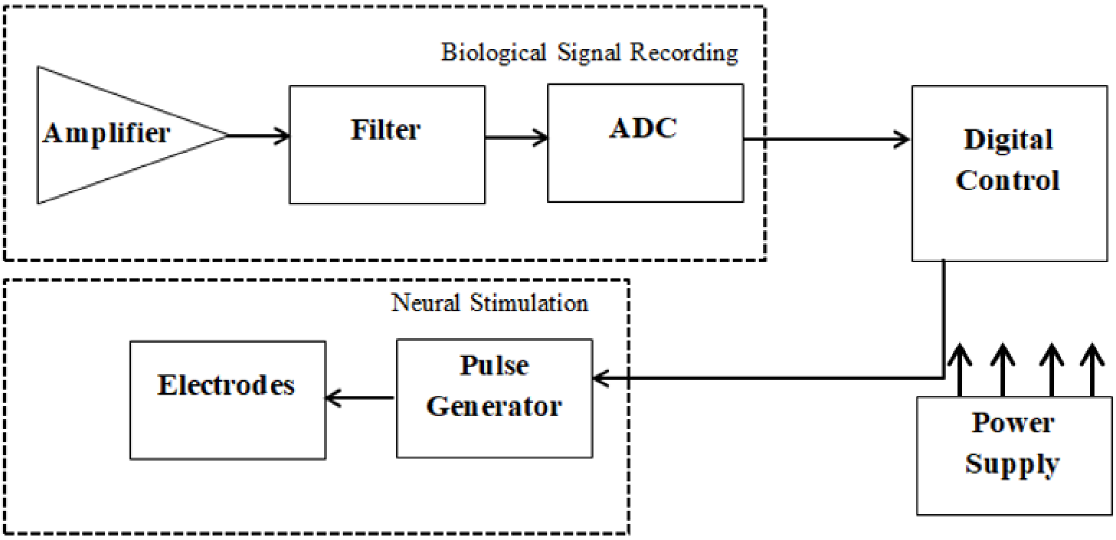

Figure 3.21: General block diagram applied to the medical devices with electrical stimulation.

and V_{eq}), and the tissue impedance itself, Z_{tis}, as is presented in Figure 3.22. The tissue impedance heavily depends on the geometry of the electrode: when the electrodes have a large contact area the impedance will be low; otherwise, small electrodes create a much smaller electric field, affecting much less neurons while using only a little current [4].

The interface of the electrode and tissue allows some interactions due to the electrons in the electrodes and the ions in the tissue. So, there are two types of interactions: charge accumulation and electrochemical reactions. The accumulation of charge is the increase of charge carriers close to the interface and there is no charge transfer between the electrode and the tissue, while in the electrochemical reactions the charge is transferred at the interface by redox reactions [4]. The use of faradaic electrodes has the disadvantage of allowing electrochemical reactions to occur and, therefore, the use of capacitive electrodes which work with capacitive charging without electrochemical reactions in the body it is advisable [54]. Rather than electrochemical reactions, the most neural damage due to stimulation derives from processes associated with passage of the stimulus current through the tissue, such as neuronal hyperactivity – too much activation might cause an imbalance in the concentrations of the various ions inside and outside the neurons [4, 55]. When a non-zero residual charge is established at stimulation site, a DC current flows into the surrounding tissue, generally thought to cause neural damage as a result of pH changes and gas formation [56]. The amplitude and pulse width are two parameters of the stimulation pulse that determine the stimulation intensity and hence the recruitment of neuron depends of this intensity/strength and duration of the stimulation, respectively. Thereby, there are two criteria to consider during the electrical stimulation so that it is done within safe levels. Previously proposed [54] charge density during the stimulation

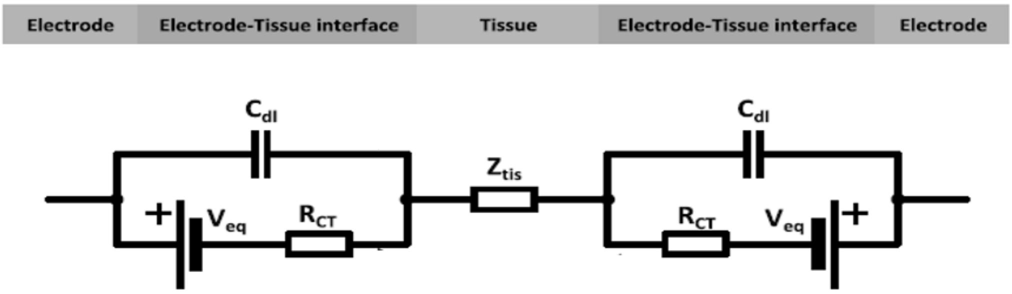

Figure 3.22: Scheme of the equivalent electrical model of the electrode system. C_{dl} – capacitive branch of the interface model; R_{CT} and V_{eq} – faradaic branch of the interface model; Z_{tis} – tissue impedance (adapted from [4]).

can be found by:

$$D = \frac{IT}{A} = \frac{Q}{A}, \tag{3.2}$$

where D is the charge density [μC/cm^2/phase], I is the stimulation current value or the pulse amplitude [A], T is the duration of each pulse phase or the pulse width [μs], A is the surface area of the electrode [cm^2] and Q is the charge [μC/phase]. The charge density limits have ranged from 15 to 65 μC/cm^2 independently of the electrode area. *McCreery et al.* observed the region of charge density where neural damage was detected (Figure 3.23a) [54]. The amplitude and pulse width determine the total electric charge contained in one stimulation pulse, by "Strength-Duration Curve" in Figure 3.23b, give us a detail about the stimulation intensity thresholds, corresponding to the different stimulation durations used. Furthermore, this curve provide us the optimum teoric pulse width (*Chonaxie*) and pulse amplitude (*Rheobase*) to generate the most efficient stimulation pulse [57]. With the purpose of stimulating the trigeminal nerve branches with the prototype to be developed, the stimulation parameters should be regulated according to Equation (3.2) and Figure 3.23 to assure safe levels.

Depending on the application, the stimulator system may have multiple channels connected to multiple electrodes. A single channel stimulator consists of one stimulation source that can be connected to two or more electrodes which provide one stimulation pattern simultaneously on the electrodes. In the prototype two electrodes fed by a stimulation pattern will be used and, therefore, the stimulation system has only one channel.

Depending on the choice of electrodes as well as how they operate, different electric field shapes and sizes are obtained. As explained previously, there are monopolar, bipolar and tripolar electrode configurations. Figure 3.24 presents a schematic of the three configurations. The monopolar configuration uses a larger electrode and it is characterized by a broad stimulation field (may result in more activated nerve fibers) which requires the use of a higher current. The bipolar configuration uses two small electrodes and produces a focused stimulus which allows for a better power efficiency. The tripolar configuration rends less power efficiency. Thence, resorting to bipolar configuration is the best solution

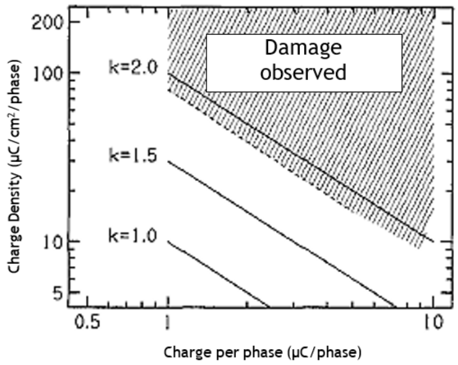

(a) Representation of charge per phase and charge density values and region above which neural damage occurs (hatched area); the solid lines and k represent a parameter of the model (adapted from [54]).

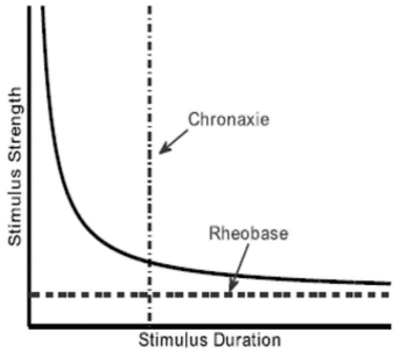

(b) Strength-Duration Curve [4].

Figure 3.23: Neuro-stimulation safe levels [4].

to acquire nerve stimulation with good power efficiency.

3.3.1 Monophasic and Biphasic Stimulation

Figure 3.25 presents a general neural current stimulator with a coupling capacitor C_c connected in series with the stimulator and the bipolar electrodes. The electrodes are represented as a resistance R_s in series with a capacitor C_dlx and a resistor R_cx, modelling the electrode-tissue interface. The stimulation source may be a monophasic current stimulator (generating a single-pulse stimulus as the number 1 in Figure 3.25 (b)) or a biphasic current stimulator (generating a stimulus with a cathodic and an anodic pulses as the number 2 in Figure 3.25 (b)) [4].

The biphasic stimulation is commonly used in the most part of the implantable devices for safety reasons such as charge-balanced. Applying a passive charge balancing, with S_1 open the capacitor C_c will be charged according to the cathodic phase; when S_1 closes occurs the discharge of C_c to the electrode and, consequently, the stimulation of the tissue. Then, the anodic phase of the biphasic stimulation is given, with the same behavior by the stimulator, but with an opposite signal charge, promoting a cancellation of the charge

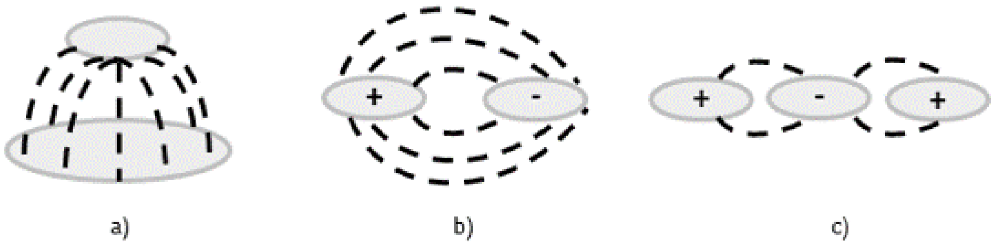

Figure 3.24: Examples of three different electrode configurations. The disks represent the electrodes and the dashed lines represent the stimulation field. a) Monopolar configuration; b) Bipolar configuration; c) Tripolar configuration.

in the tissue. In terms of power consumption, this approach is more expensive than monophasic stimulation because it is necessary to generate a current twice for the two pulses and the second phase of a biphasic stimulus reduces the effective strength of the leading stimulus phase [4, 42].

The monophasic pulses excite neurons at lower thresholds, with lower current values, and provide more spatially selective excitation of nerve fibers [42]. However, as the monophasic stimulation is a non-compensated charge method, it is not useful for high stimulation frequencies leading to increased residual charge in the body. Furthermore, monophasic stimulation is just possible to use only with non-polarizable electrodes such as Ag-AgCl electrodes, because there is no risk of charge accumulation at the interface [4].

A solution to overcome one of the problems presented by these techniques is the asymmetric biphasic stimulation, where the second phase is longer than the first phase. Here it is possible to maintain the safety charge balance [42].

The coupling capacitor C_c can become a problem if its capacitance value is high. The reason is in the increase of the footprint area, impeding the use of a chip. Furthermore, coupling capacitors introduce an offset in the electrodes [4, 56]. The passive method is not

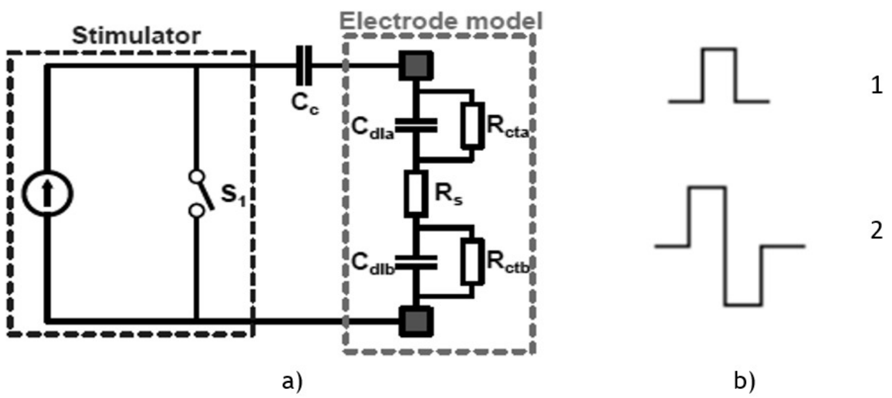

Figure 3.25: (a) Example of a current stimulator system with the stimulator in series with a coupling capacitor in series with the electrode model (adapted from [4]); (b) Representation of two typical waveforms in monophasic stimulation (1) and in biphasic stimulation (2).

the only technique to remove residual charge. In contrast to the passive method which use a natural process of the body for discharge, active methods need extra power to remove the charge being more effective but with higher consumption. Predefined current pulses at the end of each stimulation cycles, inserting short pulses, applying an offset DC current into the electrodes or introducing an inter-pulse delay are all examples of active methods of charge removal [56].

Figure 3.26 summarizes what has been discussed previously. The black line represents a general pulse in monophasic stimulation and the blue line represents biphasic stimulation. The biphasic stimulation has two phases, cathodic and anodic (the anodic phase corresponds also to the single pulse of monophasic stimulation), with amplitude I and duration t. The anodic first stimulation pulse of the electrical discharge in the nerve by the electrode leads to an increase in charge. When the cathodic charge cancellation pulse occurs, the charge increases with the opposite signal, cancelling the previous charge. As the zero net charge is difficult to achieve due to the fabrication variation of stimulation drivers, the remaining charge is passively discharged. The behavior of the charge in biphasic stimulation is represented by the green line. The simplest is the behavior of the charge in the monophasic stimulation, because as only one pulse occurs, there is an increase of charge on the body, which is then passively discharged (red line). The yellow line is the charge characteristic behavior in an active method that, as can be observed, allows a fast balance of charges. Finally, it may be observed that the red and green lines do not reach the 0 value because as explain above the device fabrication creates some offsets.

Since both types of stimulation, monophasic and biphasic, have advantages and disadvantages, the choice between them depends heavily on the duration of each phase and the stimulation frequency. During the day, the moments of bite are punctual which perfectly allows the use of monophasic stimulation with passive discharge. At meal times, the stimulation frequency is greatly increased because the bite's period is around 0,8 seconds and in that case the discharge time in monophasic stimulation may be higher than between two pulses taking to an increase in residual charge (DC currents). For this to happen, a method of discharging the residual charge that may remain in the electrodes, especially at meal times, should be devised. Since the goal of stimulation in the prototype is its minimum consumption and as the stimulation frequency will never be high to accumulate a lot of residual charge, an active method is not the best option. Thus, without the need to achieve such short discharge times, it is possible to ensure the low energy consumption.

3.4 Developments in Facial and Oral Field

The evolution of techniques such as deep brain stimulation, peripheral nerve stimulation and, more recently, motor cortex stimulation have allowed new developments in the treatment of head and face pain. There are numerous pathologic conditions which produce

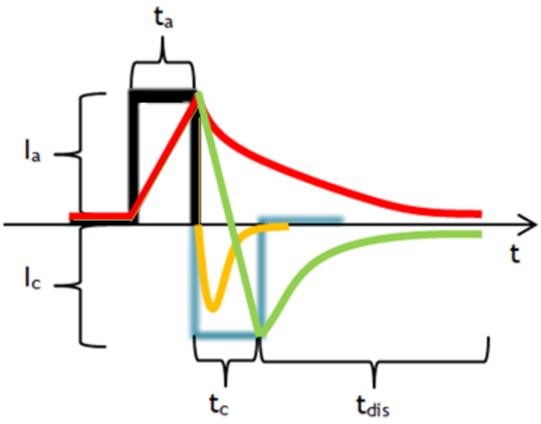

Figure 3.26: Scheme of the different examples of stimulation: monophasic (black line) and biphasic (blue line); red line represents the charge behavior in monophasic stimulation; green line the charge behavior in biphasic stimulation; yellow line the charge behavior in an active method.

craniofacial pain including trigeminal neuropathic pain (TNP), trigeminal deafferentation pain (TDP), postherpic neuralgia (PHN), and postrstroke pain. The causes of these pathologies can be in the neurovascular compression of trigeminal nerve, demyelination, facial trauma, oral surgeries, stroke, etc. Medications commonly used for the treatment of neuropathic pain are often ineffective under conditions of trigeminal nerve injury. Some of the most recent procedures for face pain treatment are portrayed in [58]. Peripheral nerve stimulation and subcutaneous stimulation of the occipital nerves have been proven to be effective for the treatment of a variety of pain conditions. Stimulation of peripheral branches (supraorbital and infraorbital nerves) of the trigeminal nerve has shown promise in the management of patients with TNP and PHN. The procedure includes insertion of standard percutaneous quadripolar electrodes just above or below the orbital edge for stimulation of the supraorbital nerve or infraorbital nerve, respectively. It is also possible to use temporary electrodes which are removed only when the treatment is finished. Motor cortex stimulation represents one of the most promising techniques available for the treatment of intractable neuropathic pain. Recently, a new procedure has been described for the treatment of intractable cluster headache (a series of relatively short but extremely painful headaches) through stimulation of the posterior hypothalamus with a hypothalamic "pacemaker".

At the dental medicine level there is still a long way to go in the area of Smart Implants. Bite force measurement techniques have been improved since *Helkimo*, in the 70s, to the present [23, 28]. Additionally, with increasing knowledge of the physiology and dental anatomy, the number of studies on the mechanoreceptors properties in teeth have also increased [26], along with test prototypes of nerve stimulation in the maxillofacial area and consequent patient behavior [59]. In prostheses there is currently an orthodontic bracket with an integrated microelectronic chip equipped with stress sensors, allowing quantitative determination and system monitoring of the 3D forces applied on the bracket [60] and a low-power miniaturized autonomous data logger capable of measuring, compensating and processing 18 different voltages simultaneously, implemented in a complementary metal oxide semiconductor (CMOS) technology [61]. With regard to neural stimulation, there are still few examples, highlighting a technology for the treatment of Xerostomia[5] through electrostimulation. The electrodes are located on the third molar area mucosa to enable stimulation of the lingual nerve and containing also a remote control that allows the patient to communicate with the device by infrared light transmission, Figure 3.27 [16].

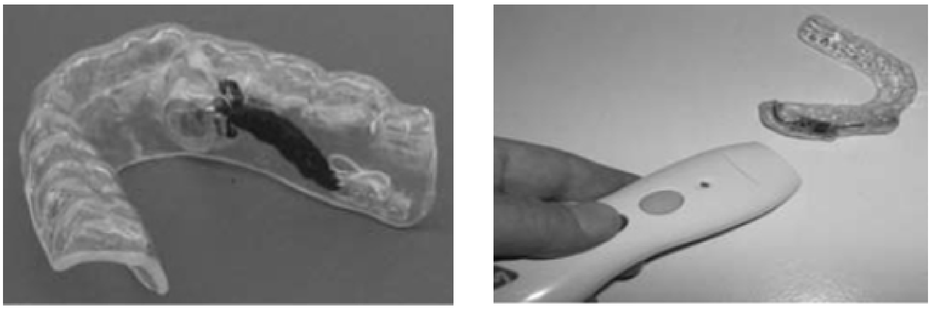

(a) *Saliwell*, electro-stimulator with the electronic system in a plastic splint.

(b) Electro-stimulator with a remote control.

Figure 3.27: Developments in Facial and Oral Field [16].

3.5 Conclusion

A review of the state of art medical devices was presented, discussing future technologies that will be on the rise. Overall, the biggest challenges in medical devices are in low power consumption and miniaturization, offering greater operating efficiency, with a higher speed of data processing power and faster wireless communication. The in-body medical devices (implantables, ingestibles and injectables) assume concerns related to powering, safety, operating frequency and antenna design. With the introduction of microsystems new challenges regarding energy transferring and harvesting methods using batteries with more energy density, acoustic waves, RF and inductive power transfer. Currently, neural stimulation have gained greater importance, using electrical, magnetic, optical and acoustic stimuli to artificially recruit neurons, providing great benefits in the treatment of neurological diseases or the restoration of sensitivity and movement. Concerning the dentistry domain, only a couple of stimulation devices were developed until now and to the best of our knowledge no such a device as a stimulator to restore dental sensitivity of people who lost their teeth was ever developed.

[5]Xerostomia – feeling of dry mouth as a result from absent or reduced saliva.

Chapter 4

Design and Implementation of Prototype Device

The present work aims at developing a smart overdenture or bridge intended to restore the broken somatosensory activity during a bite moment. The prototype to be developed is meant to detect different values of pressure exerted on the implant and to convert them into proportional levels of current that ultimately enable stimulation of the trigeminal nerve branches. For such, two different approaches were followed: one trying a different and innovative approach through the use of a Field Programmable Analog Array (FPAA), with configurable analog modules allowing to test different simulations for a proof-of-concept of this prototype; and the other through discrete components, approaching as closely as possible the future of the prototype to integrate into a SoC. However, due to problems in the execution of the first approach, the developed prototype at the end of this dissertation follows a discrete method and its architecture is presented in the block diagram shown in Figure 4.1.

This prototype comprises two modules. The first module represents the generation, processing and transmission of information. Thus, the force sensor detects the occurrence of a bite due to an increase of the exerted pressure and converts it into electrical information. The pre-amplifier is used as a signal conditioning circuit between the force sensor and the data acquisition system. The ADC quantifies this information into four levels – no pressure, low pressure, medium pressure, and high pressure. The ADC is followed by a modulator that formats this information to be transmitted to the second module. Ideally, the piezoelectric sensor and the first module will be placed inside a tooth implant or in an overdenture/bridge.

The second module performs the reception and processing of the transmitted information and provides the nerve stimulation. It is composed by a demodulation interface for data communication with the first module and a DAC which will convert the four digitized levels into the analogue current values, which will then be applied to the nerve stimulation electrodes. The second module will be implanted close to branches of the trigeminal nerve.

The communication between the two modules is meant to be wireless. However, since this work is focused on the bite pressure detection, processing, digitization, and nerve stimulation functionalities, a direct communication between the two modules is assumed now. Nevertheless, the transmitted information is presented in a serial format as it will be necessary in case the wireless transmission is included.

In the future, this prototype is meant to be realized as a system-on-chip ASIC with proper dimensions for an implantable device, the design of the different electronic circuits will be made in order to be as much as suitable for a system on a chip design, allowing simplicity, customization and low power consumption. Thus, the adopt approach aims in first place to realize a functional prototype to be used as proof of concept device and was then made with discrete components in a bread board and after woods in a single printed circuit board (PCB).

Chapter 4 is divided into different subchapters that correspond to the different blocks of Figure 4.1 together with a discussion to substantiate the approaches used.

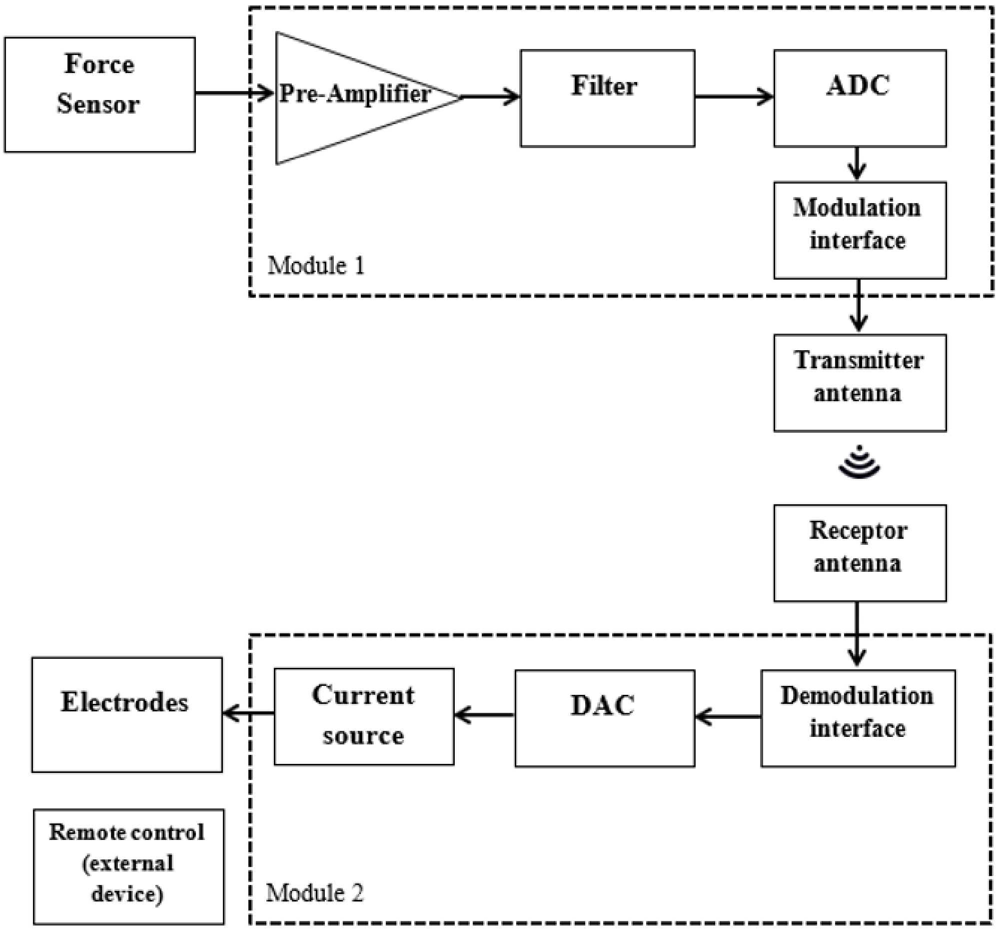

Figure 4.1: Block diagram of two different modules of the prototype. Module 1 – transmitter; Module 2 – receiver.

4.1 Field Programmable Analog Array Approach

As presented at the beginning of this chapter, this is a new method, allowing to simulate different approaches in software environment, for the proposed goal of convert different force levels into proportional electric current.

For such purpose the device used is the *OTC24000*, by *Okika Technologies*, an analog signal processor, ideally suited to signal conditioning, filtering, gain, rectification, etc. The device also accommodates nonlinear functions such as sensor response linearization and arbitrary waveform synthesis. The *OTC24000* device consists of a 2x2 matrix of fully configurable analog blocks, surrounded by programmable interconnect resources and analog input/output cells with active elements (Figure 4.2) [62].

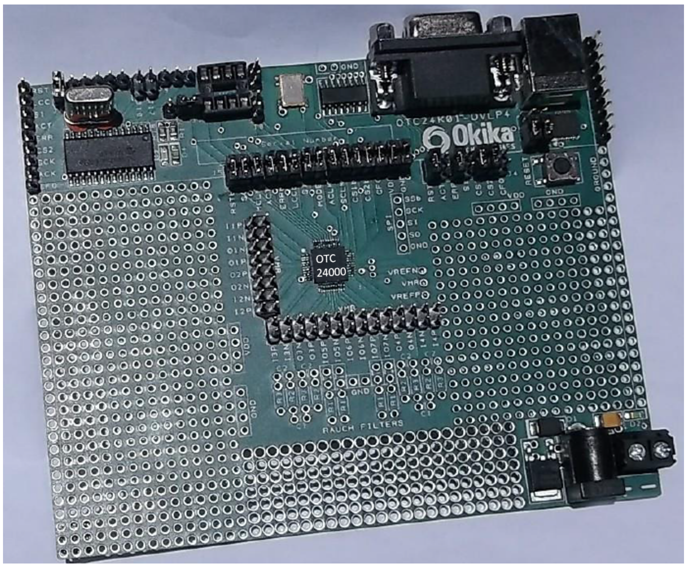

Figure 4.2: Board with *OTC24000* device in center and programmable interconnects resources and analog input/output cells around.

To implement and test circuit designs in the *OTC24000*, the *Dynamx Design Lab* Software, a high-level block diagram based circuit design entry and simulation tool, is available.

Figure 4.3 presents the dynamic scheme that conclude the operation process of this approach. Figure 4.3 (a) agrees to the environment of the *Dynamx Design Lab* Software, allowing to build analog functions through blocks and interconnect them. These analogue functions have certain specifications that can be changed so that they are configured according to the final goal of the circuit to be built (e.g: filter corner frequency) - Figure 4.3 (b). When the entire block diagram is designed and configured, it is possible to simulate the output of the circuit, as well as the input/output of each independent block (Figure 4.3 (c)). When the simulations are in accordance with the intended purpose, it connects the board to the software, programming the block diagram in the *OTC24000*, transposing to reality what was simulated (Figure 4.3 (d)).

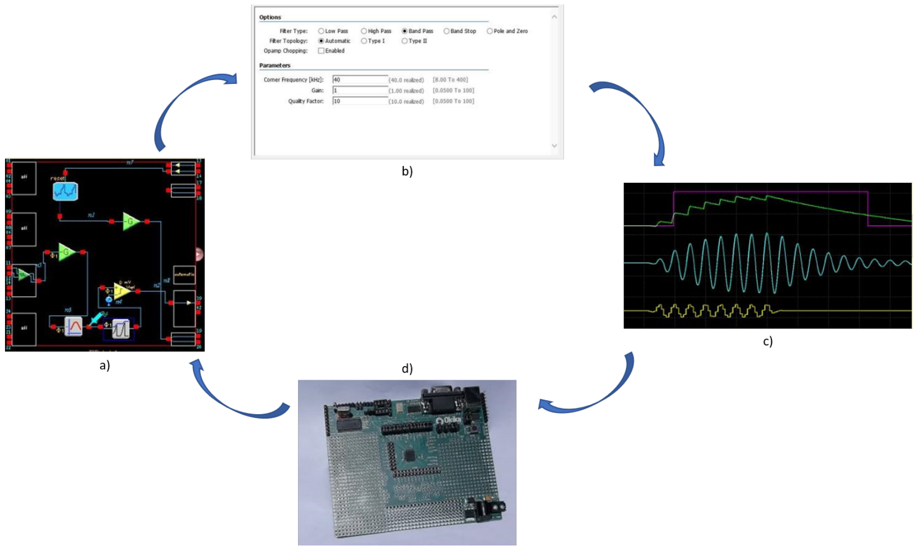

Figure 4.3: Representation of the dynamic between different steps in the field programmable analog array approach.

The use of the programmable board has the purpose of being able to simulate different blocks, adjusting the parameters of the different functions, in order to obtain the best possible result. To convert the signal of the sensor that registers the applied force at different levels of electric current, according to a varied list of blocks available in the software, it was considered that the three most viable options would be the use of a comparator circuit, a delta-sigma circuit or an ADC circuit. In all three cases a gain block is used to amplify the input signal and a signal conditioning filter. One of the disadvantages seen in the software is that it has a limit of five blocks per chip, not allowing the building of very complex circuits on a single chip (for this reason, the comparator circuit does not allow the gain block internally to exceed the five blocks, forcing it to place it outside the chip at the input).

In the comparator circuit (Figure 4.4) the signal to be simulated is routed through a bypass input, amplified, filtered, and then passed by an adjustable positive peak detector. This block output will rise toward a positive peak of the input and decay back down. Thereafter, the peak voltage value is compared to three different reference voltage values corresponding to three comparators. The output of each comparator, at the output of the chip, corresponds to a digital level that can later be entered into a DAC circuit (identical to the DAC circuit designed to the discrete method, described later in this chapter) built into the board. The advantage of this approach in the future is its simplicity, in addition to being the one that most resembles the discrete method.

In the delta-sigma circuit (Figure 4.5) the signal to be simulated is routed through a bypass input, amplified and filtered. Then, this signal enters in a delta-sigma block whose output will be a set of pulses whose density is higher or lower, depending on the voltage value of the signal being higher or lower also (bitstream). By idealizing a future

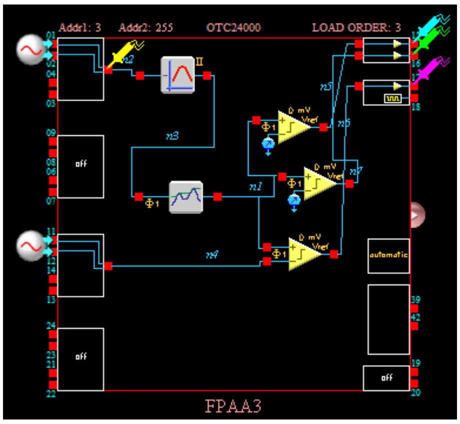

Figure 4.4: Software environment of comparator circuit approach.

application, this set of pulses can be transmitted to a second module and converted, again, into an analog signal, equal to the input signal, through a filter. To convert this analog signal to different levels of electric current, one can proceed with the previous approach with the three comparators. The advantage of this approach is the conversion into serial pulse density, facilitating wireless data transmission between modules in the future.

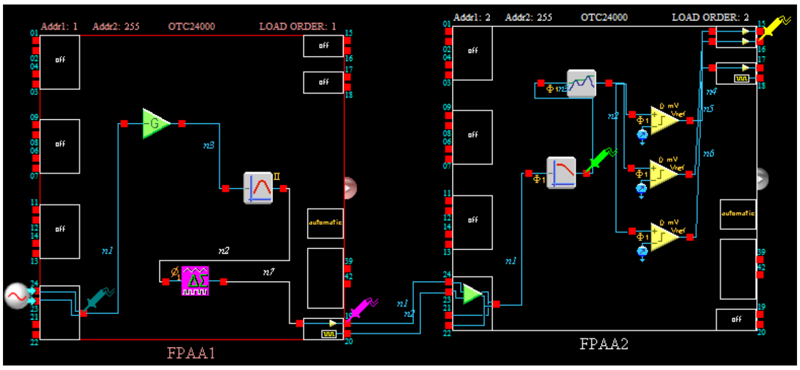

Figure 4.5: Software environment of sigma-delta circuit approach.

Finally, in the ADC circuit (Figure 4.6) the signal to be simulated is routed through a bypass input, amplified, filtered and then this signal enters in an ADC block. This block produces a serial 8-bit digital output word, beginning with the most significant bit, on the Data output branch and the other output branch, Sync, defines when the 8-bit digital word is launched (Sync = 1). In order for this digital signal to be converted into a electrical current level, there must be an external interface to the chip output that reads only the first two most significant bits, when the sync passes from 0 to 1, obtaining four different logic levels (00, 01, 10, 11), resembling the final goal of the prototype to quantify four stages of applied force. The peak detector allows only ADC bits to be collected when detecting a significant voltage signal on the same interface, so that the ADC is not constantly recording bits, which leads to high power consumption. The advantage of this approach is that the ADC directly converts the analog signal into a digital word in series, not requiring a data conversion process.

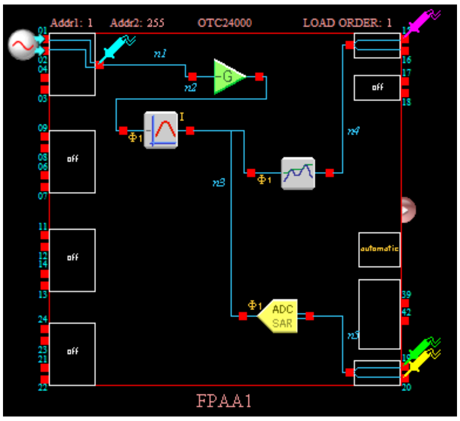

Figure 4.6: Software environment of ADC circuit approach.

4.2 Discrete Approach

4.2.1 Force Sensor

The force (or pressure) detection unit comprises sensors that convert the displacement caused by the applied force into electrical signals. This conversion is possible due to the elastic properties of the material where the force is exerted [37]. There are three different types of pressure sensors that, in a first instance, could be used here: capacitive sensors, piezoresistive sensors and piezoelectric sensors.

4.2.1.1 Capacitive Sensors

The fundamental principle of operation of these sensors is the variation of capacitance of a parallel plate capacitor given by:

$$C = \varepsilon \frac{A}{d}, \tag{4.1}$$

where ε is the dielectric constant of the medium between the parallel plates, d is the separation distance between the plates, and A is the cross-sectional area of the plates. Equation (4.1) gives us the variation of capacitance when one of the plates moves with respect to the other. The capacitance value has a hyperbolic capacitance-displacement characteristic. However, when the plate separation is maintained constant and a laterally displacement occurs the capacitance-displacement characteristic can be linear. The capacitance measurement circuit to be used can take the form of a Wheatsone bridge[5] [37]. This type of sensors has characteristics such as high sensitivity to absolute pressure;

[5]A Wheatstone bridge is an electrical circuit with two branches and usually four resistances in which an output voltage between a pair of opposite contacts is proportional to the difference of in-plane stress components.

however the hysteresis of the dielectric is a disadvantage, as well as the non-linear response to lower pressures due to residual stress [63].

Since the aim is to record changes of a base pressure value (without a bite) and not an absolute value of the exerted pressure and, in addition, the prototype can record lower pressure values characteristic of small occlusal force values, the choice of that sensor was excluded.

4.2.1.2 Piezoresistive Sensors

The piezoresistive effect describes the variation of resistivity of a semiconductor/metal with applied mechanical stress. In other words, corresponds to the amount of work needed to move a unit positive charge from a reference point to a specific point:

$$R = \rho \frac{l}{A}, \tag{4.2}$$

where ρ is the piezoresistivity coefficient, l is the conductor length and A is the cross-sectional area of the current flow. When the material suffers a traction or compression between the elastic limits the resistance values vary. The linear change of a resistance is traditionally measured by using the Wheatstone bridge circuit, the sensitivity of which depends on the excitation voltage or current [64]. This type of sensors has an anisotropic characteristic, since it implies the consideration of different properties of the material in different directions [65].

The configuration of a piezoresistive sensor is characterized by an output that allows recording absolute pressure values. However, as mentioned earlier, it is not the purpose of this prototype to record absolute pressure values. On the other hand, the piezoresistive sensors require a permanent consumption to operate, which implies higher power consumption for the prototype. For these reasons, the use of a piezoresistive sensor was also discarded.

4.2.1.3 Piezoelectric Sensors

The piezoelectricity is the electric charge that accumulates in certain solid materials in response to applied mechanical stress. A piezoelectric sensor is a device that responds with the piezoelectric effect allowing to measure changes in different variables, namely pressure or force, converting them to an electrical charge. It is typically not suited for static pressure measurements but to dynamic measurements. When a force is applied to the sensor, the material generates an electrostatic charge proportional to the applied force. A piezoelectric transducer has very high DC output impedance, to maximize the generated power, and can be modelled as a proportional voltage source, where voltage V is directly proportional to the applied force, and with an output impedance modelled with the equivalent circuit shown in Figure 4.7 (b). This effect is reversible and so a piezoelectric material that is exposed to an electric field will change its physical size. Actually, there are three basic classes of piezoelectric materials: natural, such as quartz crystals; ceramics, such as zirconate-titanate (PZT); polymers, such as polyvinylidene fluoride (PVDF). The piezoelectric sensors have outstanding advantages, such as the extremely wide dynamic range, excellent linearity, high sensitivity, and compact volume.

In the last years a new technology based on piezoelectric sensors has emerged, namely in integrated circuit domains, the Piezoelectric oxide semiconductor field effect transistor (POSFET). Here, the piezoelectric sensor is placed on the gate of a field-effect transistor and the channel charge and current are controlled by the gate voltage or by stress exerted on the gate [66]. The advantage is that the gate is very compressible and with the sensor directly embedded in the FET a resistor-capacitor circuit is not necessary, reducing the number of wires in the sensitive circuit. Furthermore, this approach is highly sensitive to pressures exerted with a high signal-to-noise ratio. The great applicability of these sensors is in touch sensing systems like tactile sensing (e-skin) or flexible POSFET chips [67].

In a first instance, this latter approach would have greater advantages for the applicability of the prototype to be developed, comparing with a piezoelectric sensor implemented in a circuit like that of Figure 4.7 (b). However, the POSFET fabrication technology is different from that of general purpose ICs technologies being used, making it difficult to integrate the sensor and the respective signal conditioning circuit in the same monolithic substrate. On the other hand, the POSFET is an active device that needs to be fed by an external source.

Therefore, the solution adopted for the prototype to be developed will resort to a passive piezoelectric element, which does not require an external supplying source, in spite of not having a high sensitivity because the goal of the work is only to record four levels of force. With one piezoelectric element there is greater implementation freedom in the dental implant, being it possible in the future to implement more than one device, to register more than one point of force.

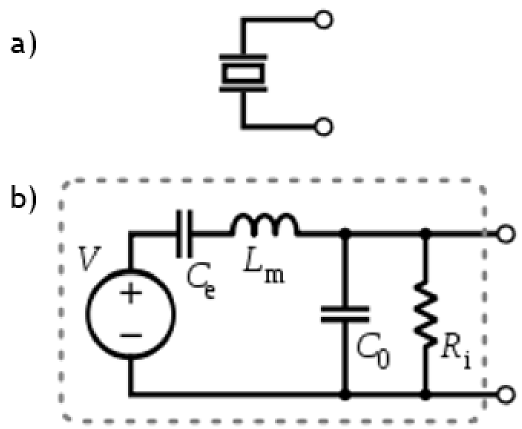

Figure 4.7: Schematic representation of the symbol (a) and the equivalent electronic circuit (b) of a piezoelectric sensor [17].

Regarding the type of material to be used in the piezoelectric sensor, is the most currently used today recur to ceramic or polymeric materials. The former ones are more advantageous for detecting higher values of pressure, but the latter are easier to implement.

According to the values suggested in the literature and discussed previously in Chapter 2, the maximum value recorded for implant-supported mandibular overdentures is approximately 350 N. For this reason, choosing the ideal sensor for bite force recording should ensure that the force range is higher than 350 N value.

In the present work the selected piezoelectric sensor has a ceramic cross-section, *PSt 150 / HPSt 150*, Figure 4.8. The sensor has a cubic shape, with 5×5 mm^2 ceramic cross-section, works for high axial resonant frequencies, and is suitable for d31 and d33 actions (the applied force is in the vertical direction, z-axis, from top to bottom, i.e., d33 action).

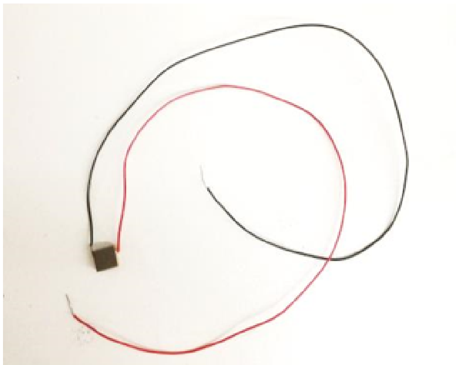

Figure 4.8: Representation of the piezoelectric sensor chosen for the prototype.

4.2.2 Signal Acquisition and Processing

A piezoelectric element produces nanocoulombs (nC) of charge in one working cycle and so a charge amplifier or a voltage amplifier is often used as a preliminary signal conditioning circuit placed between the piezoelectric element and the data acquisition system (readout device). The piezoelectric sensors usually present a high impedance and charge type output that requires a charge amplifier or an external impedance for charge-to-voltage conversion. The pre-amplifier allows mainly to transform the high impedance and charge output characteristic of these sensors into a lower impedance voltage output.

The choice between a charge amplifier and a voltage amplifier is usually made according to the distance between the sensor and the amplifier. When the distance is long one should opt for a charge amplifier, while for shorter distances one should opt for a voltage amplifier. In some cases where the distance is very short, both amplifiers are suitable [18]. In the case of the prototype to be developed, the distance is not a justification for the choice between the different amplifiers, since the distance between the piezoelectric element and the amplifier is short, never exceeding the diameter of the implant, since both will be inserted in the implant.

4.2.2.1 Voltage Amplifier

A voltage amplifier with high input impedance can be used as a signal conditioning circuit for a piezoelectric sensor placed at a short distance from the amplifier. When this amplifier is used the output of the sensor is in an open-circuit state. The link between the piezoelectric element and the voltage amplifier is expressed according to the operational amplifier's non-inverting configuration circuit. In the amplifying circuit shown in Figure 4.9 one can see: C_c – cable capacitance; C_e – capacitance of the sensor element; C_i – input capacitance of the operational amplifier; U_i - input voltage of the voltage amplifier; U_o – output voltage of the voltage amplifier; R_d – insulation resistance of the sensor; R_i – input resistance of the amplifier; q – charge source produced by the sensor element; R_f – feedback resistor; and A_u – gain of the amplifier.

The extremely high input impedance of the ideal operational amplifier allows its input current to be approximately zero, being thus the charges generated by the piezoelectric element kept in capacitors C_c and C_e without any loss. This is the reason why the piezoelectric element with a voltage amplifier can be approximately considered as an open circuit. The parallel of the insulation resistance of the sensor element, R_d, with the input

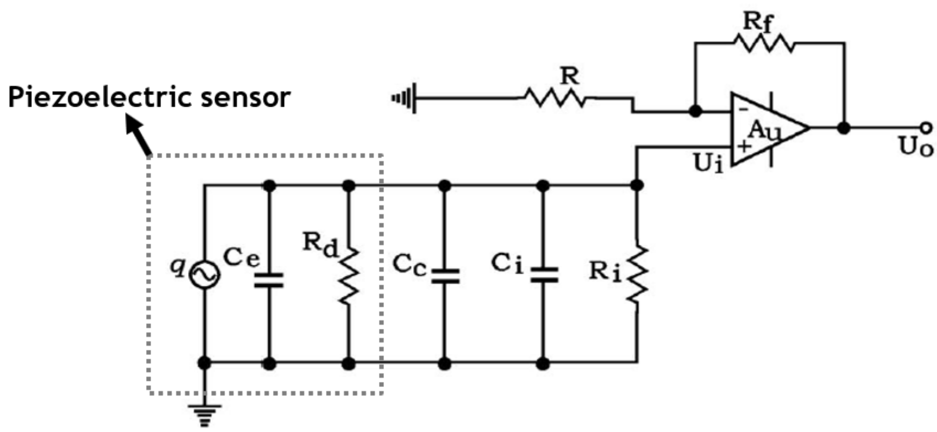

Figure 4.9: The operational amplifier's non-inverting equivalent circuit of a piezoelectric element linked to the voltage amplifier (adapted from [18]).

resistance of the amplifier, R_i, is frequently very high (>1012 Ω) and can be neglected. Therefore, the voltage amplifier output is given by:

$$U_o \approx \frac{R_f}{R} \frac{q}{C_e + C_c + C_i}, \tag{4.3}$$

once the sum of C_i and C_c is much smaller than C_e, since the length of the cable is very short, the simplified output voltage becomes approximately:

$$U_o = \frac{qR_f}{C_e R}, \tag{4.4}$$

The previous deduction allows to conclude that a stable and short interconnection ensures reduced C_c values in order to obtain a good performance of the sensor [18]. Furthermore, the feedback occurs apart from the piezoelectric element contributing to circuit stability. Although these features are advantageous in a circuit with a voltage amplifier, the output of this circuit has a non-linear response.

4.2.2.2 Charge Amplifier

The charge amplifier is the most conventionally used circuit to read the piezoelectric sensor output, since the piezoelectric sensor generates charge under the effect of stress. Contrary to the voltage amplifier, the output of the piezoelectric sensor is in a short-circuit state if a charge amplifier is used. The equivalent circuit of the measurement system when a charge amplifier is connected with a piezoelectric element is represented in Figure 4.10. The circuit elements in Figure 4.10 are the same as those in Figure 4.9, adding the C_f – feedback capacitance. In most cases, the insulation impedance of the piezoelectric sensor

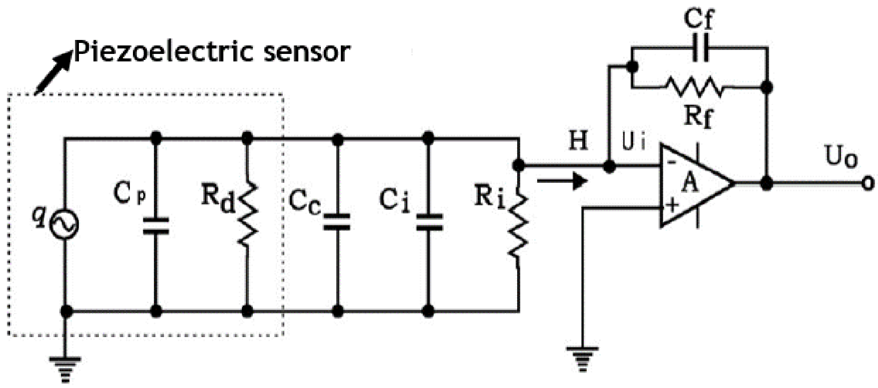

Figure 4.10: The operational amplifier's inverting equivalent circuit of a piezoelectric element linked to the charge amplifier (adapted from [18]).

and the input resistance of the amplifier can be neglected as explained above. When R_d and R_i are ignored, the output becomes:

$$U_o = -\frac{q}{(1+\frac{1}{A})C_f + \frac{C_p+C_c+C_i}{A}}, \tag{4.5}$$

The Equation (4.5) can be simplified because the values of the open-loop gain A and the feedback resistor R_f show very high values and the feedback capacitor C_f value is much higher than $(C_p+C_c+C_i)/A$, leading to:

$$U_o \approx -\frac{q}{C_f}. \tag{4.6}$$

From Equation (4.6) it can be concluded that the output of the amplifier depends mainly on the feedback capacitance and the induced charges. Comparing with the voltage amplifier, the charge amplifier exhibits a greater immunity to disturbances. In addition, the H point in Figure 4.10 works as a virtual ground and therefore, ideally, allows no current in C_p, R_d, C_c, C_i and R_i, eliminating the existence of parasitic currents at the output of the amplifier. However, the cable length should be as short as possible to not affect C_f to $(C_p+C_c+C_i)/A$ ratio.

For these reasons and combining the linearity characteristics of this circuit output, the charge amplifier presents greater advantages as a pre-amplifier for the prototype to be developed.

The charge-mode amplifier will balance the charge injected at the negative input by charging the feedback capacitor C_f. The resistor R_f bleeds the charge of capacitor C_f at a low rate to prevent the amplifier from drifting into saturation. Resistor R_f also provides a DC bias path for the negative input. The value of R_f and C_f set the low cut-off frequency of the amplifier. The action of the amplifier maintains 0 V at its input terminals, so that the parasitic capacitance associated with the interface cabling is not a problem. Resistor R_i provides protection against electrostatic discharge. Resistor R_i and capacitors C_e and C_c combine to produce high frequency roll off [19].

The dimensioning of the values C_f, R_f and R_i allows the adjustment of the frequency response of the sensor, according to Figure 4.11. Analyzing its curve behavior is possible to conclude that the charge amplifier behaves like a bandpass second order filter, eliminating low and high frequencies. The non-inverting input can be biased at 1/2 V_{DD}. The output

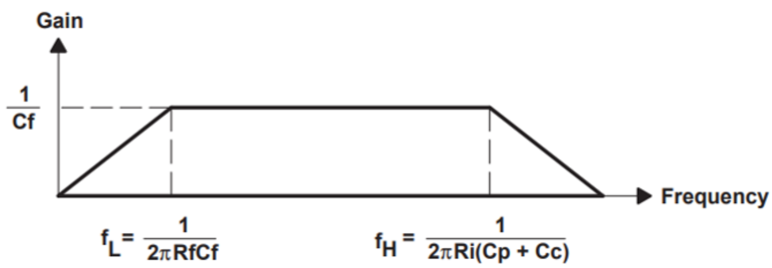

Figure 4.11: Frequency response by a charge mode amplifier circuit [19].

will swing around this DC level and therefore the result of Equation (4.6) it will be added 1/2 V_{DD} V [19].

The operational amplifier (U1A) used in the charge amplifier prototype circuit is *LM358*, powered at 5 V, as presented in Figure 4.12. The power supply voltage value is high, and the reason resides in the fact, since this is in first place a proof-of-concept prototype, priority was given to the functional aspects avoiding as much as possible constrains imposed by the available book-of-the-shelf components. In a future prototype, smaller voltages should be used to allow the modules to be fed from low-energy batteries.

To obtain the most suitable piezoelectric signal response, namely a rapid discharge of the piezoelectric sensor after peak of force is recorded, the following values were set: $R_i = 1\ k\Omega$, $R_f = 1\ M\Omega$ and $C_f = 10$ nF. A rapid discharge allows to adapt the circuit time constant to a fast mastication, where repeated peaks of force occur, preventing an accumulation of charge. With these values, the gain obtained is 1x10^8 dB and $f_L = 15,9$ Hz and $f_H = 1,4$ kHz. The capacitance of the piezoelectric sensor was found in datasheet ($C_p = 110$ nC) and the interface cable capacitance is a reference value used in the literature ($C_c = 12$ pC).

Figure 4.12 presents a second operational amplifier (U2A), also *LM358*, used to adjust the gain for the output signal. The gain is calculated by the resistors in the negative input as in Equation (4.7):

$$G = 1 + \frac{R_5}{R_4}. \tag{4.7}$$

So, according to the adjusted values for R_4 and R_5, the gain for the output signal is approximately unitary.

As noted by Figure 4.12, the reference value used is not 1/2 of V_{DD} as previously suggested, to reduce the power consumption.

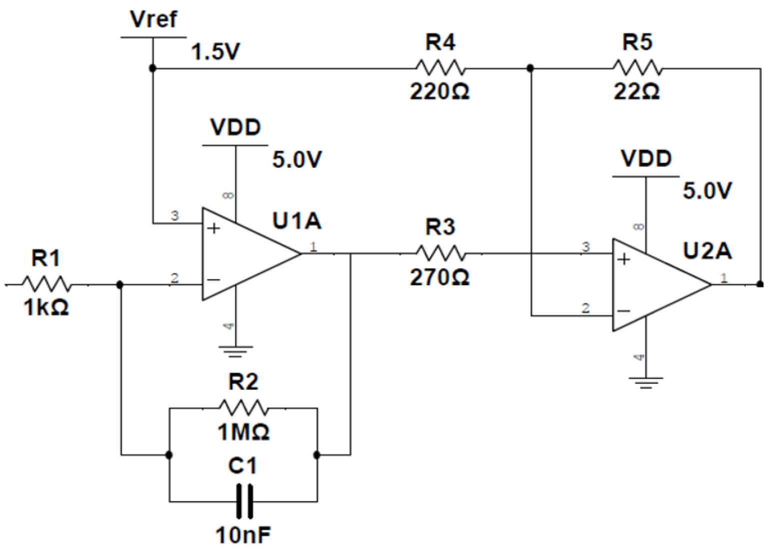

Figure 4.12: Architecture of the prototype charge and gain amplifier circuit.

4.2.3 Analogue-to-Digital Converter

The aim of the developed prototype is to detect four different levels of force (no force, low, medium and high force). For this reason, the ADC circuit produces an output signal based in these four levels through the combination of three parallel digital values between the following combinations:

$$\begin{bmatrix}0\\0\\0\end{bmatrix}, \begin{bmatrix}0\\0\\1\end{bmatrix}, \begin{bmatrix}0\\1\\1\end{bmatrix}, \begin{bmatrix}1\\1\\1\end{bmatrix}.$$

The first combination is given when no force is sensed by the sensor; the second combination corresponds to a low force level; in the third combination, a medium force level is recorded; the latter combination corresponds to a high force value. This codification is denominated thermometer encoding. This name derives from the similarity with the thermometer scale, in which the mercury column always rises to the appropriate temperature and no mercury is present above that temperature.

The architecture of the designed ADC is presented in Figure 4.13. The schematic was optimized and simplified after observing the outputs of the four levels. That is, initially feedback circuits were included between the drains and gates of transistors Q1, Q2, and Q3 in order to create an hysteresis effect so that there were no oscillations in the bit values and, therefore, the three outputs could always assume well defined states of 0 or 1. It was verified afterwards that correct operation could be obtained even without these feedback circuits. It was decided to use an ADC with this configuration, since it is a conversion of only three bits, so using a commercial converter would imply a larger number of bits, unnecessarily. In addition, it is a closer application of the full custom implementation idealized for the future of the prototype.

The type of A/D conversion performed by this circuit is inherently of a *flash* converter like type. Although this type of ADC is in general expensive in certain applications, that is not the case since the data processing is simple. There are other alternative approaches, namely the integral pulse frequency modulation (IPFM), to create a signal to be transmitted for the nerve stimulation. In an IPFM model an impulse is generated when the integral of a modulating signal reaches a threshold. Each time the threshold is reached, a spike is generated, and the integral is reset. The IPFM allows studying properties of biomedical signals, such as nerve spike trains, modelling the information coding and signal transmission through nervous fibers [68, 69]. However, this approach requires eventually the use of a capacitor in the integrator, which would force it to have high dimensions and the scale of use of the prototype is extremely reduced. On the other hand, the impulse stimulus amplitude would have to be defined after a pulse density to amplitude converter circuit, which is not trivial.

The transistors used in the ADC in Figure 4.13 are metal-oxide-semiconductor field effect-transistors (MOSFET). They have an insulated gate, whose voltage determines the conductivity of the device. This ability to change conductivity with the amount of applied voltage can be used for amplifying or switching electronic signals. Depending on the gate-source voltage (V_{GS}) and the drain-source voltage (V_{DS}) of the transistor, it may be in the triode region and behave as a switch Equation (4.8) or in the saturation region Equation (4.9).

$$V_{GS} - V_t \geq V_{DS}, \tag{4.8}$$

$$V_{GS} - V_t \leq V_{DS}. \tag{4.9}$$

The references of the n and p channel transistors used here are *ZVN2110A* and *ZVP2110A*, respectively. The V_t of both is 0,8 V, according to datasheet.

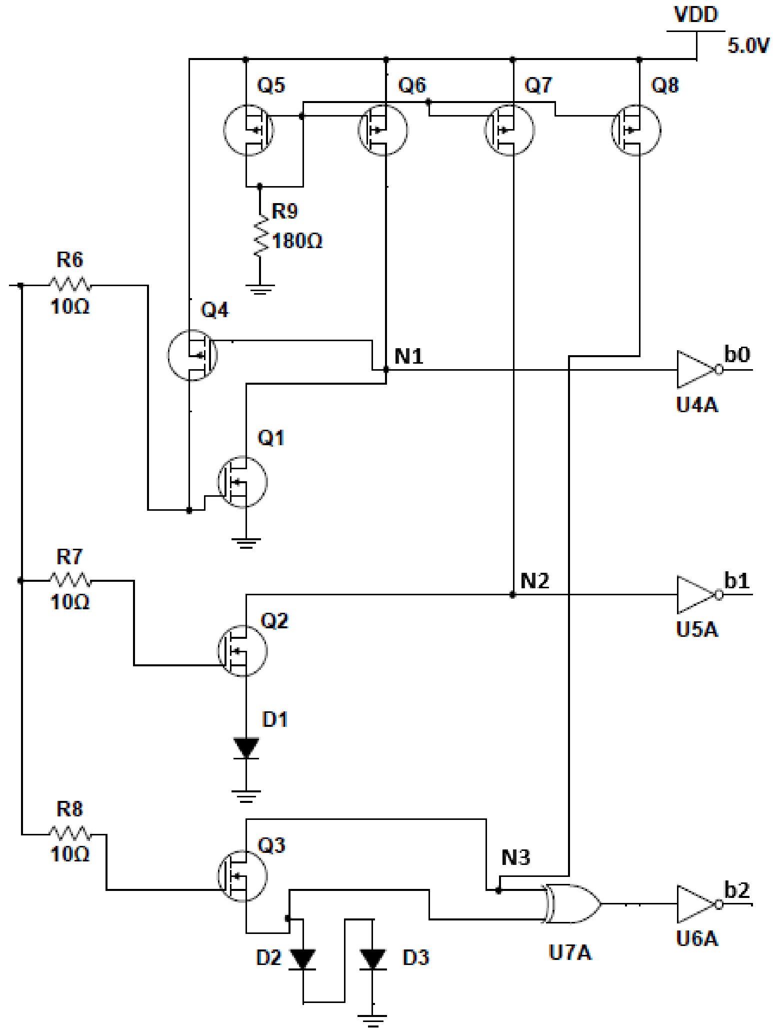

Figure 4.13: Architecture of the ADC circuit for the prototype.

Transistors Q5, Q6, Q7 and Q8 are all pMOS and perform a current source/mirror circuit that maintains the current of each bit output constant, regardless of loading. Since the goal is to build a circuit with low power consumption, the current must also be low – in this case a value in the order of mAs was adopted, somehow imposed by the transistors being used, but smaller values should be adopted in a full custom design. For this reason, resistor R9 is designed to be 180 Ω and the current in transistor Q5 is:

$$I = \frac{V}{R} = \frac{5 - 0,8}{180} = 23\ mA, \tag{4.10}$$

where 0,8 is the transistor threshold voltage and V is the voltage drop in Q5. So, the currents in the drains of Q6, Q7 and Q8 are also 23 mA.

For the detection of the second force level (b0) the attention must be focused on the first branch, namely on transistor Q1. If there is no force record, the voltage value at the gate node of Q1 is 0 and the drain of Q6 is 0 V as well. In this way, both Q1 and Q6 do not conduct, forcing the voltage value at N1 to equal V_{DD}, 5 V. U4A corresponds to an inverter, causing the value of its output to be the inverse of its input. Since the voltage at the input of U4A is 5 V, the output value is 0, imposing a 0 value for the first bit. As soon as there is a force on the sensor, V_{GS} of Q1 increases, and, when it exceeds its V_t, the transistors conduct and the voltage in N1 tends to decrease to 0 V. An input of 0 in the inverter is converted in an output 1 and the bit for the second force level is thus set.

The third level of force (b1) is detected by the second branch, being Q2 and diode D1 used to define the respective threshold level – the 1 to 0 shift occurs when $V_{G,Q2} > 1{,}6$ V.

As for the fourth level, b2 shifts from 1 to 0 for values $V_{G,Q3} > 2{,}4$ V. In this case, the use of U7A (XOR gate) allows the level transition to be more abrupt, so that level oscillations do not occur. This is because the signal from this branch is much more compromised by the analog component of both transistors and diodes.

The use of diodes instead of transistors is justified because the diodes impose more fixed voltages than the transistors.

At the output of U4A, U5A and U6A, the 3 bits corresponding to the recorded force levels will be displayed.

4.2.4 Data Transmission Interface

As this smart implant implies the communication between two modules placed in different places of the dental arch and head, a wireless transmission is required to avoid the need of using connection wires, which actually is not convenient at all to place them in the person's mouth. For the information to be transmitted wirelessly, it needs to be modulated. First, parallel data needs to be converted to serial before transmission and, afterwards, after its reception, it is converted again to the parallel format. This serial data must then be modulated in RF, in order to be wirelessly transmitted, from module 1 to module 2, namely by means of a binary to phase-shift keying modulation. After data transmission, the RF must then be demodulated in serial data.

4.2.4.1 Parallel to Serial Conversion

The Parallel-in Serial-out (PISO) circuit converts the three parallel bits from the ADC in a serial word. The parallel data is loaded into a register simultaneously and is then shifted out serially one bit at a time under clock control.

Other alternative approaches can be found in the literature for this conversion, namely the *Thermometer to Gray Encoders* for a flash ADC [70]. This modulation has been widely used in high-performance critical applications which persistently impose special design constraints in terms of high-frequency, low power consumption, and minimal area.

The PISO used here is based on the *SN74165* (Figure 4.14), an 8-bit serial shift registers which shifts the data in the direction of 1^{st} bit toward 8^{th} bit when clocked. Since only three bits are used (F, G and H inputs), the remaining five PISO inputs are short-circuited. Parallel-in access to each stage is made available by data inputs that are enabled by a low level at the shift/load (SH/$\overline{\text{LD}}$) input. Clocking is accomplished through a two-input positive-NOR gate, permitting one input to be used as a clock-inhibit function. Holding either of the clock inputs high inhibits clocking, and holding either clock input low with SH/$\overline{\text{LD}}$ high enables the other clock input. Clock inhibit (CLK INH) should be changed to the high level only while Clock (CLK) is high. Parallel loading is inhibited if SH/$\overline{\text{LD}}$ is high. Data at the parallel inputs are loaded directly into the register while SH/$\overline{\text{LD}}$ is low, independently of the levels of CLK and CLK INH. Data at the parallel inputs are loaded directly into the register while SH/$\overline{\text{LD}}$ is low. The behavior of the different pins is explained in the waves of Figure 4.15.

Since only when the SH/$\overline{\text{LD}}$ input goes to 0 the PISO activates the input of the bits for the serial conversion, it is interesting that this transition to 0 occurs if and only if the 1$^{\text{st}}$ bit equals 1, otherwise it is a signal that there was no detection of force in the piezoelectric. In other words, with this ADC combination the 2$^{\text{nd}}$ bit only has the value 1 if the 1$^{\text{st}}$ bit is 1 and the same case for the 3$^{\text{th}}$ bit (because this is a thermometer code). For this reason, the SH/$\overline{\text{LD}}$ pin is connected to the output of a NOT logic gate whose input is the 1$^{\text{st}}$ bit.

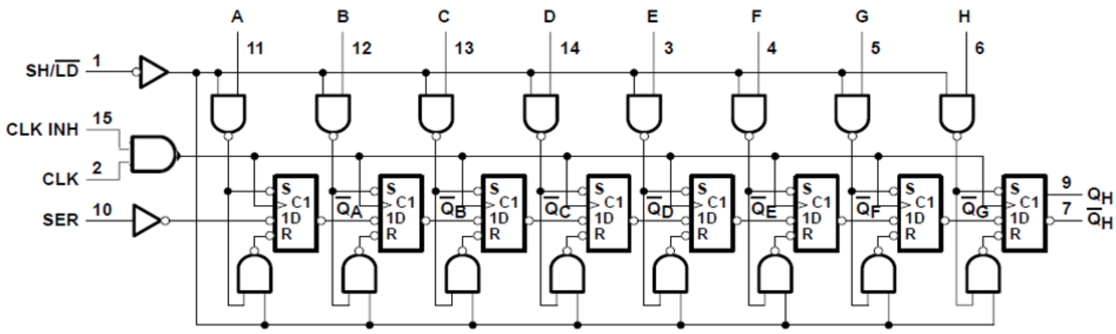

Figure 4.14: Logic diagram of the PISO used.

The CLK and CLK INH are defined by *NE555*, based clock. The CLK is defined by an astable mode of operation, where the frequency and duty cycle can be controlled independently with two external resistors and a single external capacitor; the CLK INH is defined by a mono-stable non-retriggerable mode of operation, where the timed interval is controlled by a single external resistor and a capacitor network. In future, the use of the *NE555* will not be the most suitable for clock generation because of its dimensions and the complexity of circuits it integrates, since the purpose of the prototype is to be integrated into a SoC.

The astable circuit that generates CLK is shown in the Figure 4.16. The connection between the trigger input to the threshold input causes the timer to self-trigger and run as a multi-vibrator. The capacitor C charges through R_A and R_B and then discharges

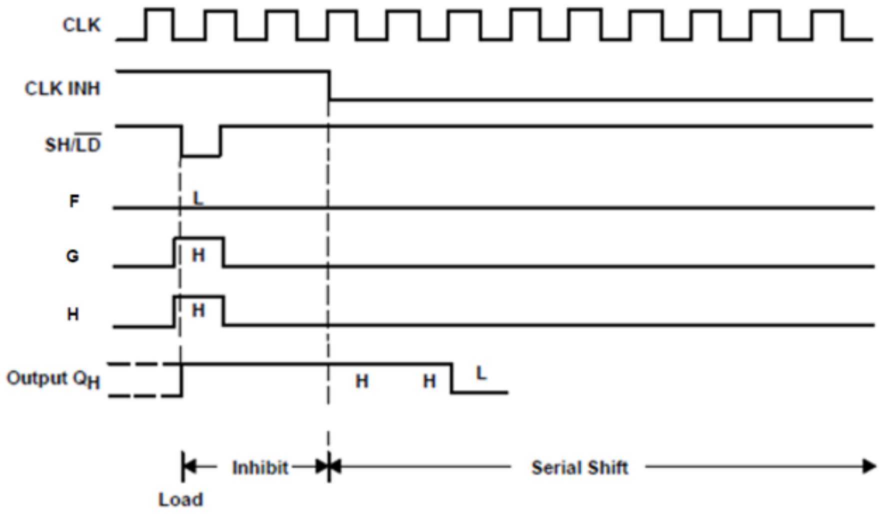

Figure 4.15: Operating sequences of the different pins in PISO.

through R_B only. Therefore, the ratio between the high clock phase and the low clock phase is given by the following equation:

$$\frac{t_L}{t_H} = \frac{R_B}{R_A + R_B}, \tag{4.11}$$

where t_L is the output low-level duration and t_H the output high-level duration. For a CLK whose phases have the same time base (ratio of t_L and t_H equal to 1), the values chosen for the resistances are $R_B = 3,3$ kΩ and $R_A = 270$ Ω. The value of capacitor C set the clock frequency value, through the following equation:

$$f = \frac{1,44}{(R_A + (2R_B))C}. \tag{4.12}$$

As the human biting frequency is relatively low, a clock frequency of 1 kHz is more than enough for the modulation of the data, and so, according to Equation (4.12), the capacitor used has a capacitance $C = 210$ nF.

CLK INH is the inhibition time before serial shift. In this way, it is important that this clock is activated when the transition of the 1^{st} bit to 1 occurs, because only in this case it is important that the serial shift happens. Thus, the time that the CLK INH is high should be slightly longer than the passage of the three bits, just to ensure that all of them are recorded by PISO. The circuit for mono-stable non-retriggerable operation which defines CLK INH is shown in the Figure 4.17. This operation allows to set a high output pulse duration, through the discharge time of a capacitor. When an input pulse occurs (in this case given by the value of the 1^{st} bit), the TRIG is started, and an output pulse is generated. The non-retriggerable mode allows that there is no other output pulse until the end of the first output discharge, even if there is another input pulse. The output

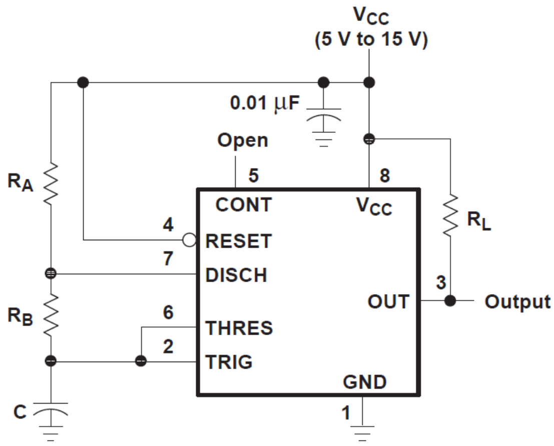

Figure 4.16: Circuit for astable operation in *NE555*. R_L is a reference value of 1 kΩ, according to datasheet.

pulse duration is approximately:

$$t = 1{,}1\, R_A C. \tag{4.13}$$

Defining a CLK INH time of 100 ms and $R_A = 10$ MΩ, the capacitance is $C = 100$ nF.

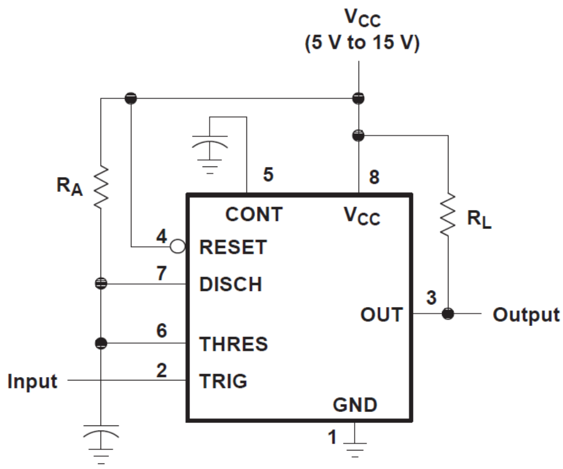

Figure 4.17: Circuit for monostable operation in NE555. R_L is a reference value of 1 kΩ,according to datasheet.

4.2.4.2 Serial to Parallel Conversion

In the reception of the second module the reverse processing must occur, that is, the received signal must be demodulated to obtain the transmitted bit stream and the serial data should be converted to the parallel format. This section describes a Serial-in Parallel-out (SIPO) circuit that converts a serial word of three bits into three parallel bits.

For the SIPO construction, we used six D flip-flops, three of them functioning as data shift that go into series and the other three functioning as latch of the shifted data

Figure 4.18. The first flip-flop receives the serial input in D_2, transmitted by the PISO, and for three clock cycles it moves the three bits in series along the three shift flip-flops through the connection of the output of the previous one with the input of the following (i.e. Q_2 for D_1, Q_1 for D_0). At the end of the three clock cycles, the bit shift ends and b0 is at Q_0, b1 at Q_1 and b2 at Q_2. The following three flip-flops work as latch, that is, they allow to receive data from the shift Q_x outputs to their internal registers, D_x', respectively, while their clock is low and, at the moment the clock is activated, throw the data out in parallel. Then, reset in the latch occurs and it is ready to receive new bits. Figure 4.19 represents the three different behaviors of clock shift, clock latch and reset

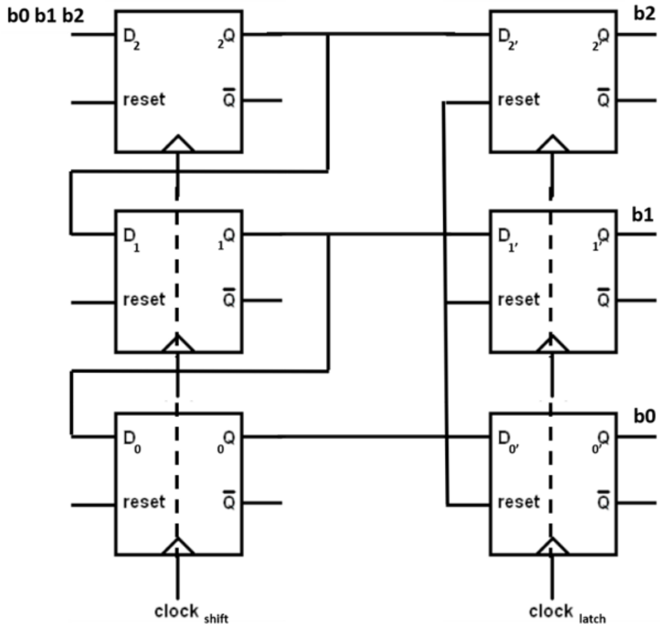

Figure 4.18: Representation of the SIPO architecture.

latch.

The shift clock has the same duration of PISO clock, i.e., a frequency of 1 kHz. Each bit is thus shifted 1 in 1 ms from the serial input to the respective flip-flop output. After 3 ms the bit shift is complete. For this reason, the shift clock follows the same operating method of PISO clock, the use of an astable *NE555*.

When the serial input arrives (black arrow), at that same time the latch clock must be low for a time greater than 3 ms to ensure that the three bits are shifted before being latched. To do this, a *NE555* monostable non-retriggerable with 4 ms ($C = 10$ nF and $R_A = 390$ kΩ), approximately, is used, which trigger is the serial input and its output is negated to allow the latch to be deactivated during arrival and displacement serial input and otherwise is always enabled.

The latch reset has the same operation of the latch clock, however with a low period superior to the low period of latch clock. This allows the output of the parallel bits of the latch before its reset (shaded area). When the latch reset returns to 1, the bits are cleared, and all latch outputs are set to 0. For this reason, a *NE555* monostable non-retriggerable with 6 ms ($C = 10$ nF and $R_A = 560$ kΩ), approximately, is used, which trigger is the serial input and its output is negated, so that there is no reset while the latch is receiving the registers internally.

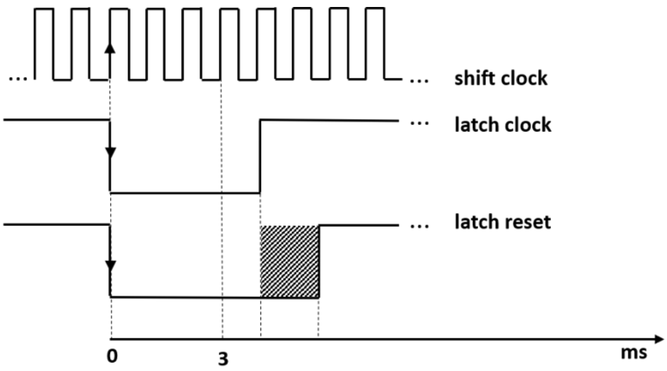

Figure 4.19: Operating sequences of the different clocks and reset in SIPO.

After the implementation of the SIPO of Figure 4.17, an identical solution was devised, however, without requiring a clock and therefore with a lower energy consumption.

The mode of operation of this new approach is shown in Figure 4.20. In this case, the SIPO is also composed of six flip-flops, each of the first three flipping each bit of the serial input to the three other flip-flops, which receive them in their internal registers and that allow the output of the 3 bits in parallel.

When the serial data appears, bit b0, corresponding to the first bit of the serial input, enters the first flip-flop and is shifted to its output in a time of 1 ms - since the clock of this flip-flop is connected to the serial input and each bit has a duration of 1 ms. This output is connected to the input of the first flip-flop of the latch, allowing the b0 to be stored internally.

The detection of b1 by the second flip-flop arises when its clock is high. To do this, the clock of this flip-flop is connected to the output of the circuit shown in Figure 4.21. This RC circuit allows that when giving a voltage pulse, the capacitor C loads according to a time interval defined by the following equation:

$$\tau = RC, \tag{4.14}$$

where τ is the time constant which corresponds to 63% of the total capacitor load. Thus, when the logic input 1 of the serial input is given, the output of the XNOR logic port is 0 until the RC circuit exceeds 50% of the load of its capacitor and then returns to 1. Since the times used are so small, we can consider $\Delta T = \tau$, as the time whose output remains at 0. In the case of the detection of bit 1 it is convenient that $\Delta T = 1$ ms, so that the second flip-flop clock active after the duration of the passage of the first bit, thus allowing extraction of bit b1.

Consequently, the clock of the third flip-flop must be low for 2ΔT, so that after 2 ms, the bit in the input of the flip-flop (D) is b2.

In the same order of operation as the SIPO latch operation explained above, it must be idle for at least 3ΔT so that all three bits of time are stored in their internal registers. After this time interval, its clock is active and the bits are sent to the output (Q) in a parallel format. Whenever the latch clock is active, its reset must be inactive and vice versa. In this way, an inverter is used that allows this time inversion.

However, in the security of the latch launching the three bits before being reset, a delay is set after 3ΔT. This delay is defined by an RC circuit with a time constant of 0,5 ms.

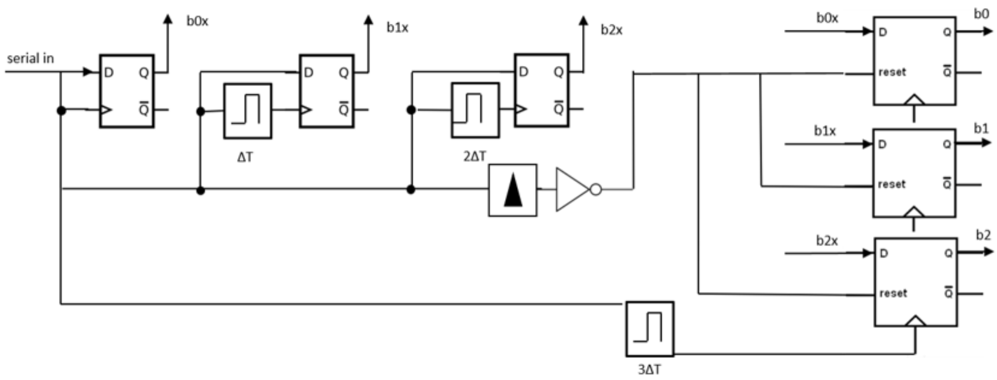

Figure 4.20: Representation of the another SIPO approach.

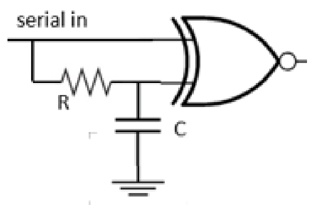

Figure 4.21: RC circuit to define ΔT.

4.2.5 Digital-to-Analogue Converter

A thermometric current-steering digital-to-analog converter is used to convert the 3-bit stimulus data in a variable amplitude current stimulus [71, 72, 73].

The architecture of the DAC is shown in Figure 4.22. The transistors used in this circuit have the same characteristics of the transistors used in the ADC circuit. The 3-bit inputs b0, b1, and b2 switch the transistors Q4, Q6 and Q8, respectively. In other words, if b0, b1 and b2 have the logic value 1 (analogue value of 5 V), the transistors Q4, Q6 and Q8 conduct. For the transistors to behave as switches, they must be in the triode region and, therefore, Equation (4.8) must be verified. In case Q4, Q6 and Q8 conduct, transistors Q5, Q7 and Q9 conduct, in the saturation region, respectively. The goal is the I_{DS} currents of each of the saturation transistors to add up as they conduct. That is, if there is no force exerted on the piezoelectric sensor, b0, b1 and b2 are 0 and none of the transistors Q5, Q7 and Q9 conducts and its $I_{DS} = 0$, respectively. When the force level is reduced and $b0 = 1$, only transistor Q5 conducts and the current will correspond only to $I_{D,Q5}$. When the level of force exerted increases, the remaining transistors conduct and there is a sum of that currents. To the transistors Q5, Q7 and Q9 operate in the saturation region, must comply with Equation (4.9).

U1A is an operational amplifier (*LM358*), and as such the voltage drop between its non-inverting and inverting input is equal to 0. Thus, we ensure that the voltage in the branch connecting $V_{DS,Q5}$, $V_{DS,Q7}$ and $V_{DS,Q9}$ is equal to V_{ref}. To adjust V_{ref}, it should be attention to Equation (4.17):

$$V_{ref} = V_{GS} + V_{DS}, \tag{4.15}$$

where V_{GS} is the gate-source voltage in Q5, Q7 and Q9 and V_{DS} is the drain-source voltage in Q4, Q6 and Q8. V_{GS} in transistors Q5, Q7 and Q9 can be calculated by Equation (4.15), for a drain current of 1 mA and a transconductance gain (β) of 0,0008, according to the saturation curve of transistors by:

$$I_D \approx \frac{\beta}{2}(V_{GS} - V_t)^2, \tag{4.16}$$

and therefore $V_{GS} = 2,4$ V. Once the voltage of gate inputs in Q4, Q6 and Q8 is, for one side, equal to V_{GS} of these transistors plus V_{GS} of Q5, Q7 and Q9, and, for another side, equal to 5 V, when the bits are 1, V_{GS} in Q4, Q6, and Q8 is 2,6 V. Consequently, for Q4, Q6 and Q8 work in the triode region, by Equation (4.8), and since the threshold voltage of all transistors used is 0,8 V, its V_{DS} must be at most 1,6 V. Focusing the attention in Equation (4.15), again, the maximum V_{ref} for transistor Q5, Q7 and Q9 operate in saturation region is 4 V. With the aim of the minimum power consumption, the V_{ref} chosen is 2 V.

Transistors Q5, Q7 and Q9 could be replaced by resistors, however, this technology was chosen to be as similar as possible to the future purpose of this circuit which is to be implemented in a SoC.

The DAC current ($I_{D,Q5}$ + $I_{D,Q7}$ + $I_{D,Q9}$) is mirrored to the branch with R1 through the current mirror Q1 and Q2. There is the possibility of using a cascode current mirror (with four transistors instead of two), having the advantage of allowing a higher output resistance, by reducing the channel modulation effect, leading to a lower variation of the output current with the output voltage. However, the cascode current mirror requires two more transistors and therefore the voltage drop of these would be greater than in the non-cascode current mirror, leading to a reduction of the admissible output voltage range.

After the concepts considered in Chapter 3 about nerve stimulation, the circuit of

Figure 4.22 is designed according to a single-phase stimulation. As previously mentioned, the sum of the currents of the transistors Q5, Q7 and Q9 will be mirrored, being able to reach a maximum value of 3 mA, according to Table 3.2 of Chapter 3, because the stimulation current values vary in the order of the milli-amperes to amperes, depending on the area of the body to be stimulated, namely the losses that exist due to the amount of tissue that this current must penetrate to the target [9]. In the case of the implantation of the module 2, for the stimulation of the trigeminal nerve, there are no great losses because the stimulation is done in the gingiva, where the trigeminal branches are located. In addition, stimulation current values should be minimal. Thus, the value for the stimulation current considered is 1 mA for each force level, i.e., in the case of excessive force there is a stimulus of 3 mA. Therefore, R1 functions as the load, that is, the impedance value of the tissue-electrode [9]. To calculate the maximum R1 value, it comes:

$$(V_{DD} - V_{SD,Q2}) = R1\, I_{stim\ max}, \tag{4.17}$$

where $V_{DD} = 5$ V, $V_{SD,Q2} = 0{,}8$ V and $I_{stim\ max} = 3$ mA, then $R1 = 1{,}4$ kΩ.

The Q10 transistor acts as an electrode charge remover when there is no stimulation. To this end, the gate is connected to the output of an inverter (U2A), whose input is bit b0. Thus, when the bit $b0 = 0$, the force on the sensor is zero, and after the negation of the bit, the logic value at gate input is 1 and the transistor is conducting.

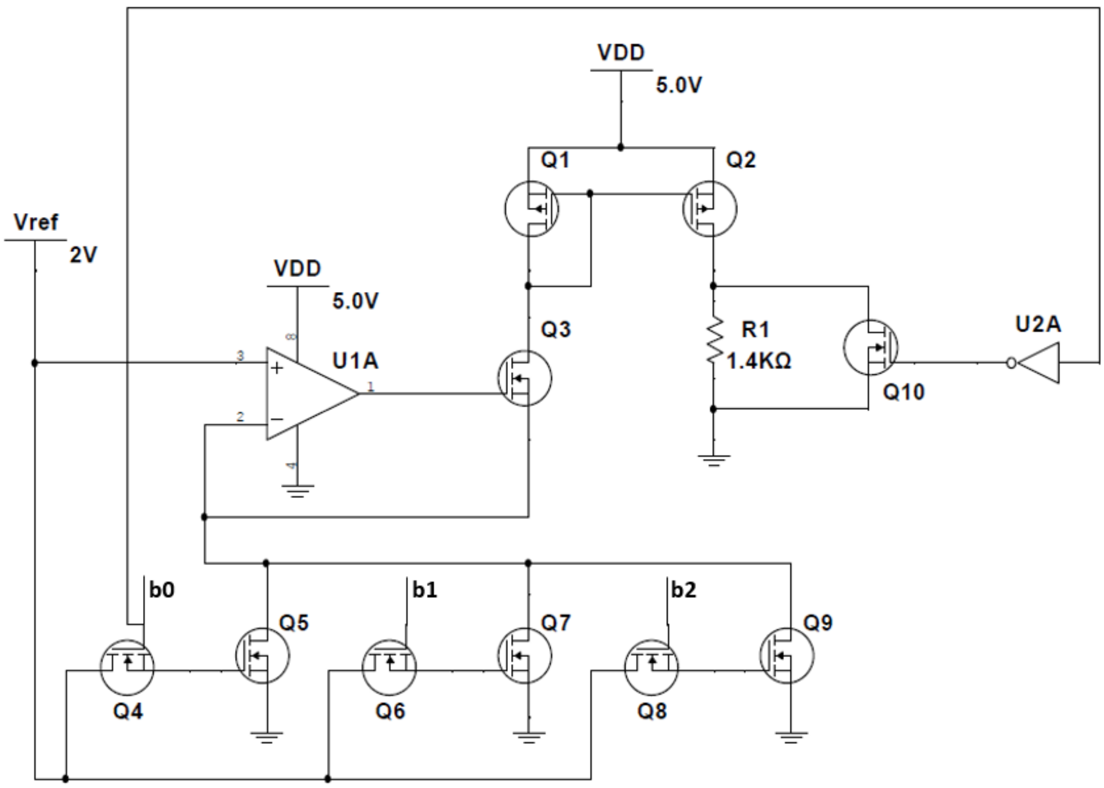

Figure 4.22: Architecture of the DAC circuit for the prototype.

In conclusion, it is possible to design a prototype with the aim of mimicking the action of periodontal mechanoreceptors, absent in a dental implant, according to the circuit of Figure 4.23. Here, the complete process is demonstrated, since a force is exerted on the piezoelectric sensor and an electric signal proportional to that force is generated, followed by a signal conditioning circuit (filtering and amplification), ADC conversion in four proportional logic levels to the force exerted, serial modeling and parallel demodulation for future wireless transmission of the three bits, DAC conversion and, finally, generation of a stimulation current, proportional to the force exerted.

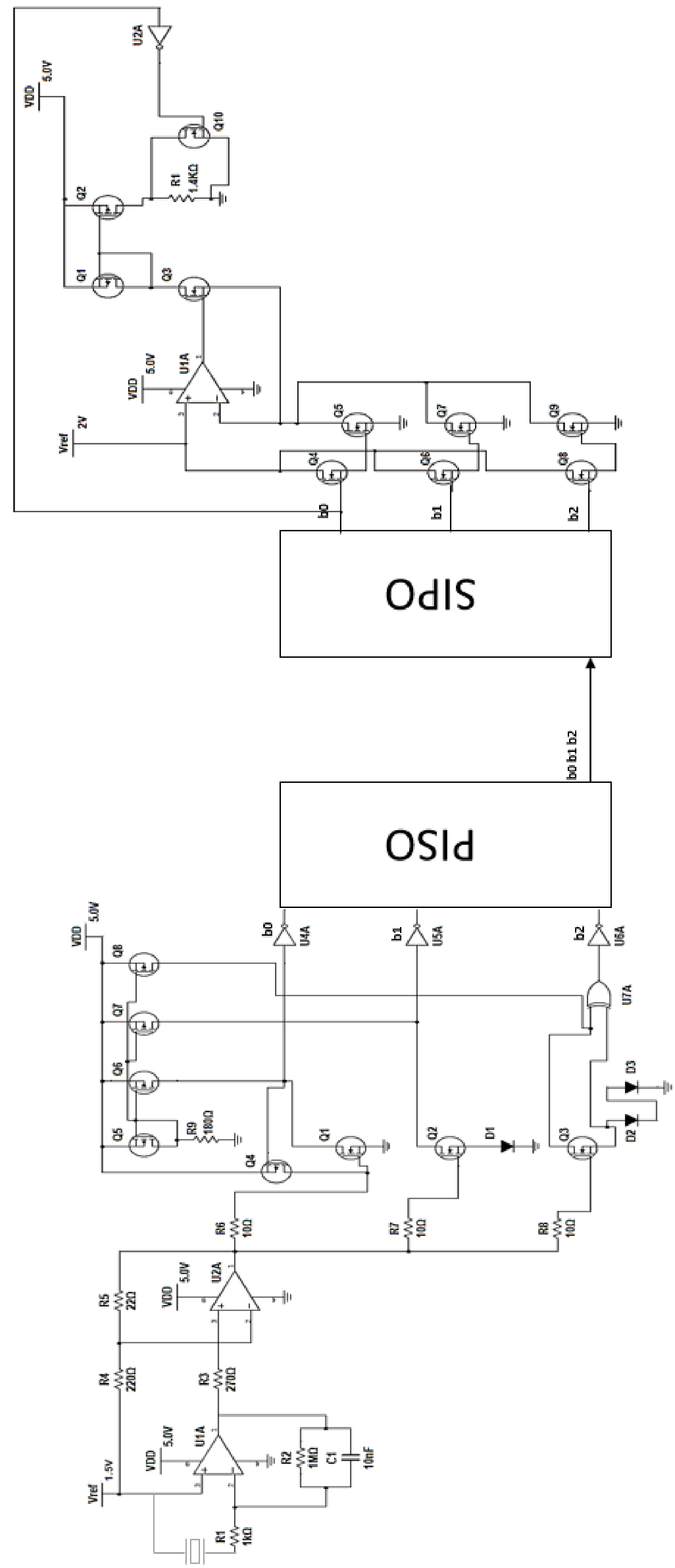

Figure 4.23: Global architecture of the prototype to be developed.

Chapter 5

Results and Discussion

This chapter presents the verification and discussion of the two methods presented in Chapter 4. In the Field Programmable Analog Array Method, it was only possible to simulate the three different circuit approaches in software, since problems appeared in the interface of the board with the software. As the waiting time for the recession of a new board was high, it was considered relevant to test the different blocks of the discrete method. The evaluation of the simulations on the programmable board can be completed for future work.

5.1 Field Programmable Analog Array Approach

5.1.1 Comparator Circuit

To simulate the operation mode of the comparator circuit four sinusoidal waves with increasing amplitudes were generated (Figure 5.1). On the other hand, the three comparators have a set reference level in software. Thus, for the proposed goal, the following reference levels were defined: 1 V, 2 V and 3 V. The first reference level is defined according to a DC signal (as seen in Figure 4.4), since the software does not allow three comparators with integrated reference levels. Thus, the generated sinusoidal waves have a defined amplitude, so as to simulate the four cases of applied force (no force, low, medium and high force), of: 0,5 V, 1,5 V, 2,5 V and 3,5 V.

It is possible to observe that in case (a) the three comparators have an output 0 V, as expected, since the amplitude of the input signal is so low that it does not reach the reference voltage of the first comparator.

In case (b) only the first comparator (channel 1) has an output different from 0 (in the software, the output of 3.30 V corresponds to digital value 1), since its reference voltage is exceeded.

In case (c) and (d), in the same point of view, the level of the second and third comparators is reached, respectively.

Note that here it is dealing with a thermometric code as well, since, for example, the reference of the second comparator is only reached if the reference of the first comparator is reached.

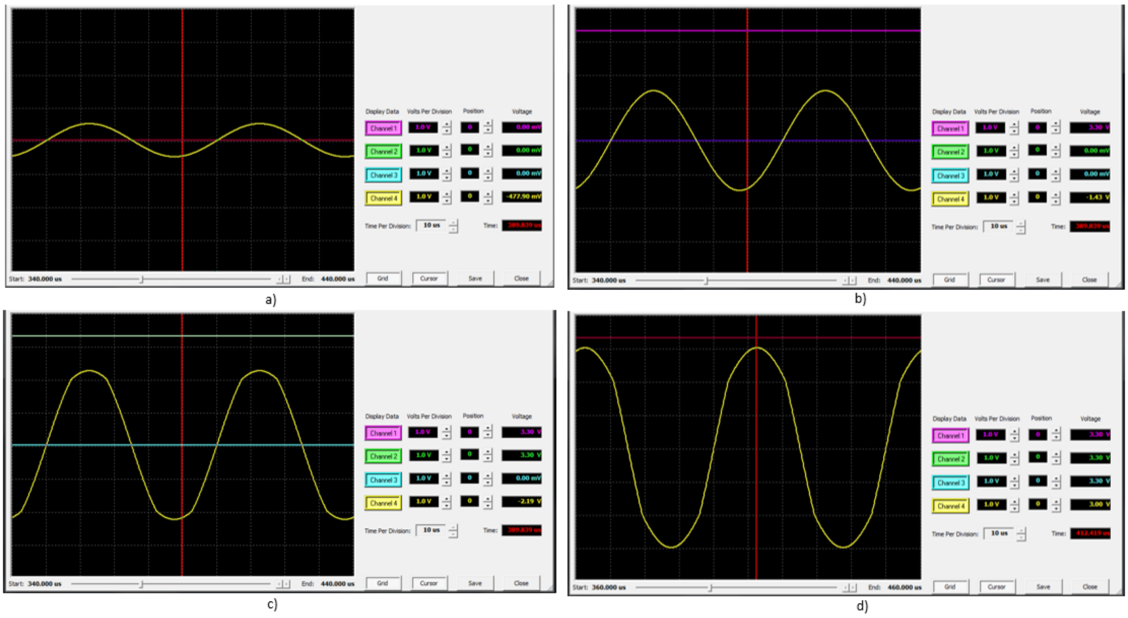

Figure 5.1: Simulation of circuit comparator operation mode with different input waveforms.

5.1.2 Delta-sigma Circuit

In the case of the delta-sigma simulation circuit (Figure 5.2), the simulation probes, as observed in the Figure 4.5, were placed at: the output of the delta-sigma block (channel 1), the output of the low-pass filter (channel 2), the input waveform (channel 3) and the output of the second comparator (channel 4).

Note that, as expected, the density of the pulse set is higher at the positive and negative peaks of the sine wave. On the other hand, channel 2 and channel 3 overlap since the filter allows the conversion of the delta-sigma signal into an analogue signal identical to the input signal. Channel 4 has a peak of 3,30 V during the period when the signal at the filter output exceeds the reference voltage value of the respective comparator (defined as 2,15 V). That is, by cursor observation, when the sine wave reaches 2,11 V, channel 4 rapidly changes to 0 V.

5.1.3 ADC Circuit

In the case of the ADC simulation circuit (Figure 5.3), the simulation probes, as observed in the Figure 4.6, were placed at: the output of peak detector (channel 1), the sync output ADC(channel 2), the input waveform (channel 3), and the data output of the ADC (channel 4). The results are not so visible, in this case, since the operating clock

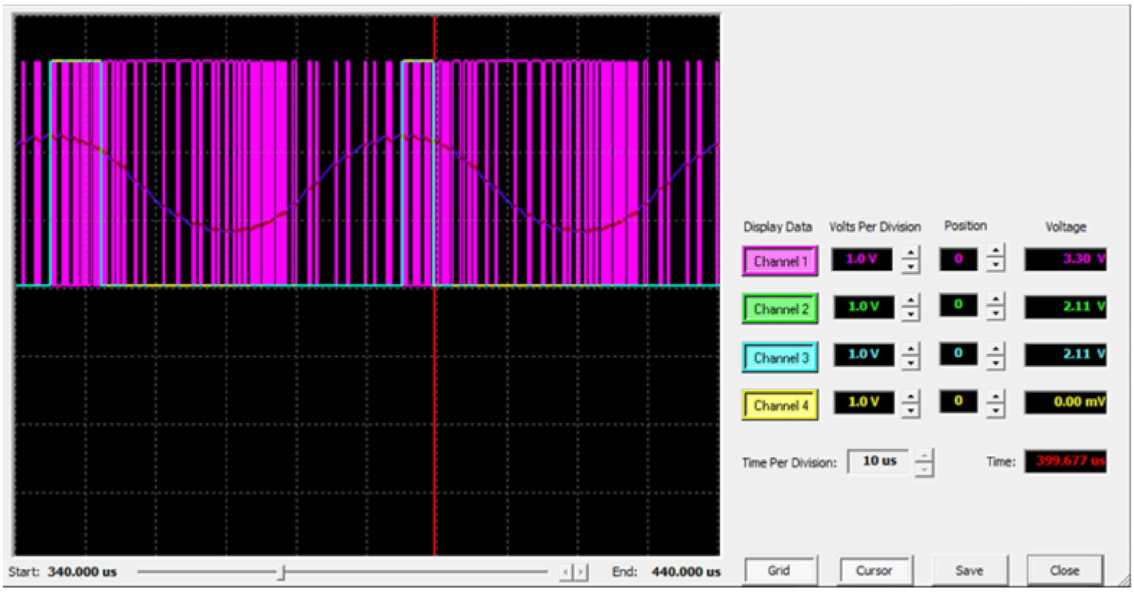

Figure 5.2: Simulation of delta-sigma circuit operation mode.

of the ADC is 4 MHz, causing the bits to be sent on a very fast time scale (in the order of 250 ns). For this reason, an interface of recording the data at these frequencies began to be developed, so as to obtain only the first two bits, however it has not been tested. Nevertheless, it is possible to verify that when there is peak detection, the bit density sent by the ADC is much higher than that verified when the input signal reduces its voltage to minimum values.

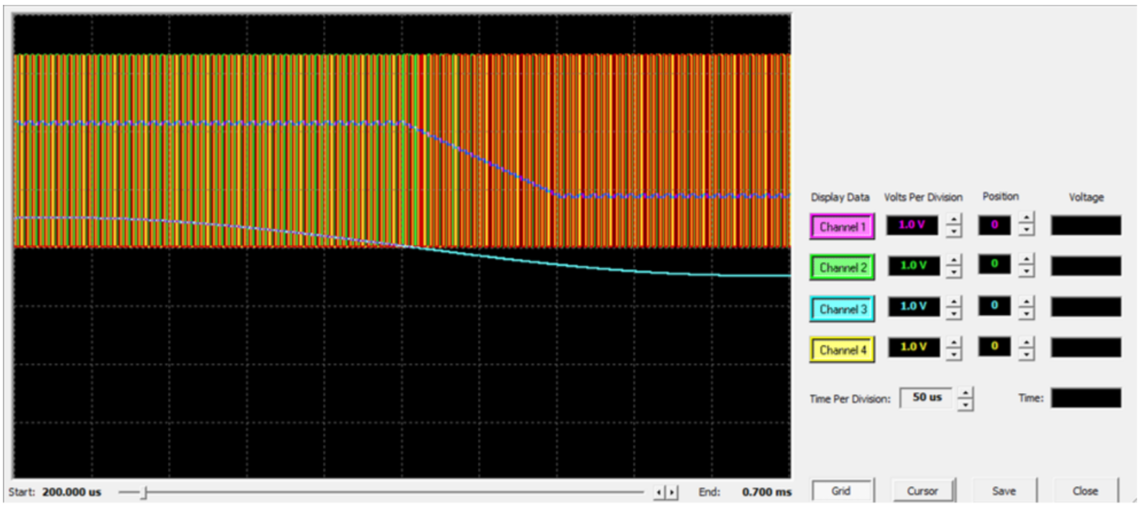

Figure 5.3: Simulation of ADC circuit operation mode.

5.2 Discrete Approach

The prototype device of the Discrete Method was designed and tested in a breadboard, but to obtain a better quality implementation, namely with lower noise, a PCB with the entire circuit of Figure 4.23 was built. Interferences in the breadboard may result from: intermittent connections, bad lead connections; capacitive coupling between neighbor connections; use of long wires which can act as antennas and pick up noise. All the results presented here were obtained with the PCB implementation. The board layout and PCB details are presented in the Appendix A.

The equipment used to acquire the waveforms of the signals observed within the different circuits of the prototype included two oscilloscopes (*Rigol DS2102A* and *Rigol DS1074*) and a waveform generator (*Topward 8110*). To simulate the other approach for SIPO, with the RC circuit rather *NE555*, was used *Multisim* Software.

5.2.1 Piezoelectric Signal Acquisition and Processing

Figure 5.4 shows the signals generated by the piezoelectric sensor when different force levels are applied with a finger. Increasing levels of force were applied, leading to the increasing amplitudes of the waveforms (a), (b) and (c). When no force is applied, the signal is maintained at 1,5 V, the voltage value used as reference level.

According to Equation (4.6), it is possible to calculate the piezoelectric charge produced in the different cases studied. For this and by observing the peak voltage value of each waveform, we obtain the output voltage: $U_{o,a} = 2$ V, $U_{o,b} = 3$ V and $U_{o,c} = 3{,}5$ V. With a feedback capacitance of 10 nF, the piezoelectric charges produced are: $q_a = -5$ nC, $q_b = -15$ nC and $q_c = -20$ nC, respectively. The negative signal represents the movement of charges between the piezoelectric sensor plates. As expected, charge generation increases with increasing forces applied to the sensor.

According to the piezoelectric datasheet, the sensitivity of the sensor is 1 mV per 0,1 nm of stroke displacement. Further, the stiffness of the sensor is 500 N/μm. With these two references and the output voltages of the different waveforms, it is possible to establish a relationship between sensitivity and stiffness and then calculate the force applied to the sensor. Thus, given the sensor sensitivity ratio referred to above, and according to the output voltages observed in Figure 5.4, the sensor suffers a stroke of 200 nm in (a), 300 nm in (b) and 350 nm in (c). Relating these values to the stiffness of the sensor it is concluded that the three force levels imposed are, respectively: $F_a = 100$ N, $F_b = 150$ N and $F_c = 175$ N. According to article [29], the maximum bite force varies with implant type between 170 and 325 N, for complete dentures or maxillary dentures and implant-supported mandibular overdentures. The value obtained for a maximum force applied in this prototype is within the maximum levels recorded in the literature. However, if the prototype is applied to implants that allow higher force levels than those obtained in these results, the solution is to change the sensitivity of the piezoelectric sensor to the applied force by adjusting the gain of the U2A op amp of Figure 4.12 and thus changing the values of the resistors R4 and R5.

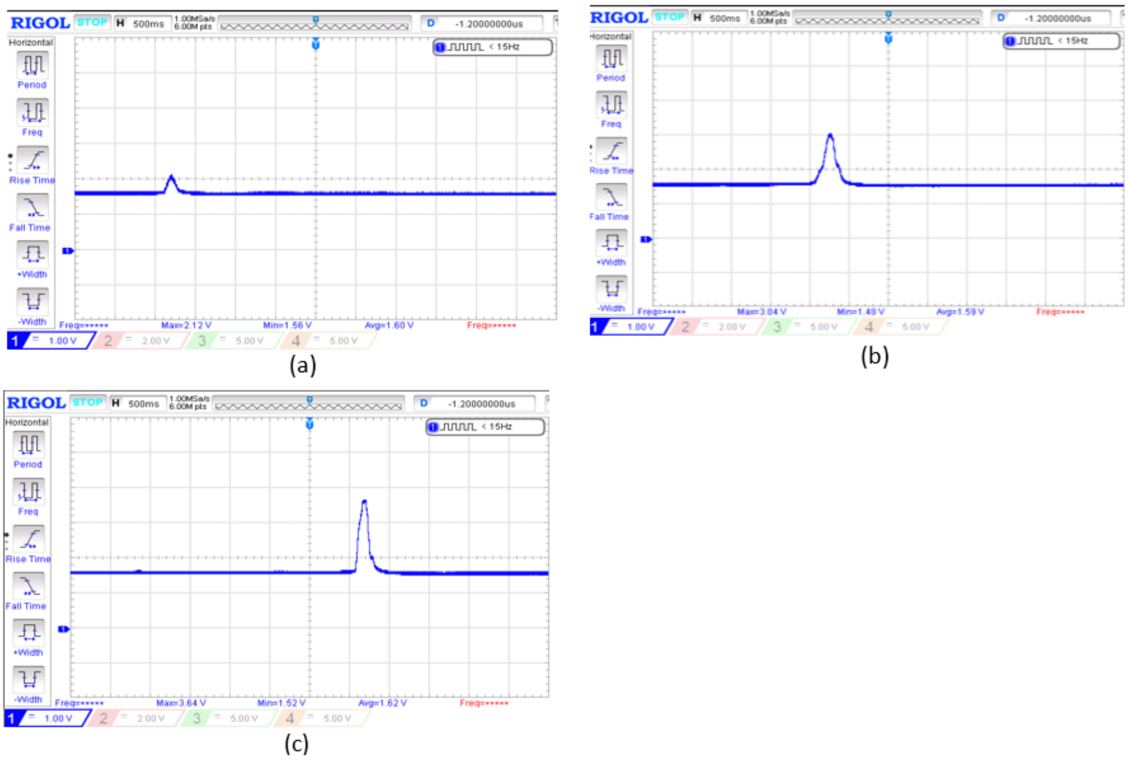

Figure 5.4: Waveforms of the piezoelectric sensor signal when different force levels are applied. (a) Low level force; (b) Medium level force and (c) High level force, with a temporal scale of 500 ms and a vertical scale of 1 V, per division.

It was verified that the waveform of the piezoelectric signal tends to saturate between 3,5 V and 4 V, not reaching the 5 V of the power supply voltage. The reason lies in the fact that the operational amplifiers used in the charge amplifier are not rail-to-rail amplifiers. The usable dynamic range of the amp-op is an important feature because it affects several parameters such as noise susceptibility, and signal-to-noise ratio (SNR). For that reason, the use of a rail-to-rail amplifier in future designs will be a good practice.

Figure 5.5 presents pulses generated by the piezoelectric sensor in response to a sequence of forces with intervals of approximately 0,5 s. It is estimated that, in average, human chewing is done with intervals of 0,8 s between bites [25]. The rapid discharge observed occurs due to the values of input resistance of the amplifier, feedback capacitor and feedback resistor.

5.2.2 Analogue-to-Digital Converter

After implementing the ADC circuit presented in Figure 4.13 on bread board, it was observed that when the p-MOS Q4 and n-MOS Q1 transistors conduct, an oscillation occurs. Since the p-MOS Q4 transistor was introduced with the purpose of creating a

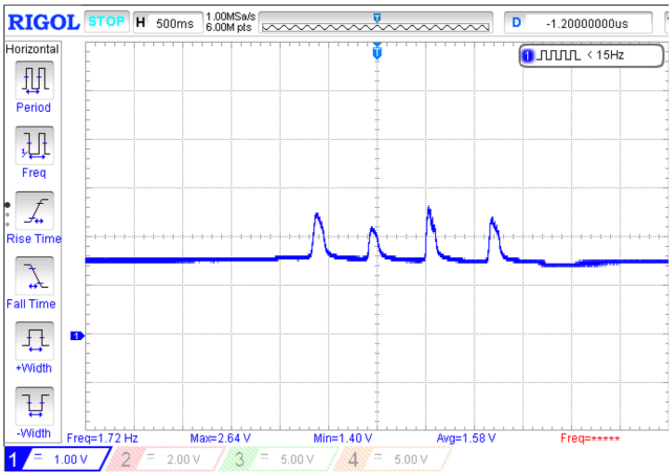

Figure 5.5: Piezoelectric signal waveform observed after application of successive forces, mimicking a chewing action, with a time scale of 500 ms and a vertical scale of 1 V, per division.

hysteresis effect, which actually is already forced by the inverters, it was found that the p-MOS Q4 transistor can be removed from the ADC circuit. The resistors R6, R7 and R8 can also be removed from the circuit, since the output without these references is not change.

To test the behavior of the ADC circuit at different voltage levels, a triangular waveform was applied at its input (Figure 5.6). Note that as the voltage amplitude of the triangle wave increases (channel 1), the three bit outputs (bit 0/channel 2, bit 1/channel 3 and bit 2/channel 4) switch according to a thermometric code – the second and third bit levels only switch to 5 V after the passage of the first and the second level, respectively. When the triangular wave reaches 1,8 V, channel 2 switches to 5 V, corresponding to the second discrete level. Then, the third discrete level occurs when the input voltage reaches 2,4 V. Finally, the fourth and last level (bit 2/channel 4) is reached when the triangular wave exceeds 3,8 V.

Then, the signal acquisition and conditioning circuit was connected to the ADC circuit, and the three output bits were observed when applying four different forces in the piezoelectric sensor. In Figure 5.7, channel 1 corresponds to the signal at the output of the conditioning circuit, and therefore to the input of the ADC circuit, channel 2 corresponds to the bit 0 output, channel 3 is the bit 1 output, and channel 4 to the bit 2 output. When there is no force on the sensor, the input of the ADC circuit (channel 1) maintains the reference voltage level 1,5 V and the value of the three bit outputs is 0 (a situation that occurs from the moment 0 s to 2,5 s on the time scale). Afterwards a force peak occurs, but since its magnitude does not reach the first transition level, channels 2, 3, and 4 remain at 0. In the next three peaks, since the three transition levels are gradually exceeded, the three bits outputs shift to 1 at the corresponding transition levels.

In order to verify the hysteresis behavior of the different ADC levels, Figure 5.8 presents

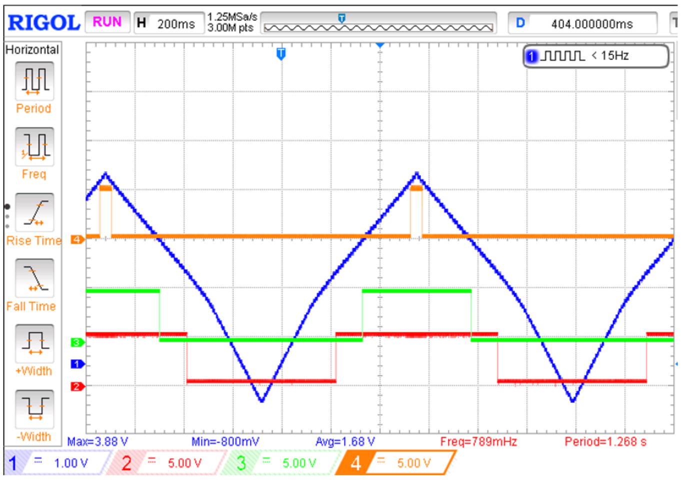

Figure 5.6: Operation of the 3-bit, thermometer code, ADC circuit in response to a triangular waveform, with a temporal scale of 200 ms and a vertical scale of 5 V, per division.

a situation in which small oscillations are caused around the threshold of the first transition level (channel 1). Note that the oscillations around the transition level are so minimal that they can hardly be observed in the figure, however when the first threshold is reached there is a drastic 0 to 5 V switching of the first bit, without any fluctuations.

5.2.3 Parallel-to-Serial Conversion

In order to test the Parallel-in Serial-out conversion of the three bits, the PISO output, that provides the serialized ADC output, was analysed imposing simultaneously a $\simeq$1 kHz clock generated by the *NE555* oscillator. The results are shown in Figure 5.9. The left images of each sub-figure were captured by a two channel oscilloscope and the right images by a four channel oscilloscope, both in the single mode option, to detect the voltage edge of the PISO output, simultaneously. Channel 1 of the left images corresponds to the clock of the *NE555* and channel 2 to the PISO output; in the right images channel 1, 2 and 3 correspond to the output of the ADC bits b0, b1 and b2, respectively, and channel 4 to the PISO output, again.

Focusing the attention in Figure 5.9a, the left image shows the detection of bit b0. The occurrence of this bit in the PISO output can be seen in the right image.

In Figure 5.9b and Figure 5.9c the same conclusions can be drawn, in this case for bit b1 and b2, respectively. In the case of (b) the PISO output is active at 5 V for two clock cycles and in case (c) the same output is active at 5 V for three clock cycles. It should be noted that, in these two cases, the time scale is 5 ms, by division.

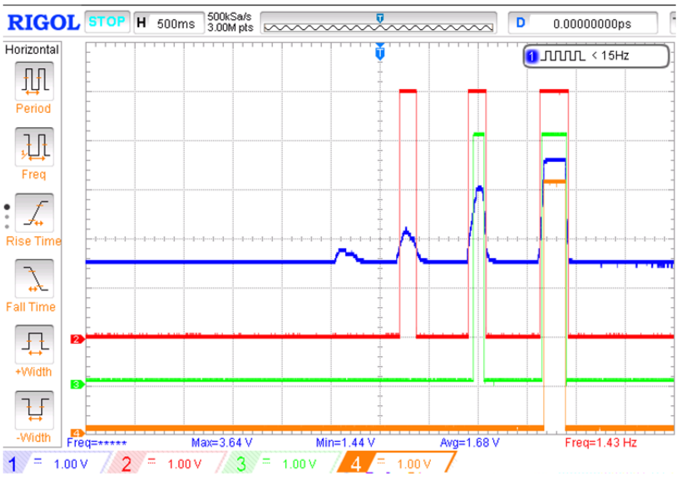

Figure 5.7: Occurrence of the four ADC discrete levels, 000, 001, 011, and 111, in response to four force levels applied to the piezoelectric sensor. Temporal scale of 500 ms and a vertical scale of 1 V, per division.

5.2.4 Serial-to-Parallel Conversion

Figure 5.10 shows the results obtained in the SIPO output, when applying three different force levels. Thus, the probes to test the conversion from series to parallel were placed in each of the SIPO parallel outputs, corresponding to each one of the bits, more concretely b0 in channel 1, b1 in channel 2, b2 in channel 3, and the SIPO serial input in channel 4. The images were captured in the single mode option, detecting the voltage edge of the SIPO input.

What is actually observed is the opposite of that presented in the previous section, i.e., one can notice the pulse width to digital conversion performed by the SIPO block - when the SIPO input shows a 1 ms pulse, it corresponds to only bit b0 at status “1” (Figure 5.10 (a)); when the SIPO input shows 2 ms duration pulse, both bits b0 and b1 are “1” (Figure 5.10 (b)), and finally, if the serial input is a 3 ms duration pulse, the three bits are “1” (Figure 5.10 (c)). Note that the time during which the bits are active is the interval between the end of the latch release and the start of the reset, defined by the two *NE555* clocks, which corresponds to a 2 ms period, approximately, as verified.

To test the other approach of SIPO, three situations of increasing force were simulated, that is, in each of the simulations of Figure 5.11 a square wave with a period of 1, 2 and 3 ms was generated, representing the series entry of the 3 bits. The waveforms obtained in Figure 5.11 correspond to: D (bx) - bx input of the latch flip-flop; D (bxp) - bx output of the latch flip-flop; D (lclk) - latch clock; D (deltat) - output of the XNOR gate with a time constant of 1ms; D (delta2t) - output of the XNOR gate with a time constant of 2 ms; D (rst) - reset. X1 attends the jump to 1 of the serial input and X2 its return to 0.

In any of the three situations it is verified that since b0 arrives with the value 1, the entry in the latch is 1 since the flip-flop clock that throws b0 to the latch is the only one

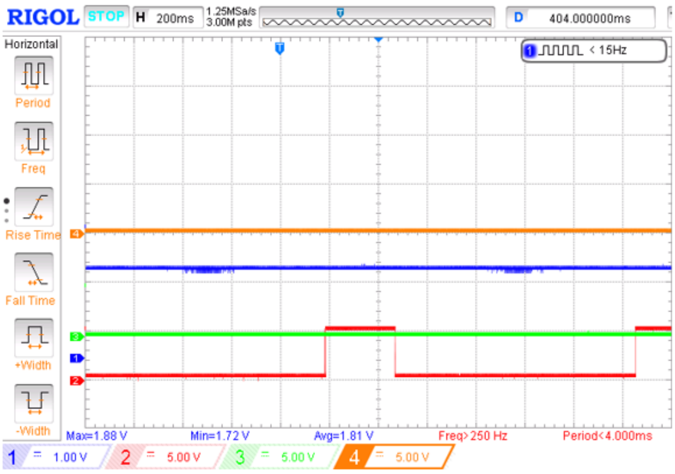

Figure 5.8: Hysteresis behavior of the ADC circuit, with a temporal scale of 200 ms and a vertical scale of 5 V, per division.

that does not have an RC circuit.

In the situation where only $b0 = 1$ (Figure 5.11 (a)), it is verified that the latch clock is active after 1 ms of the register, sending the bit b0 with the value 1 and the remaining ones to 0 during the time in that the reset is inactive (delay). After approximately 0,3 ms delay the reset is activated and the latch outputs return to 0.

In the situation where b0 and b1 have a value of 1, the latch clock is only activated 2 ms after the serial input jump. Deltat is active 1 ms after the arrival of b0, that is, at the moment of entrance of $b1 = 1$ the RC circuit has exceeded the time constant of 1 ms and therefore XNOR is switching, releasing b1 to the latch. When it reaches maximum load, the RC circuit starts to discharge and XNOR tends to uncouple.

In the situation where the three bits are equal to 1, the situation is identical to the previous one, however, the latch clock is only activated 3 ms after the jump of the serial input and delta2t is active 2 ms after the arrival of b0 launching b2 for the latch, since the time constant of the respective RC circuit is double the previous one.

The reason why the waveform of b1 and b2 at the input of the latch in situations (b) and (c) is more than 1 ms is precisely due to the charge and discharge time of the deltat and delta2t RC circuit, respectively.

In this simulation XNOR ports were assumed with well defined switching levels (2,5 V). In practice, these switching levels may vary, which can lead to delays in launching the bits or in receiving them.

5.2.5 Digital-to-Analogue Converter

Finally, to evaluate the digital to stimulus current amplitude process, a probe was placed in each gate of the transistors controlled by the SIPO output (b0 in channel 1, b1 in channel 2 and b2 in channel 3) and the electrode terminal (drain of the transistor Q2

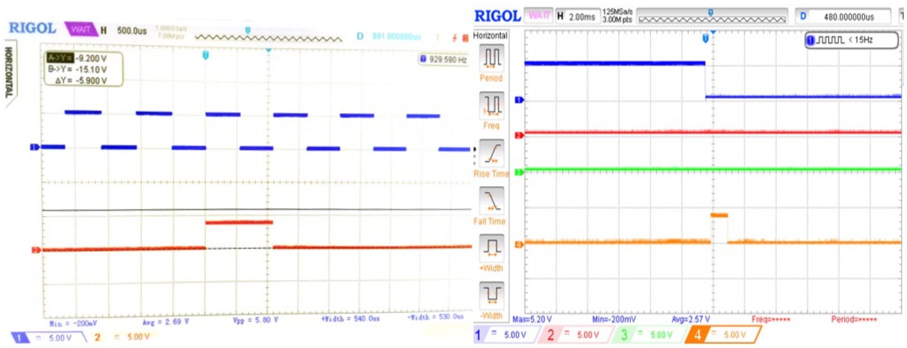

(a)

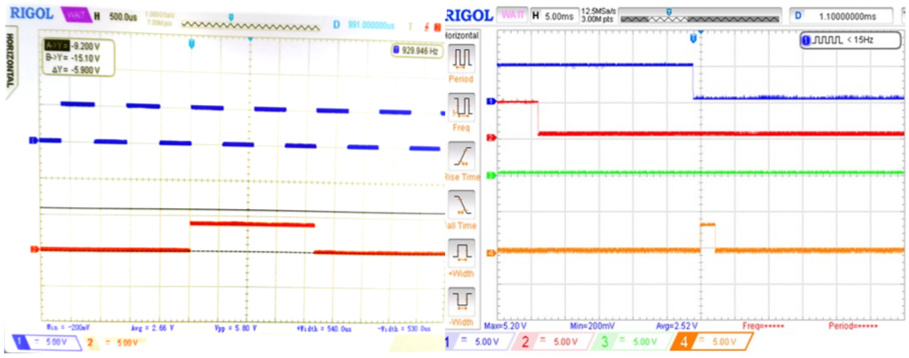

(b)

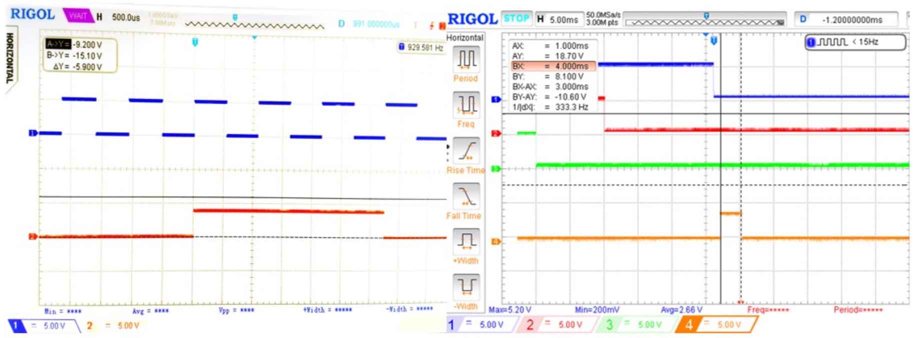

(c)

Figure 5.9: Waveforms of clock and PISO outputs, on the left images (time scale: 500 μs/division); waveforms of the three ADC bits and PISO output, on the right images (time scale: 2 ms/division in (a) and 5 ms/division in (b) and (c)).

and resistor R1 node in Figure 4.22) in channel 4. The obtained results are shown in Figure 5.12. The images were captured in the single mode option, to detect the edge of the DAC output voltage in channel 4.

Since the load resistance used was 1 kΩ, in order for the stimulus output current to be 1 mA for each level of force applied, an increase of 1 V of the output voltage must be observed for each bit that is activated. As can be seen from Figure 5.11 (a), in the situation where $b0 =$ "1", an ouput voltage of 1 V is observed. A proportional situation is seen in Figure 5.11 (b), in this case for the activation of bits b0 and b1, leading to an amplitude of 2 V, therefore, 2 mA at the output to the electrode. Finally, in the situation where

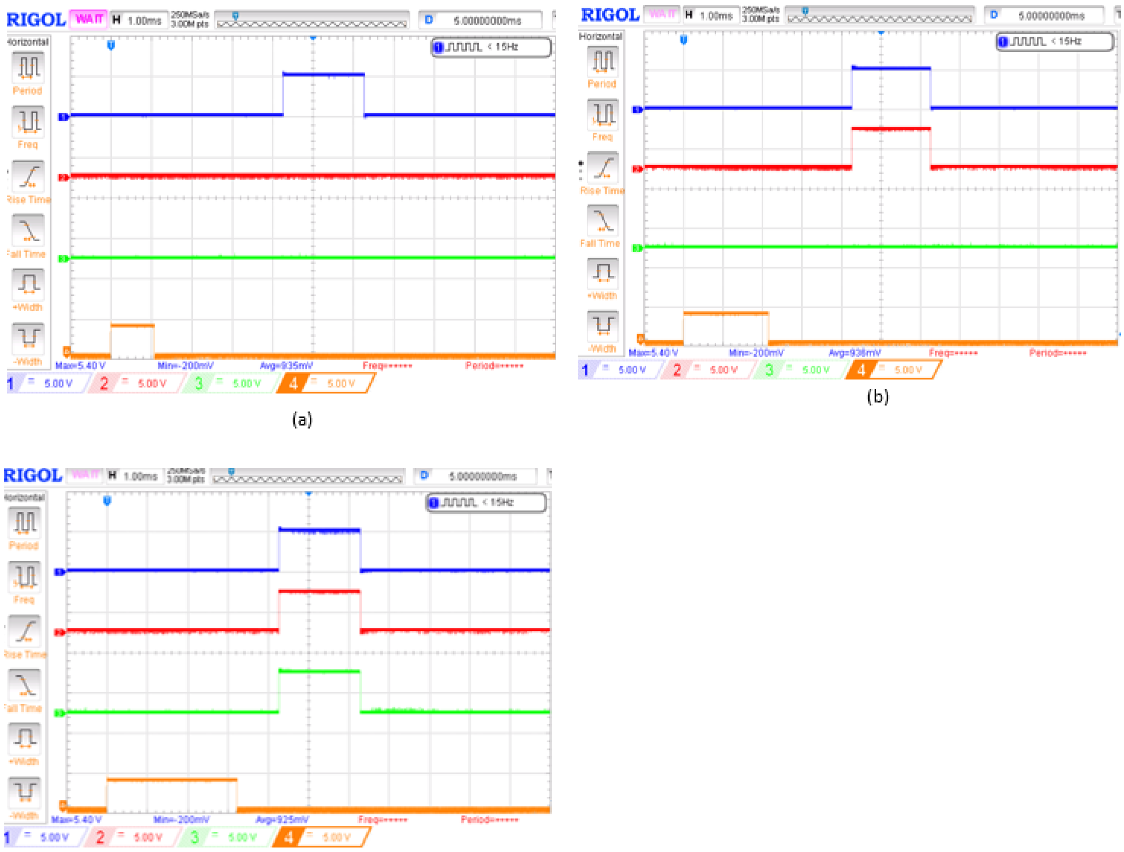

(a) (b) (c)

Figure 5.10: Generation of the three parallel bits at the SIPO output for three SIPO input cases (time scale of 1 ms/div and a vertical scale of 5 V/div).

the three bits are active, the voltage amplitude should be 3 V, but in fact, as depicted in Figure 5.11 (c), the voltage amplitude is about 2,5 V. This occurs because, as the output voltage increases, the V_{SD} voltage of the p-channel transistor (Q2 of Figure 4.22) decreases and, when it reaches the saturation limit the transistor operation enters the triode mode, and, consequently, the I_{DS} to V_{DS} characteristic changes. To reverse this problem a lower resistance value could be used, however as this resistance R1 functions as the tissue impedance, it cannot be changed. Thus, a way to increase the voltage in the resistor, so that the p-channel transistor does not reach the triode limit, is to opt for a transistor with a lower threshold voltage.

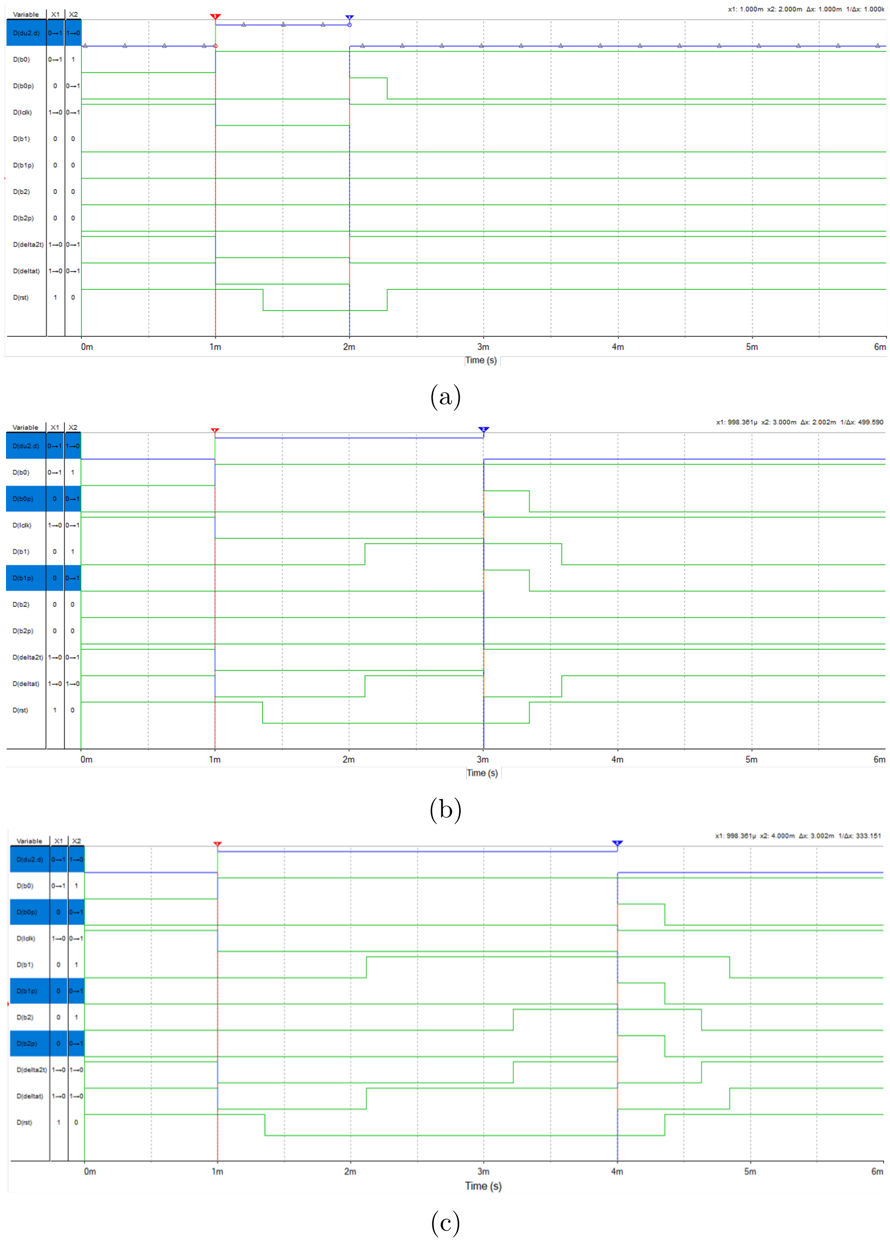

Figure 5.11: Simulation obtained on *Multisim* of the SIPO approach operation, without a clock.

Figure 5.12: Representation of the three parallel bits from DAC input and the voltage signal to nerve stimulation, with a temporal scale of 1 ms and a vertical scale of 1 V in (a) and 2 V in (b) and (c), per division.

Chapter 6

Conclusion

This is the final chapter of this document. Throughout the document the advantages and challenges of implanted medical devices in the human body, the evolution of Smart Implants at the micro-scale, and the integration of electrical neuro stimulation in these systems for the rehabilitation of the most varied cases of disorders is discussed. Overall, the biggest challenges in medical devices are in low power consumption and miniaturization, offering greater operating efficiency, with a higher speed of data processing power and faster wireless communication.

With the focus on dental medicine and orthodontics, the purpose of the system to be developed is to respond to the consequences of missing teeth, such as failures in dental mechanical implants as a result of excessive forces exerted on them due to the absence of sensory structures that communicate with the brain. In other words, it is intended to mimic a natural tooth in a Smart Implant, restoring its sensitivity to the force exerted during mastication.

First is carried out a global analysis of all the work that was developed. Finally, it is addressed the future work to be done in order to build a fully optimized in-situ implantable device, including its powering and remote external control, in order for this device to be ready for the next prototype evaluation.

6.1 Work Conclusion

The proposed work for the dissertation addresses the design of a first prototype of implantable neuro electrical stimulation in-situ able of translating the record of different applied force levels during chewing and mandibular occlusion. To the best of our knowledge, it is a totally new approach to a bionic device for in-situ stimulation of the trigeminal nerve branches in order to create an appropriate response of the brain to certain activities of patients with dental implants.

The dissertation started with an explanation of the stomatognathic system, functional and structural complexities that are fundamental to provide humans capabilities such as biting and chewing, dependents of the sensorial organs activity, namely of the periodontal mechanoreceptors. Due to oral problems there is often the need for extraction of one or more teeth. Studies show that 6-10% of the world population is completely edentulous and that only in the developed world, about 130 million teeth are lost annually. When a dental extraction occurs, the alveolar bone is reabsorbed and the periodontal ligament ceases to exist and, consequently, leads to loss of periodontal receptors and of dental sensitivity in the region. Due to this absence, there are numerous mechanical complications in the implants that can be caused by overloads and that carry costs for patients.

Then, a review of the state of art medical devices was presented as well as neural stimulation technologies. There are some cares to have with nerve stimulation techniques, specially amplitude and pulse width, frequency of stimulation, pulse duration and charge removal to comply with the security of the system to the patient.

Two different approaches were followed to develop the final purpose of the prototype, one trying an approach through the use of a programmable analog array, and another with discrete components. Due to some mishaps with the board used in the first approach, the final prototype device design follow a method with discrete components. The proposed prototype was designed and tested on a PCB and integrates two modules. The first module represents the generation, processing and transmission of information and the second module performs the reception and processing of the transmitted information and provides the nerve stimulation.

The solution adopted to acquire the exerted pressure on teeth is a passive piezoelectric element, which does not require an external supplying source. A charge amplifier placed between the piezoelectric element and the data acquisition system is used as a preliminary signal conditioning which transform the high impedance and charge output characteristic of piezoelectric sensor into a lower impedance voltage output. Adjusting the sensitivity and gain values of the circuit, three reference levels were obtained to test the prototype: 100 N, 150 N and 175 N. To detect four different levels of force (no force, low, medium and high force) it was decided to use a flash ADC, converting the analogue signal in a thermometric code (000, 001, 011 and 111). The ADC follows a configuration in order to create a hysteresis effect so that there are no oscillations in the bit values and, therefore, the three outputs can always assume well defined states of 0 or 1. In addition, it is a closer application of the full custom implementation idealized for the future of the prototype.

For the information to be transmitted wirelessly, a PISO circuit converts the three parallel bits from the ADC in a serial word to be transmitted for second module. The parallel data is loaded into a register simultaneously and is then shifted out serially one bit at a time under clock control. In the reception of the second module the reverse processing occurs, that is, the received serial signal is converted to the parallel format with a SIPO.

A thermometric current-steering digital-to-analog converter is used to convert the 3-bit stimulus data in a variable amplitude current stimulus of 1 mA, 2 mA or 3 mA, depends of the pressure level exerted. The stimulation circuit is designed according to a single-phase stimulation with an electrode charge removal technique.

All prototype developed is powered at 5 V, due to the characteristics of the electrical components used.

Chapter 5 presents the verification and discussion of the implemented blocks in order to validate the idealized proof-of-concept for this prototype. It could be concluded that all the blocks perform their tasks correctly.

6.2 Future Work

As mentioned before, the work done during the dissertation is just a proof-of-concept to design the prototype of a medical device that should be released in the market in a few years and therefore further work is needed. Firstly, it would be interesting to get the results with the programmable board, which were not achieved throughout the dissertation, since the different simulations in board can be more advantageous comparing with the currently ADC in the prototype. After, in the discrete approach, it is necessary to develop the wireless communication between two models. Furthermore, to improve the designed circuits namely to reduce the power consumption and size of the prototype, in order of getting closer to the idealized future, integrating the prototype modules into a SoC. To reach this miniaturized solution, the next step is to convert the developed design into an IC, simulate it and finally create its layout. Due to the time for prototype development and eventualities during its implementation, there was no possibility of working on the remote control of the stimulator, through an external device. This external controller should be used by the physician in order to adjust the trigger levels of the stimulation and change the stimulation parameters according to each patient and should be another step to be developed. For the device to be deployed, in the future, it needs a clean and biocompatible permanent and sufficient source of energy to operate, like a microbattery, which should be also studied. When the entire system is constructed, it is necessary to conduct in vivo experiments to test for dental sensitivity. After the experimental operation is validated, the next step should be the design of an extremely safe and efficient final prototype with the ideal dimensions to be implanted in the dental arch.

Appendix A

PCB

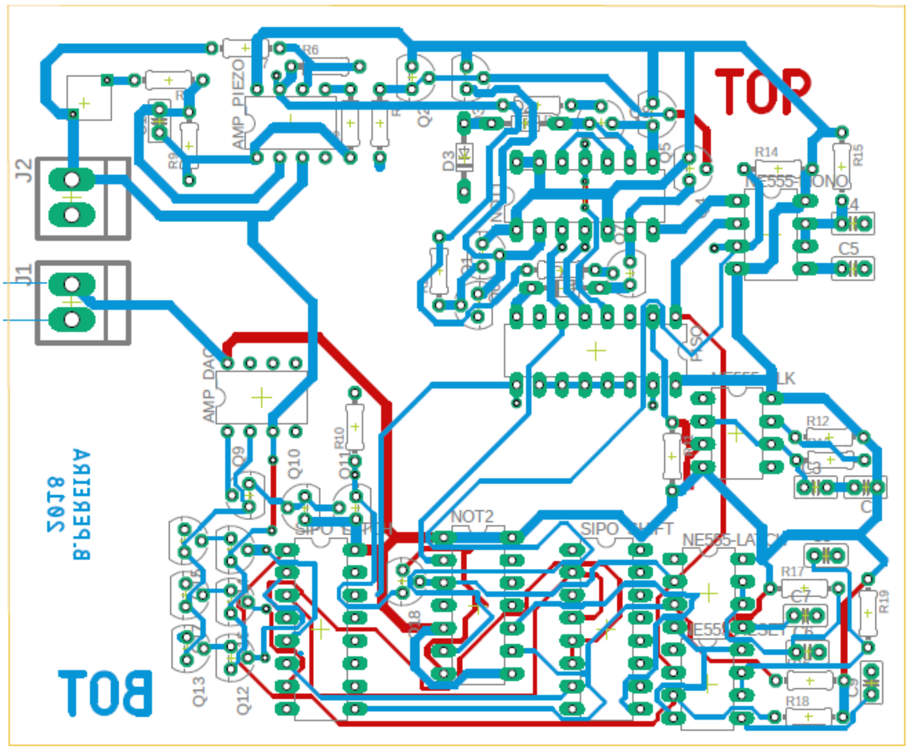

Figure A.1: Scheme of the board layout of PCB, on Eagle Software.

References

[1] D. Irnich and J. M. P Duc. Head. *Elsevier*, 26, 2013.

[2] F. Borges. Desenvolvimento de um Dispositivo de Sensorização da Oclusão. Master's thesis, Faculdade de Engenharia da Universidade do Porto, Porto, Portugal, December 2015.

[3] Medical Exhibits, Demonstrative Aids, Illustrations and Models. (Consulted November 8, 2017). URL: http://medicalexhibits.com/details.php?return=demonstratives&exhibit=12129_02X&type=exhibit&searchfor=trigeminal%20nerve.

[4] M. Dongen and W. Serdijn. *Design of Efficient and Safe Neural Stimulators: A Multidisciplinary Approach*. Springer, February 2016.

[5] U. F. O. Themes. 2. Functional Neuroanatomy and Physiology of the Masticatory System. *Pocket Dentistry*, January 2015.

[6] Prosthetic Techniques used for the insertion of a dental implant. (Consulted November 8, 2017). URL: http://www.isi-clinic.ch/en/prosthetic-techniques-used-for-the-insertion-of-a-dental-implant/.

[7] A. Kiourti and K. S. Nikita. A Review of In-Body Biotelemetry Devices: Implantables, Ingestibles, and Injectables. *IEEE Transactions on Biomedical Engineering*, 64(7):1422–1430, July 2017.

[8] J. Shimizu and K. I. Trovato. Electronic capsule for treating gastrointestinal disease, April 2012. (Patent consulted August 30, 2018).

[9] D. Prutchi and M. Norris. *Design and Development of Medical Electronic Instrumentation: A Practical Perspective of the Design, Construction, and Test of Medical Devices*. John Wiley & Sons, January 2005.

[10] J. G. Webster. *Medical Instrumentation Application and Design*. John Wiley & Sons, February 2009.

[11] C. A. Edwards, A. Kouzani, K. H. Lee, and E. K. Ross. Neurostimulation Devices for the Treatment of Neurologic Disorders. *Mayo Clinic Proceedings*, 92(9):1427–1444, September 2017.

[12] S. Simcox, G. Davis, A. Barriskill, J. Middleton, I. Bruinsma, M. Duncan, and R. Smith. A portable, 8-channel transcutaneous stimulator for paraplegic muscle training and mobility–a technical note. *Journal of Rehabilitation Research and Development*, 41(1):41–52, February 2004.

[13] P. Kerrebroeck and T. Marcelissen. Sacral neuromodulation for lower urinary tract dysfunction. *World Journal of Urology*, 30(4):445–450, August 2012.

[14] H. Basaeri, D. B. Christensen, and S. Roundy. A review of acoustic power transfer for bio-medical implants. *Smart Materials and Structures*, 25(12):123001, 2016.

[15] A. Demosthenous. Advances in Microelectronics for Implantable Medical Devices. *Advances in Electronics*, 2014, 2014. URL: https://doi.org/10.1155/2014/981295.

[16] H. Aggarwal, M. Pal-Singh, H. Mathur, S. Astekar, P. Gulati, and S. Lakhani. Evaluation of the effect of transcutaneous electrical nerve stimulation (TENS) on whole salivary flow rate. *Journal of Clinical and Experimental Dentistry*, 7(1):e13–e17, February 2015.

[17] Introduction to Piezoelectric Force Sensors. (Consulted January 3, 2018). URL: http://www.pcb.com/resources/technical-Information/Tech_Force.

[18] W. Q. Liu, Z. H. Feng, R. B. Liu, and J. Zhang. The influence of preamplifiers on the piezoelectric sensor's dynamic property. *Review of Scientific Instruments*, 78(12):125107, December 2007.

[19] J. Karki. Signal Conditioning Piezoelectric Sensors. *Texas Instruments*, 2000.

[20] C. J. Goodacre, G. Bernal, K. Rungcharassaeng, and J. Y. K. Kan. Clinical complications with implants and implant prostheses. *The Journal of Prosthetic Dentistry*, 90(2):121–132, August 2003.

[21] J. A. Porter and J. F. Von. Success or failure of dental implants? A literature review with treatment considerations. *General dentistry*, 53(6):423–32; quiz 433, 446, 2005.

[22] C. E. Misch. *Dental Implant Prosthetics - E-Book; Second Edition.* Elsevier Health Sciences, June 2014.

[23] E. Helkimo, G. E. Carlsson, and M. Helkimo. Bite force and state of dentition. *Acta Odontologica Scandinavica*, 35(6):297–303, January 1977.

[24] B. Serralheiro. Influência da perda de dentes sobre a função postural. Master's thesis, Universidade Católica Portuguesa, Viseu, Portugal, July 2015.

[25] Y. Ono. Occlusion and brain function: Mastication as a prevention of cognitive dysfunction. *Journal of Oral Rehabilitation*, 37:624–640, 2010.

[26] M. Trulsson. Sensory-motor function of human periodontal mechanoreceptors. *Journal of Oral Rehabilitation*, 33(4):262–273, April 2006.

[27] J. Malmivuo and R. Plonsey. *Bioelectromagnetism: Principles and Applications of Bioelectric and Biomagnetic Fields.* Oxford University Press, 1995.

[28] J. Regan, A. Russo, and C. Putte. *Seeley's essentials of anatomy & physiology; Nineth Edition.* McGraw-Hill, 2015.

[29] M. Trulsson, A. van der Bilt, G. E. Carlsson, K. Gotfredsen, P. Larsson, F. Müller, B. J. Sessle, and P. Svensson. From brain to bridge: masticatory function and dental implants. *Journal of Oral Rehabilitation*, 39(11):858–877, November 2012.

[30] J. Andreu-Perez, D. R. Leff, H. M. D. Ip, and G. Yang. From Wearable Sensors to Smart Implants-–Toward Pervasive and Personalized Healthcare. *IEEE Transactions on Biomedical Engineering*, 62(12):2750–2762, December 2015.

[31] A. Amar, A. Kouki, H. Cao, A. B. Amar, A. B. Kouki, and H. Cao. Power Approaches for Implantable Medical Devices. *Sensors*, 15(11):28889–28914, November 2015.

[32] M. Nathan. Microbattery Technologies for Miniaturized Implantable Medical Devices. *Current Pharmaceutical Biotechnology*, 11(4):404–410, June 2010.

[33] N. Beurskens, F. Tjong, and R. Knops. End-Of-Life Management Of Leadless Cardiac Pacemaker Therapy. *Arrhythmia and Electrophysiology Review*, 6(3), August 2017.

[34] X. Chen, B. Assadsangabi, Y. Hsiang, and K. Takahata. Enabling Angioplasty-Ready "Smart" Stents to Detect In-Stent Restenosis and Occlusion. *Advanced Science*, 5(5):1700560, May 2018.

[35] B. McAdams, A. Rizvi, B. H. McAdams, and A. Rizvi. An Overview of Insulin Pumps and Glucose Sensors for the Generalist. *Journal of Clinical Medicine*, 5(1):5, January 2016.

[36] K. Kalantar-zadeh, N. Ha, J. Ou, and K. Berean. Ingestible Sensors. *ACS Sensors*, 2(4):468–483, April 2017.

[37] J. D. Bronzino. *Biomedical Engineering Handbook*. CRC Press, December 1999.

[38] X. Li, S. Zhong, and J. Morizio. 16-Channel biphasic current-mode programmable charge balanced neural stimulation. *BioMedical Engineering OnLine*, 16(1):104, August 2017.

[39] Z. Yue, S. E. Moulton, M. Cook, S. O'Leary, and G. Wallace. Controlled delivery for neuro-bionic devices. *Advanced Drug Delivery Reviews*, 65(4):559–569, April 2013.

[40] P. Lopes and P. Baudisch. Demonstrating Interactive Systems Based on Electrical Muscle Stimulation. In *Adjunct Publication of the 30th Annual ACM Symposium on User Interface Software and Technology*, UIST '17, pages 47–49, New York, NY, USA, 2017. ACM.

[41] J. T. Hashmi, Y. Huang, S. K. Sharma, D. B. Kurup, L. Taboada, J. D. Carroll, and M. R. Hamblin. Effect of pulsing in low-level light therapy. *Lasers in Surgery and Medicine*, 42(6):450–466, August 2010.

[42] C. Miller, B. Robinson, J. Rubinstein, P. Abbas, and C. Runge-Samuelson. Auditory nerve responses to monophasic and biphasic electric stimuli. *Hearing Research*, 151(1):79–94, January 2001.

[43] S. Sardarzadeh and M. Pooyan. An implantable electrical stimulator for phrenic nerve stimulation. *Journal of Biomedical Science and Engineering*, 05(03):141–145, 2012.

[44] J. Lefaucheur. Cortical neurostimulation for neuropathic pain: state of the art and perspectives. *Pain*, 157, February 2016.

[45] A. Rezai, D. Finelli, J. Nyenhuis, G. Hrdlicka, J. Tkach, A. Sharan, P. Rugieri, P. Stypulkowski, and P. Shellock. Neurostimulation systems for deep brain stimulation: In vitro evaluation of magnetic resonance imaging–related heating at 1.5 tesla. *Journal of Magnetic Resonance Imaging*, 15(3):241–250.

[46] D. Scribner, L. Johnson, P. Skeath, R. Klein, F. K. Perkins, L. Wasserman, W. Bassett, D. Ilg, J. Peele, and J. Friebele. Microelectronic Array for Stimulation of Retinal Tissue. Technical report, Naval Research Laboratory, January 2005.

[47] S. Jezernik, M. Craggs, W. M. Grill, G. Creasey, and N. J. M. Rijkhoff. Electrical stimulation for the treatment of bladder dysfunction: Current status and future possibilities. *Neurological Research*, 24(5):413–430, July 2002.

[48] W. Ngamkham, M. N. van Dongen, and W. A. Serdijn. Biphasic stimulator circuit for a wide range of electrode-tissue impedance dedicated to cochlear implants. In *2012 IEEE International Symposium on Circuits and Systems*, pages 1083–1086, May 2012.

[49] F. Sun and M. Morrell. Closed-loop Neurostimulation: The Clinical Experience. *Neuroterapeuthics*, 11(3):553–563, July 2014.

[50] B. M. Doucet, A. Lam, and L. Griffin. Neuromuscular Electrical Stimulation for Skeletal Muscle Function. *The Yale Journal of Biology and Medicine*, 85(2):201–215, June 2012.

[51] K. Ann Ng, E. Greenwald, Y. Xu, and N. Thakor. Implantable neurotechnologies: a review of integrated circuit neural amplifiers. *Medical & Biological Engineering & Computing*, 54(1):45–62, January 2016.

[52] W. Ngamkham, M. N. van Dongen, and W. A. Serdijn. Biphasic stimulator circuit for a wide range of electrode-tissue impedance dedicated to cochlear implants. In *2012 IEEE International Symposium on Circuits and Systems*, pages 1083–1086, May 2012.

[53] D. Braeken, R. Huys, D. Jans, J. Loo, S. Severi, F. Vleugels, G. Borghs, G. Callewaert, and C. Bartic. Local electrical stimulation of single adherent cells using three-dimensional electrode arrays with small interelectrode distances. In *2009 Annual International Conference of the IEEE Engineering in Medicine and Biology Society*, pages 2756–2759, September 2009.

[54] R. V. Shannon. A model of safe levels for electrical stimulation. *IEEE Transactions on Biomedical Engineering*, 39(4):424–426, April 1992.

[55] D. B. McCreery, W. F. Agnew, T. G. H. Yuen, and L. A. Bullara. Comparison of neural damage induced by electrical stimulation with faradaic and capacitor electrodes. *Annals of Biomedical Engineering*, 16(5):463–481, September 1988.

[56] Y. Lo, R. Hill, K. Chen, and W. Liu. Precision control of pulse widths for charge balancing in functional electrical stimulation. In *2013 6th International IEEE/EMBS Conference on Neural Engineering (NER)*, pages 1481–1484, November 2013.

[57] D. Abejón, T. Cameron, C. Feler, and J. Pérez-Cajaraville. Electric Parameters Optimization in Spinal Cord Stimulation. Study in Conventional Nonrechargeable Systems. *Neuromodulation: Technology at the Neural Interface*, 13(4):281–287, October 2010.

[58] R. Osenbach. Neurostimulation for the Treatment of Intractable Facial Pain. *Pain Medicine*, 7(suppl_1):S126–S136, May 2006.

[59] C. Arcuri, F. Muzzi, R. Docimo, E. Fusco, F. Pauri, and P. Rossini. Somatosensory Evoked Potentials of Inferior Alveolar Nerve. *Elsevier*, 64(4):594–599, April 2006.

[60] B. G. Lapatki and O. Paul. Smart Brackets for 3d-Force-Moment Measurements in Orthodontic Research and Therapy – Developmental Status and Prospects. *Journal of Orofacial Orthopedics / Fortschritte der Kieferorthopädie*, 68(5):377–396, September 2007.

[61] W. Claes, R. Puers, W. Sansen, M. DeCooman, J. Duyck, and I. Naertb. A low power miniaturized autonomous data logger for dental implants. *Elsevier*, 97-98:548–556, April 2002.

[62] I. Cioc, I. Lita, D. Visan, and I. Bostan. FPAA Implementation of Signal Processing Circuits for Radiation Sensors. In *2009 32nd International Spring Seminar on Electronics Technology*, Electronics and Computers Department, University of Pitesti, Pitesti, Romania, 2009. IEEE.

[63] E. Pritchard, M. Mahfouz, B. Evans, S. Eliza, and M. Haider. Flexible capacitive sensors for high resolution pressure measurement. In *2008 IEEE SENSORS*, pages 1484–1487, October 2008.

[64] A. Thanachayanont and S. Sangtong. Low-Voltage Current-Sensing CMOS Interface Circuit for Piezo-Resistive Pressure Sensor - Thanachayanont - 2007 - ETRI Journal - Wiley Online Library, February 2007.

[65] D. A. Bittle, J. C. Suhling, R. E. Beaty, R. C. Jaeger, and R. W. Johnson. Piezoresistive Stress Sensors for Structural Analysis of Electronic Packages. *Journal of Electronic Packaging*, 113(3):203–215, September 1991.

[66] Y. Wu and J. Singh. Metal piezoelectric semiconductor field effect transistors for piezoelectric strain sensors. *Applied Physics Letters*, 85(7):1223–1225, August 2004.

[67] S. Gupta, H. Heidari, A. Vilouras, L. Lorenzelli, and R. Dahiya. Device Modelling for Bendable Piezoelectric FET-Based Touch Sensing System. *IEEE Transactions on Circuits and Systems I: Regular Papers*, 63(12):2200–2208, December 2016.

[68] R. Bailón, G. Laouini, C. Grao, M. Orini, P. Laguna, and O. Meste. The Integral Pulse Frequency Modulation Model With Time-Varying Threshold: Application to Heart Rate Variability Analysis During Exercise Stress Testing. *IEEE Transactions on Biomedical Engineering*, 58(3):642–652, March 2011.

[69] E. J. Bayly. Spectral Analysis of Pulse Frequency Modulation in the Nervous Systems. *IEEE Transactions on Biomedical Engineering*, BME-15(4):257–265, October 1968.

[70] Y. Gupta and S. Saini. *Performance Optimization Techniques in Analog, Mixed-Signal, and Radio-Frequency Circuit Design.* Engineering Science Reference, 2015.

[71] V. Valente, A. Demosthenous, and R. Bayford. Design of a current-steering implantable stimulator with electric field shifting for deep brain stimulation. In *2010 Biomedical Circuits and Systems Conference (BioCAS)*, pages 162–165, Paphos, Cyprus, November 2010. IEEE.

[72] S. Yi. An 8-bit current-steering digital to analog converter. *AEU - International Journal of Electronics and Communications*, 66(5):433–437, May 2012.

[73] V. Valente, A. Demosthenous, and R. Bayford. A Tripolar Current-Steering Stimulator ASIC for Field Shaping in Deep Brain Stimulation. In *2012 Biomedical Circuits and Systems Conference (BioCAS)*. IEEE, June 2012.